Georg Franz Sommerbauer, BSc.

Commissioning of a tubular reactor system: Investigations on the thermal stability of selected carbonates

Master's Thesis

submitted for the degree

Diplom-Ingenieur

in

Chemical and Pharmaceutical Engineering

(NAWI Graz studies)

Graz University of Technology
Advisor: Ass.-Prof. Dipl.-Ing. Dr.techn. Susanne Lux
Institute of Chemical Engineering and Environmental Technology

Graz, January 2014

I want to thank everybody who supported me throughout my life and years of study. Especially my parents, Gertrude and Werner, who made everything possible and always gave me the feeling that what I am doing is wright, and that I do it well. My fiancée Elisabeth for simply being there. My sister Barbara, my brothers Konrad and Thomas, and all of my friends for growing up with me, having fun with me, and helping me to form my personality. Susanne Lux for guiding me and treating me as an equal research partner. The Austrian society for providing me with funds to facilitate my studies in the form of a 'Studienbeilhilfe' during the last six years.

Deutsche Fassung: Beschluss der Curricula-Kommission für Bachelor-, Master- und Diplomstudien vom 10.11.2008, Genehmigung des Senates am 1.12.2008

Eidesstattliche Erklärung

Ich erkläre an Eides statt, dass ich die vorliegende Abeit selbstständig verfasst, andere als die angegebenen Quellen/Hilfsmittel nicht benutzt, und die benutzen Quellen wörtlich und inhaltlich entnommenen Stellen als solche kenntlich gemacht habe.

Graz, am .....

.....
(Unterschrift)

Statutory Declaration

I declare that I have authored this thesis independently, that I have not used other than the declared sources/resources, and that I have explicitly marked all material which has been quoted either literally or by content from the used sources.

.....
date

.....
(signature)

Abstract

This thesis deals with the commissioning of a Parr tubular reactor system and thermodynamic calculations for the hydrogenation of inorganic carbonates. Furthermore, carbonates mentioned (nickel and magnesium carbonate) and not mentioned (iron and manganese carbonate) in the literature were investigated experimentally in nitrogen and hydrogen atmosphere. The objective was to install a working reactor system coupled to an analyzer rack for gaseous reaction products, to compare the experimental results to the literature, and to identify possible effects of the hydrogen atmosphere on the reaction conditions and products.

Calculations of the standard free reaction energy $\Delta_R G^{\ominus}$ showed that the hydrogenation of magnesium, lead, manganese, iron, cobalt, nickel, copper, zinc, silver, and cadmium carbonate to the metal oxide and methane is thermodynamically favorable between zero and 550 °C at 1.013 bar. The literature review of publications on the hydrogenation of inorganic carbonates revealed that calcium, mixed calcium transition metal, and magnesium carbonates have already been thoroughly studied experimentally. Additionally, some data has been published on the hydrogenation of nickel, cobalt, barium, lithium, sodium, potassium, and strontium carbonate.

Iron, magnesium, manganese, and nickel carbonate were investigated in thermogravimetric experiments. 50 vol% hydrogen atmosphere led to a decrease of the decomposition temperature compared to pure nitrogen atmosphere. In the case of iron and nickel carbonate 50 vol% hydrogen atmosphere led to a significantly higher mass loss than expected for the loss of carbon dioxide in a thermal decomposition. This higher mass loss could correspond to the reduction of the carbonate to the metal.

The heating experiments with the reactor showed that the heat is relatively equally distributed in the central part of the reactor tube. At the outermost positions, on the contrary, the temperature drops notably. Magnesium carbonate was heated to 459 ± 8 °C for 125 minutes at 0.70 ± 0.03 bar overpressure in nitrogen atmosphere. Carbon dioxide was detected and the sample mass loss presumably corresponded to the complete decomposition to magnesium oxide. The same stays true for the use of 20 vol% hydrogen and a temperature of 442 ± 16 °C for 130 minutes at 0.8 ± 0.2 bar overpressure. Heating of iron carbonate to 479 ± 12 °C for 150 minutes at 0.9 ± 0.2 bar overpressure in nitrogen atmosphere resulted in the detection of carbon dioxide and a sample mass loss of 9.96 wt%. Heating of iron carbonate to 473 ± 25 °C for 200 minutes at 0.76 ± 0.05 bar overpressure in 20 vol% hydrogen produced carbon dioxide and carbon monoxide. The carbon monoxide production could be due to a reverse water-gas-shift reaction. The mass loss increased to 39.81 wt%, possibly due to complete thermal decomposition.

Kurzfassung

Diese Masterarbeit behandelt die Inbetriebnahme eines Parr Rohrreaktorssystems und thermodynamische Berechnungen zur Hydrierung von anorganischen Carbonaten. Es wurden Experimente mit Carbonaten, die in der Literatur erwähnt werden (Nickel- und Magnesiumcarbonat), durchgeführt, aber auch mit Carbonaten, die bisher keine Erwähnung fanden (Eisen- und Mangancarbonat). Ziel dieser Arbeit war es ein funktionierendes Reaktorsystem mit gekoppelter Gasanalyse aufzubauen, die experimentellen Ergebnisse mit der Literatur zu vergleichen und die Auswirkung einer Stickstoff- bzw. Wasserstoffatmosphäre auf den Reaktionsverlauf zu untersuchen.

Die Berechnung der freien Standard-Reaktionsenthalpie $\Delta_R G^{\ominus}$ für die Hydrierung von Magnesium-, Blei-, Eisen-, Kobalt-, Nickel-, Kupfer-, Zink-, Silber- und Cadmiumcarbonat zum Metalloxid und Methan zeigte, dass diese Reaktionen zwischen Null und 550 °C bei 1,013 bar thermodynamisch begünstigt sind. Publikationen in diesem Forschungsbereich beschäftigen sich hauptsächlich mit der experimentellen Durchführung der Hydrierung von Magnesium-, Kalzium- und Kalzium-/Übergangsmetallcarbonaten. Zusätzlich wurden Daten zur Hydrierung von Nickel-, Kobalt-, Barium-, Lithium-, Natrium-, Kalium- und Strontiumcarbonat publiziert.

Eisen-, Magnesium-, Mangan- und Nickelcarbonat wurden thermogravimetrisch untersucht. Dabei zeigte sich, dass eine 50 volumsprozentige Wasserstoffatmosphäre, im Vergleich zur reinen Stickstoffatmosphäre, zu einer signifikanten Erniedrigung der Zersetzungstemperatur führt. Der Masseverlust war bei Eisen- und Nickelcarbonat deutlich höher als durch den Verlust von Kohlendioxid in einer Zersetzungsreaktion erklärbar. Dies könnte auf eine Reduzierung der carbonatischen Proben bis zum elementaren Metal hinweisen.

Die Aufheizexperimente im Reaktor zeigten, dass die Wärme nur im zentralen Teil der Reaktorröhre gleichmäßig verteilt ist. An den Randpositionen kommt es zu einem signifikanten Temperaturabfall. Magnesiumcarbonat wurde in Stickstoffatmosphäre bei 0,70 ± 0,03 bar Überdruck für 125 Minuten auf 459 ± 8 °C gehalten. Dabei wurde Kohlendioxid detektiert und der Masseverlust der Probe wies auf eine vollständige thermische Zersetzung zu Magnesiumoxid hin. Selbiges gilt für 20 volumsprozentige Wasserstoffatmosphäre, 130 Minuten Haltezeit, 442 ± 16 °C und 0,8 ± 0,2 bar Überdruck. Beim Erhitzen von Eisencarbonat auf 479 ± 12 °C für 150 Minuten bei 0,9 ± 0,2 bar Überdruck in Stickstoffatmosphäre wurde Kohlendioxid detektiert und der Masseverlust betrug 9,96 Gewichtsprozent. Wurde Eisencarbonat hingegen in 20 volumsprozentiger Wasserstoffatmosphäre für 200 Minuten bei 0,76 ± 0,05 bar Überdruck auf 473 ± 25 °C gehalten, konnte neben Kohlendioxid auch Kohlenmonoxid detektiert werden. Der Grund für die Kohlenmonoxid-Erzeugung könnte in einer umgekehrten Wassergas-Shift-Reaktion liegen. Weiters erhöhte sich der Masseverlust auf 39,81 Gewichtsprozent, was auf eine vollständige thermische Zersetzung hinweisen könnte.

Contents

1 Introduction

This Master's thesis deals with two interconnected subjects. Firstly, the commissioning of a Parr tubular reactor system and an analyzer rack. Secondly, the theoretical and experimental examination of the behavior of selected inorganic carbonates in nitrogen and hydrogen atmosphere. These subjects are interconnected by investigating the thermal decomposition and possible reactions of selected carbonates in thermogravimetric experiments and by heating experiments in the reactor system commissioned.

Inorganic carbonates are normally found in nature in minerals or saline lakes. They have been used by mankind over several thousand years, for instance in construction. Alkaline (earth) carbonates find the widest application considering the annual production, with calcium carbonate in the top position with several 1000 Mt/yr (2005) [1]. Section 2: *Inorganic carbonates* presents an overview of the natural occurrence of inorganic carbonates in the geosphere as well as preparation methods and applications.

As we are interested in the hydrogenation of inorganic carbonates, Section 3: *Literature review* gives an overview of publications on this subject. Section 4: *Thermodynamic considerations* discusses the chemical thermodynamics of the hydrogenation of selected carbonates to produce methane. Therefore, elemental chemical thermodynamics are recapitulated in Sections 4.1 through 4.6. Section 4.7: *Thermodynamic calculations* presents the calculation of the standard free reaction energy of selected carbonates.

Section 5: *Thermogravimetric experiments - Preliminary studies of the thermal stability of selected carbonates* introduces the experimental method and presents the experimental findings for siderite and magnesium, manganese, and nickel carbonate. Section 6: *Commissioning of the tubular reactor system* includes a description of the reactor system, the gas analysis equipment, and the commissioning experiments. The final section summarizes the findings of this Master's thesis and highlights possible future improvements of the experimental setup, applicability of advanced analytic techniques, and outlines possible further experiments.

2 Inorganic carbonates

2.1 Carbonic acid

Introduction of carbon dioxide into water leads to the formation of aqueous carbonic acid according to reaction equation (2.1). Most of the carbon dioxide does not react to form carbonic acid at standard conditions (STP) and remains as a solved, hydrated gas [2].

$$CO_2 + H_2O \leftrightharpoons H_2CO_3 \tag{2.1}$$

$$\left(\frac{c_{CO_2}}{c_{H_2CO_3}}\right)_{eq,STP} \approx 600 \tag{2.2}$$

The first dissociation constant K_{s1,H_2CO_3} for carbonic acid lies in the range of $1.3 * 10^{-4}$ [2] to $2.5 * 10^{-4}$ [3]. Most of the aqueous carbonic acid does not consist of the free acid but of hydrated carbon dioxide (see equation (2.2)). Hence, the first dissociation constant for dissolved carbon dioxide K^*_{s1,H_2CO_3} is three orders of magnitude lower than that of the free acid. K^*_{s1,H_2CO_3} lies in the range of $4.27 * 10^{-7}$ [3] to $4.45 * 10^{-7}$ [2].

Until the end of the 20th century the conventional wisdom was that free carbonic acid is too unstable to be isolated as a pure compound, as decomposition to carbon dioxide and water readily proceeds. At the turn of the 20th century special techniques were developed to isolate pure carbonic acid, and to verify its existence with analytic methods like NMR-spectroscopy [4]. The carbonic acid etherate $H_2CO_3 \cdot O(CH_3)_2$ can be synthesized from hydrogen chloride and soda in dimethly ether at -35 °C. Pure carbonic acid can be synthesized in high vacuum at -100 °C from potassium bicarbonate and hydrogen chloride [2].

2.2 Carbonic acid salts

Two classes of carbonic acid salts can be distinguished: hydrogen carbonates or bicarbonates with the monovalent HCO_3^- anion and carbonates with the bivalent CO_3^{2-} anion. Most of the elements that have stable monovalent and bivalent cations can form bicarbonates and carbonates. Except for sodium hydrogen carbonate, most hydrogen carbonates are readily soluble in water. Most carbonates are hardly or insoluble, except for alkaline earth metal carbonates [2].

The solubility of alkaline earth metal carbonates and the insolubility of most other carbonates opens an easy synthetic route to inorganic carbonates: the precipitation of insoluble salts with water-soluble alkaline metal carbonates like soda. This synthetic route is frequently used for the preparation of carbonates.

In the following sections 2.3 to 2.6 a review of the natural occurrence in the geosphere, preparation, and applications of inorganic carbonates is given. Only compounds found in

the widely used introductory textbooks *Lehrbuch der Anorganischen Chemie* [2] and *Anorganische Chemie* [3] and *Ullmann's encyclopedia of industrial chemistry: Online version* [5] in the version available by end of June 2013 are described.

2.3 Main group elements

2.3.1 Lithium

Lithium carbonate Li_2CO_3 occurs in the lithosphere as an ore companion and in saline lakes. It is mainly produced by precipitation of lithium brines with sodium carbonate Na_2CO_3. Lithium carbonate is the starting material for most lithium applications like in aluminium, glass, battery, and ceramics production. Pure lithium carbonate can be used as a drug for the treatment of manic-depressed patients [2, 3].

2.3.2 Sodium

Sodium carbonate (also called soda) Na_2CO_3 can be found in saline lakes and minerals like trona $Na_3(CO_3)(HCO_3) \cdot 2\,H_2O$. The two main ways for soda production are the Solvay-process with the sum reaction equation (2.3). A less expensive way for soda production is the mining of minerals like trona.

Solutions of sodium carbonate react basic according to reaction equation (2.4). Crystallization of the carbonate from a saturated aqueous solution gives sodium carbonates with different amounts of water depending on the temperature. Bellow 32.5 °C ten molecules of water of crystallization are bound producing the decahydrate $Na_2CO_3 \cdot 10\,H_2O$. Above 32.5 °C the heptahydrate $Na_2CO_3 \cdot 7\,H_2O$ is created. This compound loses six water molecules above 35.4 °C giving the monohydrate $Na_2CO_3 \cdot H_2O$. The monohydrate loses one molecule of water above 107 °C giving water free sodium carbonate.

$$2NaCl + CaCO_3 \rightleftharpoons Na_2CO_3 + CaCl_2 \tag{2.3}$$

$$CO_3^{2-} + H_2O \rightleftharpoons HCO_3^- + OH^- \tag{2.4}$$

Soda and sodium hydroxide are the most important bases used in industry. Soda is used at a 50 Mt/yr scale. The glass industry needs 40-50 % of the world soda production. Other applications for soda are found in chemical industry, detergent production, and pulp and paper industry [2, 3].

2.3.3 Potassium

There are no potassium carbonate K_2CO_3 containing ores known that would be worth mining. Potassium is found in diverse other ores like silicates and sulfates. Potassium carbonate is also called potash as it was historically produced by treating wood ash with water in a pot.

$$2KOH + CO_2 \rightleftharpoons K_2CO_3 + H_2O \tag{2.5}$$

Potash cannot be produced from potassium chloride in a process like the Solvay-process used for sodium. This is because of the higher solubility of potassium bicarbonate com-

pared to sodium bicarbonate. Therefore, it is produced from electrolytically produced potassium hydroxide and carbon dioxide (see reaction equation (2.5)). Other sources for potash are waste products like wood ash and treacle residues among others. Potassium carbonate is mainly used in soft soap and valuable glass production [2, 3].

2.3.4 Rubidium, Cesium, Francium

Rubidium and cesium are naturally found together in low concentrations accompanying sodium and potassium containing ores. Like the other alkaline metals, they are also found in saline lakes. All known francium isotopes are radioactive and can only be found in traces in the lithosphere. One possibility to produce rubidium carbonate Rb_2CO_3 is the thermal oxidation of dirubidium zinc hexacyanoferrate [6]. Cesium carbonate Cs_2CO_3 can be synthesized by thermal decomposition of cesium oxalate or reacting carbon dioxide with cesium hydroxide [7].

Due to scarce exploitable rubidium resources there are only few industrial and commercial applications at a two ton scale per year. Rubidium compounds are used as drugs and as parts of solid state lasers among other special applications [6]. Cesium salts find various special applications at a 20 ton scale per year [8]. Cesium carbonate can, for example, be used as a base catalyst in organic synthesis [9].

2.3.5 Beryllium

Beryllium carbonate $BeCO_3$ is hardly found in minerals. Beryllium is mainly found in the mineral beryl, an aluminosilicate, which is also the main source for the element. Precipitation of soluble beryllium salts like beryllium sulfate or chloride with aqueous alkaline metal carbonates produces basic beryllium carbonate $BeCO_3 \cdot nH_2O$ (n =2-5).

Beryllium carbonate is easily decomposed to beryllium oxide and carbon dioxide. This compound is therefore only stable in carbon dioxide atmosphere. It hydrolyzes in aqueous solution to form $[Be(H_2O)_4]^{2+}$ ions. Due to the toxicity of beryllium salts, they are hardly commerically used [2, 3].

2.3.6 Magnesium

Magnesium carbonate $MgCO_3$ is found in the lithosphere as magnesite $MgCO_3$ and dolomite $CaMg(CO_3)_2$ like in the Southern Alps - the Dolomites. Mining of magnesite is one of the main resources for magnesium carbonate.

The formation of magnesium carbonate in aqueous solutions can only be performed with abundant Mg^{2+} ions and excess free carbonic acid. Otherwise, basic magnesium carbonate $Mg(OH)_2 \cdot 4\,MgCO_3 \cdot 4\,H_2O$ is formed.

Magnesium carbonate is produced worldwide in megatons as a filling and insulation material. Basic magnesium carbonate is used as ‘magnesia alba’ in medicine as a neutralization agent for abundant gastric acid (e.g. patients with heartburn) and for the production of diverse powders in pharmaceutical applications among various other applications [2, 3].

2.3.7 Calcium

Calcium carbonate $CaCO_3$ occurs in the lithosphere as calcite $CaCO_3$ and dolomite $CaMg(CO_3)_2$. Mining of those minerals is the main resource for calcium carbonate. There exist three different naturally occurring crystal structures of calcium carbonate: calcite, aragonite and vaterite. In calcite the central Ca^{2+}-ion is coordinated by six oxygen atoms whereas in aragonite nine oxygen atoms coordinate the central Ca^{2+}-ion. For special applications, precipitated calcium carbonate (PCC) is produced by the introduction of carbon dioxide into an aqueous calcium hydroxide suspension.

$$CaCO_3 \rightleftharpoons CaO + CO_2 \qquad \Delta_R H^{\ominus} = +178.5 kJ/mol \tag{2.6}$$

Calcination (see reaction equation (2.6)) is an industrially widely applied process for caustic lime production. Caustic lime is a starting material for the building and fertilizer industry, produced in hundreds of megatons per year. Other applications for calcium carbonate are glass production and use as a filling material [2, 3].

2.3.8 Strontium

Strontium carbonate $SrCO_3$ is found in the naturally occurring mineral strontianite. Ores containing this mineral are the main source for elemental strontium and strontium carbonate. Strontium carbonate is produced at a kiloton scale per year. It is used for the production of television sets and produces the red color of Bengal firework [2, 3].

2.3.9 Barium

Barium carbonate $BaCO_3$ is found in the lithosphere as witherite. Barium carbonate is mined from natural deposits and also produced by precipitation of barium sulfide solutions with carbon dioxide or sodium carbonate. Barium carbonate is produced at a kiloton scale per year. It is used for the production of ceramics, special glasses, and for some other special applications [2, 3].

2.3.10 Lead

Lead carbonate $PbCO_3$ is found in the lithosphere as cerussite. It can be produced by introduction of carbon dioxide into an aqueous lead acetate solution, giving the carbonate $PbCO_3$ in cold conditions and basic lead carbonates like $2\,PbCO_3{\cdot}Pb(OH)_2$ as a precipitate in warm conditions. Basic lead carbonate, also called 'white lead', is used as a color because of its opacity. Nevertheless, it is harmful to human health [2, 3].

2.3.11 Aluminum

Basic aluminum carbonate is found in the mineral dawnsonite $NaAl(CO_3)(OH)_2$. The dawnsonite-like compound ammonium aluminum carbonate hydroxide (AACH) can be prepared relatively easily [10]. The products of thermal treatment of AACH, mainly aluminum oxides, have gained some interest lately. They have interesting properties such as high surface area, chemical, and thermal stability [11]. Nevertheless, basic aluminum carbonate is only used in special applications.

2.4 Transition metals

2.4.1 Manganese

Manganese is found in the lithosphere nearly as frequently as carbon or phosphorus. Manganese carbonate $MnCO_3$ is found in the mineral rhodocrosite and as an ore companion of iron [2].

Manganese carbonate can be synthesized by precipitation of an aqueous manganese sulfate solution with soda or ammonium bicarbonate. This procedure normally gives basic manganese carbonate $xMnCO_3 \cdot yMn(OH)_z$ [3]. Manganese carbonate is used as a fertilizer, for the production of elemental manganese by electrolysis, or for the production of other manganese compounds [2].

2.4.2 Iron

Iron carbonate $FeCO_3$ is found in the lithosphere as siderite, for example at the Erzberg in Styria. This ore is mined and used for the production of elemental iron in blast furnaces.

Precipitation of iron(II)-solutions with alkaline metal carbonates to yield iron carbonate must be done in the absence of oxygen. In an oxygen containing atmosphere, iron carbonate can be oxidized to yield iron hydroxide $Fe(OH)_3$ (see reaction equation (2.7)). Iron(III)-carbonate $Fe_2(CO_3)_3$ is not stable and decomposes according to reaction equation (2.8) [2].

$$4FeCO_3 + 6H_2O + O_2 \rightleftharpoons 4Fe(OH)_3 + 4CO_2 \tag{2.7}$$

$$Fe_2(CO_3)_3 \rightleftharpoons Fe_2O_3 + 3CO_2 \tag{2.8}$$

2.4.3 Cobalt

Cobalt is found in diverse forms in the lithosphere, often as an ore companion. Nevertheless, no major cobalt carbonate $CoCO_3$ containing ore is known. Cobalt carbonate can be produced by precipitation of water soluble cobalt(II)salts with alkaline earth carbonates. This procedure is also used to separate cobalt from other metals found in ores, because of different solubilities depending on the precipitation conditions. Cobalt carbonate is mostly used as a precursor for the production of other cobalt compounds [12].

2.4.4 Nickel

Nickel is found in diverse forms in the lithosphere, but no nickel carbonate ores are known [2]. The industrially most important nickel carbonate is basic nickel carbonate $2\,NiCO_3 \cdot 3\,Ni(OH)_2 \cdot 4\,H_2O$ [3], normally produced by precipitation of aqueous nickel sulfate with sodium carbonate. Changes in temperature and compound concentration produce different compositions of the basic carbonate.

Basic nickel carbonate can be dehydrated to give anhydrous nickel carbonate or the hexahydrate $NiCO_3 \cdot 6\,H_2O$. Basic nickel carbonate is used in catalyst production, the manufacture of nickel pigments, and nickel electroplating baths. Heating of basic nickel carbonate to above 450 °C in air gives a reactive nickel oxide with a high specific surface area [13].

2.4.5 Copper

Copper carbonate $CuCO_3$ is found in the lithosphere as azurite $2\,CuCO_3 \cdot Cu(OH)_2$ (blue) and malachite $CuCO_3 \cdot Cu(OH)_2$ (green). Synthesis of pure copper carbonate can be done by treating azurite or malachite with carbon dioxide at 20 kbar and 500 °C. For technical applications basic copper carbonate of the general composition $xCuCO_3 \cdot yCu(OH)_2$ is used. It can be synthesized by precipitation of Cu^{2+}-solutions with alkaline carbonates [2]. Basic copper carbonates are used for the production of other copper salts, as hydrogenation catalysts, and in some other special applications [14].

2.4.6 Silver

Silver carbonate $Ag_2(CO_3)_3$ is not found in minerals. It can be precipitated from water using soluble silver compounds, for example silver sulfate Ag_2SO_4 or silver fluoride AgF, and alkaline metal carbonates like soda. The main application for the silver carbonate is the production of powdery silver [15].

2.4.7 Zinc

Zinc carbonate $ZnCO_3$ is found in the lithosphere as smithsonite. It can be synthesized by precipitation of the aqueous solution of zinc sulfate heptahydrate with alkaline carbonates giving basic zinc carbonate $xZnCO_3 \cdot yZn(OH)_2$ of varying compositions. Zinc carbonate and basic zinc carbonate are used in research [16] but no industrial applications are known [17].

2.4.8 Cadmium

Cadmium carbonate $CdCO_3$ is mostly found in the lithosphere as an ore companion of smithsonite (see section 2.4.7, p. 14) [2]. It can be synthesized by precipitation of the aqueous solution of cadmium sulfate with sodium carbonate, often giving basic cadmium carbonate of varying compositions $xCdCO_3 \cdot yCd(OH)_2$ with water difficult to remove. Cadmium carbonate is used as a starting material for the production of other cadmium salts and for the production of cadmium pigments [18].

2.5 Rare earth elements

According to the *International Union of Pure and Applied Chemistry* (IUPAC) [19] the rare earth elements comprise of scandium Sc, yttrium Y, and the lanthanoids: lanthanum La, cerium Ce, praseodymium Pr, neodymium Nd, promethium Pr, samarium Sm, europium Eu, gadolinium Gd, terbium Tb, dysprosium Dy, holmium Ho, erbium Er, thulium Tm, ytterbium Yb, and lutetium Lu.

The rare earth elements are not as rare in nature as their name suggests, with cerium as the relatively most abundant one. Only the radioactive promethium is relatively scarce. Scandium, yttrium, and lanthanum are nearly as frequently found as copper, lead, or cobalt. The most stable oxidation number for the rare earth elements is +III. Subsequently, they are normally found in this oxidation state in the lithosphere. The ionic radiuses of the trivalent rare earth elements are in the range of 89 pm for Sc^{3+} as the lower boundary

and 117 pm for La^{3+} as the upper boundary. Because of this relatively small radius range, the rare earth elements are normally found together in ores. There exists only one known mineral containing considerable amounts of scandium alone, i.e. thortveitite $Sc_2Si_2O_7$. As the rare earth ores contain at least two of the rare earth elements, a separation process is needed to get hold of the pure elements. Therefore, fractional crystallization, fractional extraction, and fractional precipitation techniques are used among others [2].

The carbonates of scandium, yttrium, and lanthanum $M_2(CO_3)_3$ can be synthesized by solving the hydroxides $M(OH)_3$ in carbonic acid and evaporating the solvent. However, there are no major applications for these carbonates of the third group elements [2, 3]. The carbonates of the other rare earth elements $(RE)_2(CO_3)_3$ can be synthesized by precipitation of aqueous solutions of the trivalent sulfate or halide salts with sodium bicarbonate [2]. Rare earth elements and their compounds find various applications in industry, metallurgy, and as catalysts. The carbonates are mainly used in preparative and analytical chemistry [20].

2.6 Actinoids

According to the *International Union of Pure and Applied Chemistry* (IUPAC) [19] the actinoids comprise of actinium Ac, thorium Th, protactinium Pa, uranium U, neptunium Np, plutonium Pu, americium Am, curium Cm, berkelium Bk, californium Cf, einsteinium Es, fermium Fm, mendelevium Md, nobelium No, and lawrencium Lr.

Actinium, thorium, protactinium, uranium, and traces of neptunium and plutonium are found in nature. There are no carbonates of these elements found in the lithosphere. The elements with atomic numbers greater than 95 (americium) can only be produced by radio-chemical techniques and are radioactive. The trivalent and quadrivalent actinoid cations can form, mostly basic, carbonates. These carbonates are normally water soluble, except for plutonium carbonate $Pu(CO_3)_4^{4-}$. These compounds are primarily of scientific interest and have no commercial or industrial application [2].

3 Literature review

3.1 Reller et al. 1987: "Formation of organic carbon compounds from metal carbonates"

Reller et al. [21] investigated the behavior of magnesite $MgCO_3$, calcite $CaCO_3$, dolomite $CaMg(CO_3)_2$, and mixed carbonates in hydrogen atmosphere. The mixed carbonates investigated were prepared by co-precipitation of the respective nitrates of magnesium and calcium with 10 wt% of cobalt, nickel, or copper. The measurements were carried out in a thermo-microbalance combined with a mass spectrometer at a hydrogen pressure of 1 bar.

The heating of magnesite in hydrogen atmosphere produced magnesium oxide, even amounts of carbon monoxide and dioxide, and water. When calcite was treated the same way, carbon monoxide was the dominating carbon species with a ratio of carbon monoxide to dioxide of about 10:1. This is not only explainable by the (reverse) water-gas-shift reaction (see reaction equation (3.1)), but was interpreted as a reduction process different to the hydrogenation of magnesite. The product ratio for dolomite lay in between magnesite and calcite. For all three samples, the decomposition temperature decreased considerably - more than 150 °C - compared to the decomposition in non-reducing atmosphere. The oxides formed in the hydrogenation were investigated with electron microscopy. This investigation revealed the formation of conglomerates of magnesium and calcium oxide microcrystals with a diameter in the range of 10 to 20 nm.

$$CO + H_2O \rightleftharpoons CO_2 + H_2 \tag{3.1}$$

Co-precipitates with 10 wt% of the transition metals copper, nickel, and cobalt revealed a further reduction of the decomposition temperature in hydrogen atmosphere. The addition of these transition metals resulted in a reduction of the decomposition temperature in the range of 200 to 400 °C compared to the decomposition of the pure carbonates in nitrogen atmosphere. Furthermore, the transition metals had an influence on the gaseous products. The use of copper led to the detection of mixtures of carbon monoxide and dioxide. Doping with cobalt produced mostly methane, some carbon monoxide, and low concentrations of carbon dioxide. In the case of magnesium and calcium carbonate co-precipitated with ten percent nickel, the main product was methane. An investigation of the solid reaction product with electron microscopy and X-ray diffraction showed the formation of that microcrystalline oxides and elemental transition metals.

Hence, Reller et al. [21] concluded that a hydrogen atmosphere decreases the degradation temperature. This decrease is further enhanced by addition of the transition metals cobalt, copper, and nickel. The degradation products depend on the transition metal used. This finding indicates that different degradation mechanisms proceed. At the end of the

article they mention that "[t]he fact that the solid products [...] act as an effective CO_2-trapping system, renders these systems interesting with respect to the problems arising from the increasing atmospheric CO_2 concentration." [21, p. 529]

3.2 Padeste et al. 1990: "The influence of transition metals on the thermal decomposition of calcium carbonate in hydrogen"

Padeste et al. [22] reported the thermal decomposition behavior of calcium carbonate co-precipitated with transition metals. The transition metals investigated were iron, nickel, cobalt, copper, ruthenium, rhodium, palladium, and silver. Solids were analyzed by X-ray diffraction. Gaseous reactants and products were analyzed with a combined thermogravimetry/mass spectrometry unit.

The structural analysis showed that the bivalent cations of iron, copper, nickel, cobalt, and the trivalent rhodium cation formed calcite-like co-precipitates with calcium carbonate. Bivalent palladium and silver, on the other hand, formed vaterite-like co-precipitates. In the case of ruthenium, a mixture of vaterite and traces of calcite were found in the co-precipitate. Below 327-427 °C transition metal carbonate decomposition and reduction occurred with water as one of the reaction products. Padeste et al. [22] suggested four possible reasons:

1. Loss of co-precipitated water
2. Decomposition of hydroxides to oxides
3. Reduction of evolved carbon dioxide to either carbon monoxide or methane
4. Reduction of the metal oxide with hydrogen

The experimental setup did not allow to distinguish between the loss of co-precipitated water, the decomposition of hydroxides to oxides, and the reduction of metal oxides with hydrogen. Carbon monoxide formation was not observed and methane was only produced from nickel and cobalt co-precipitates.

Above 327-427 °C calcium carbonate decomposition and reduction took place. Three possible reactions were further discussed from a thermodynamic and kinetic point of view: carbon dioxide (reaction equation (3.2)), carbon monoxide (reaction equation (3.3)), and methane formation (reaction equation (3.4)).

$$CaCO_3 \rightleftharpoons CaO + CO_2 \tag{3.2}$$

$$CaCO_3 + H_2 \rightleftharpoons CaO + CO + H_2O \tag{3.3}$$

$$CaCO_3 + 4H_2 \rightleftharpoons CaO + CH_4 + 2H_2O \tag{3.4}$$

When hydrogen was present most of the carbon dioxide was reduced to either carbon monoxide and/or methane. At lower decomposition temperatures mostly methane was produced, at higher decomposition temperatures carbon monoxide predominated. Iron, copper, and silver co-precipitates showed a minor influence on the thermal decomposition behavior in hydrogen. The decomposition temperature ranged from 457 to 607 °C with

carbon monoxide as the main product. Cobalt and palladium showed a medium influence. The decomposition temperature ranged from 407 to 577 °C with a methane yield in the range of 20 to 70 %. Ruthenium, rhodium, and nickel showed the greatest influence. The decomposition temperature ranged from 347 to 507 °C with methane as the main product.

The equilibrium constants for the reactions (3.2)-(3.4) were given in equations (3.5)-(3.7). The activity a of a solid x was abbreviated as a_x and the partial pressure p of compound x was abbreviated as p_x.

$$K_{Ca/CO_2} = \frac{a_{\mathrm{CaO}} \cdot p_{\mathrm{CO_2}}}{a_{\mathrm{CaCO_3}}} \tag{3.5}$$

$$K_{Ca/CO} = \frac{a_{\mathrm{CaO}} \cdot p_{CO} \cdot p_{\mathrm{H_2O}}}{a_{\mathrm{CaCO_3}} \cdot p_{H_2}} \tag{3.6}$$

$$K_{Ca/CH_4} = \frac{a_{\mathrm{CaO}} \cdot p_{CH_4} \cdot p_{\mathrm{H_2O}}^2}{a_{\mathrm{CaCO_3}} \cdot p_{H_2}^4} \tag{3.7}$$

The activity of the solids was assumed to equal one. All reaction were started with carbonates and pure hydrogen. Hence, by applying the stoichiometry of reactions (3.3) and (3.4) and using the equilibrium constants, the equilibrium partial pressure of carbon monoxide and methane could be calculated with equations (3.8) and (3.9).

$$p_{CO} = \sqrt{K_{Ca/CO} \cdot p_{H_2}} \tag{3.8}$$

$$p_{CH_4} = \sqrt[3]{\frac{K_{Ca/CH_4} \cdot p_{H_2}^4}{4}} \tag{3.9}$$

Padeste et al. [22] used tabulated reaction enthalpies to calculate the equlibrium constants. Their thermodynamic calculations led to the following conclusions: Reaction (3.3) should proceed at slightly lower temperatures than reaction (3.2); the formation of methane according to reaction equation (3.4) should be possible at significantly lower temperatures than the non-reductive decomposition (3.2) and the formation of carbon monoxide (3.3). However, experiments showed that methane and carbon monoxide formation are kinetically hindered. This hindrance could be partly overcome with internal catalysts produced during the reaction. Nickel, ruthenium, and rhodium showed a higher catalytic activity than cobalt and palladium.

3.3 Padeste et al. 1991: "The thermal behaviour of pure and nickel doped hydromagnesite in different atmospheres"

Padeste et al. [23] investigated the decomposition of the basic magnesium carbonate hydromagnesite $\mathrm{Mg_5(OH)_2(CO_3)_4 \cdot 4\,H_2O}$ in nitrogen and carbon dioxide atmosphere. In separate experiments they investigated the decomposition of nickel-doped hydromagnesite in nitrogen and hydrogen atmosphere. Measurements were carried out in a combined thermogravimetry (TG)/differential thermal analysis (DTA) and TG/mass spectrometry apparatus at normal pressure or under vacuum conditions ($< 10^{-5}$ torr) with 8.2 mg sample weight and 30 ml/min gas flow. Solids were analyzed with X-ray diffraction and electron microscopy.

The TG/DTA curves for the decomposition of hydromagnesite in nitrogen were analyzed and interpreted to correspond to reactions (3.10) and (3.11). The run of the TG/DTA curve changed when carbon dioxide was used as the atmospheric gas. Therefore, Padeste et al. [23] suggest that instead of reaction (3.11) two separate reactions (3.12) and (3.13) took place. The crystallization of magnesium carbonate (3.12) at 517 °C is strongly exothermic, all other reactions (3.10), (3.11), (3.12) are endothermic.

$$Mg_5(OH)_2(CO_3)_4 \cdot 4\,H_2O \rightleftharpoons Mg_5(OH)_2(CO_3)_4 + 4H_2O \tag{3.10}$$

$$Mg_5(OH)_2(CO_3)_4 \rightleftharpoons 5MgO + H_2O + 4CO_2 \tag{3.11}$$

$$Mg_5(OH)_2(CO_3)_4 \rightleftharpoons MgO + 4MgCO_3 + H_2O \tag{3.12}$$

$$MgCO_3 \rightleftharpoons 4MgO + 4CO_2 \tag{3.13}$$

Nickel-doped hydromagnesite was produced by co-precipitation of the respective nitrates with sodium carbonate. However, X-ray diffraction analysis did not allow to decide whether nickel was built into the hydromagnesite lattice or not. Regarding the decomposition behavior in carbon dioxide atmosphere, no major changes were noticed compared to pure hydromagnesite. When hydrogen was used as the atmospheric gas, the TG/DTA curves showed that carbon dioxide and hydroxide water got lost in one single, exothermic step. Mass spectrometry showed that instead of carbon dioxide methane was the major gaseous product. Hence, instead of simple decomposition the strongly exothermic methanation reaction (3.14) occured.

$$CO_2 + 4\,H_2 \rightleftharpoons CH_4 + 2H_2O \tag{3.14}$$

3.4 Reller et al. 1991: "Thermochemical reactivity of metal carbonates"

Reller et al. [24] investigated the influence of temperature, gas atmosphere, and type of energy on the thermal decomposition of alkaline earth metal and transition metal carbonates. Experiments were conducted with a combined thermogravimetry/mass spectrometry unit. Solids were analyzed with scanning electron microscopy. The heating rate was set to 10 °C/min, the hydrogen and nitrogen flow was kept at 30 ml/min, and the amount of sample was approx. 15 mg.

The thermal decomposition of strontium, calcium, and magnesium carbonate showed that the decomposition temperature increases with the atomic mass of the cation of the alkaline earth metal carbonate. This finding is also true for non-reducing and reducing atmosphere. A reducing hydrogen atmosphere significantly lowered the decomposition temperature. Mass spectrometry showed that hydrogen reacts with carbon dioxide to carbon monoxide and water in a reverse water-gas-shift reaction (3.1). Morphological investigations indicated that decomposition in nitrogen causes a greater destruction of the solid crystals than decomposition in hydrogen. Reller et al. [24] assume that this is due to easier diffusion of hydrogen into the solid and diffusion of carbon monoxide and water out than diffusion of carbon dioxide into the crystal carbonate network.

Transition metal carbonates are subject to the general redox reaction (3.15) (sic!) (M ... transition metal) during thermal decomposition. Hydrogen atmosphere in thermal

decomposition of transition metal carbonates facilitates the formation of reduced carbon species like methane. Reller et al. [24] explain this finding by the formation of catalytically active transition metal species formed during the thermal degradation.

$$MCO_3 \rightleftharpoons MO_{1+x} + (1-x)CO_2 + xCO \quad (sic!) \tag{3.15}$$

Mixed calcium carbonate co-precipitated with nickel, ruthenium, and rhodium lowered the decomposition temperature around 200 °C compared to pure calcium carbonate. Theoretically, mixed transition/alkaline earth metal carbonates could be reduced to C_xH_y and $C_xH_yO_z$ species in hydrogen atmosphere. At a pressure of 1.1013 bar methane could be produced. $C_xH_yO_z$ species, on the other hand, could not be detected.

With reference to their earlier publication [21] Reller et al. [24] state that mixed transition metal alkaline earth metal carbonates such as nickel-calcium carbonate can undergo decarbonization/recarbonization cycles. Such a cycle could open a possibility to trap carbon dioxide and convert it to reduced carbon species like methane. Nickel-calcium carbonates could also be used as catalysts for methane production from carbon dioxide/hydrogen gas mixtures.

Experiments on the impact of UV radiation instead of thermal energy did not show conclusive results. This was ascribed to changing absorption behavior of the samples used and the limitation of the radiation to the surface area of the samples.

3.5 Tsuneto et al. 1992: "Hydrogenation of solid state carbonates"

Tsuneto et al. [25] reported the reduction of lithium, sodium, potassium, basic magnesium, calcium, barium, basic nickel, and cobalt carbonate with hydrogen at atmospheric pressure. The reactions were carried out with powders of the respective carbonate in a fixed bed flow reactor. Products were analyzed by gas chromatography (GC). All reactions were carried out with 2.00 g of the carbonate and 40 mg of catalyst powder if a catalyst was used. The gas flow rate was 4.8 ml/min for hydrogen and 4.8 ml/min for helium.

Table 3.1 (p. 21) shows the results of the study. The reduction of nickel and cobalt carbonate was carried out without catalyst. Entries one and two of Table 3.1 show that the temperature of 200 °C was high enough to decompose basic nickel carbonate and copper carbonate to the respective oxides and carbon dioxide. Tsuneto et al. [25] observed an induction period for the formation of methane. X-ray diffraction analysis of the solids confirmed the formation of metallic cobalt and nickel particles during the induction period. They concluded that metallic nickel and cobalt would work as a catalyst for methane formation. At temperatures above 250 °C the formation of carbon dioxide and methane proceeded explosively.

The reduction of lithium, sodium, potassium, basic magnesium, calcium, and barium carbonate was carried out with 20 nm nickel powder as a catalyst. The products of the reactions carried out are shown in entries three to seven in Table 3.1.

The reduction of calcium carbonate was further examined. Entries eight to ten in Table 3.1 show that the production of methane increases with temperature. Entries eleven to 15 in Table 3.1 show that the influence of the catalyst powder on methane yield can

Table 3.1: Reduction of several carbonates, adapted from Tsuneto et al. 1992 [25]

Nr.	Carbonate	Cat.	T [°C]	CO_2[1] [μmol/h]	CH_4[1] [μmol/h]	CtM[2] [%/h]
1	$NiCO_3 \cdot Ni(OH)_2 \cdot 4\,H_2O$	-	200	770	72	1.02
2	$CoCO_3$	-	200	13	97	0.577
3	Li_2CO_3	Ni	400	nd	1.3	0.005
4	Na_2CO_3	Ni	400	nd	2.5	0.013
5	K_2CO_3	Ni	400	trace (< 2)	1.8	0.012
6	$4\,MgCO_3 \cdot Mg(OH)_2 \cdot 5\,H_2O$	Ni	300	290	1600	38.9
7	$BaCO_3$	Ni	400	nd	1.8	0.018
8	$CaCO_3$	Ni	200	nd	3.7	0.019
9	$CaCO_3$	Ni	300	nd	8.5	0.043
10	$CaCO_3$	Ni	400	nd	95	0.475
11	$CaCO_3$	Fe	400	nd	6.4	0.032
12	$CaCO_3$	Co	400	nd	45	0.225
13	$CaCO_3$	Pd black	400	nd	0.7	0.004
14	$CaCO_3$	Pt black	400	nd	26	0.130
15	$CaCO_3$	Cu	400	nd	2.4	0.012
16	$CaCO_3$	-	400	nd	nd	-
17[3]	$CaCO_3$	Ni	400	nd	nd	-

[1] GC-analysis after 55 hours for entry 1, after 7 hours for entry 2, and 0.5-1 hours for all other entries
[2] Column added by the author of this thesis
[3] Without hydrogen

be ordered in the following sequence: Ni > Co > Pt > Fe > Cu > Pd. The control experiments showed that without any catalyst (entry 16) and without hydrogen (entry 17) neither methane nor carbon dioxide was formed. The reaction residue consisted of calcium oxide and calcium hydroxide. This was confirmed by X-ray diffraction analysis. In the nickel-catalyzed hydrogenation at 400 °C 95 % of the calcium carbonate was converted to methane after 15 days. Tsuneto et al. [25] suggest that methane is directly produced at the solid/gas interface and not via carbon dioxide.

The GC-analysis of the gas produced in the hydrogenation reactions was performed 55 hours after the reaction started for basic nickel carbonate and after seven hours for cobalt carbonate. The GC-analysis for all other reactions was performed 0.5 to 1 hour after the reaction started. It is unclear how 'the start of a reaction' was determined. In addition, the unit of methane and carbon dioxide in Table 3.1 is [μmol/h] in the original paper. There is no statement that the GC-analysis was carried out neither continuously nor more than once.

However, to estimate the reaction rate, the hourly conversion CtM [%/h] of the respective carbonate to methane was calculated by the author of this Master's thesis using equation (3.16). The results of the calculations were added to Table 3.1.

$$CtM = \left(1 - \frac{n_{0,carb} - \dot{n}_{CH4}}{n_{0,carb}}\right) \cdot 100 \quad \left[\frac{\%}{h}\right] \tag{3.16}$$

The conversion rate CtM is relatively small for the uncatalyzed reaction (1.02 % for basic nickel carbonate, and 0.58 % for cobalt carbonate). In comparison to all other hydrogenations examined, only the nickel catalyzed hydrogenation of basic magnesium carbonate (entry six in Table 3.1) showed a relatively high conversion rate of 38.9 [%/h].

Tsuneto et al. [25] were able to show that the hydrogenation of basic nickel carbonate and cobalt carbonate is possible without a catalyst. Catalysis facilitated the hydrogenation of lithium, sodium, potassium, basic magensium, calcium, and barium carbonates. In addition, the nickel-catalyzed hydrogenation of basic magnesium carbonate produced considerable amounts of methane at 300 °C.

3.6 Yoshida et al. 1999: "Methane formation by metal-catalyzed hydrogenation of solid calcium carbonate"

Yoshida et al. [26] studied the kinetics of the hydrogenation of pure calcium carbonate, calcium carbonate mixed with 5 wt% palladium, and calcium carbonate mixed with 5 wt% iridium. The experimental studies were carried out in two apparatuses: a Cahn electrobalance with a reaction volume of 3.620 ml and a closed circulation apparatus with a reaction volume of 275 ml. Product analysis was performed with gas chromatography and X-ray diffraction.

Temperature-programmed hydrogenation (TPH) in the temperature range of 325-725 °C was used to compare the catalyzed and uncatalyzed hydrogenation of calcium carbonate with the thermal decomposition of calcium carbonate. The experiments showed that addition of catalysts shifts the peak of the TPH-curve from about 625 °C for pure calcium carbonate to about 525 °C for calcium carbonate with 5 wt% palladium and roughly 475 °C for calcium carbonate with 5 wt% iridium. The peak of the thermal decomposition of calcium carbonate was detected at about 690 °C. Hence, the peaks of the TPH-curves of pure calcium carbonate and calcium carbonate mixed with 5 wt% palladium and iridium, respectively, lie bellow the peak of the thermal decomposition. Therefore, the authors concluded that the "[...] hydrogenation reaction is initiated by a direct interaction of $CaCO_3$ and spilt-over H species." [26, p. 120]

Isothermal hydrogenation of varying amounts of pure calcium carbonate at 475 °C and 133 mbar was used to conduct kinetic studies. The initial rate for carbon monoxide formation was the same for varying calcium carbonate amounts. Therefore, Yoshida et al. [26] concluded that carbon monoxide is formed according to reaction equations (3.17) and a reverse water-gas-shift reaction (3.18).

$$CaCO_3 \rightleftharpoons CaO + CO_2 \tag{3.17}$$

$$CO_2 + H_2 \rightleftharpoons CO + H_2O \tag{3.18}$$

$$CaCO_3 + 4H_2 \rightleftharpoons CaO + CH_4 + 2H_2O \tag{3.19}$$

The isothermal palladium- and irdium-catalyzed hydrogenation according to reaction equation (3.19) were investigated in the electrobalance and the closed-circuit apparatus. The reaction curves observed in both apparatuses showed a retardation with lower hydrogen pressure. However, the hydrogenation proceeded 2.7 times slower in the electrobalance. This phenomenon was attributed to adsorbed water vapor on the catalyst and/or reactant

surface.

Activation energies were established using Arrhenius plots. The activation energy for the carbon monoxide formation was calculated to be 236 kJ/mol and the activation energy for the decomposition of calcium carbonate was calculated to be 199 kJ/mol. The activation energy for the iridium-catalyzed hydrogenation of calcium carbonate accounted for 111 kJ/mol (closed-circuit apparatus) and 105 kJ/mol (electrobalance). The activation energy for the palladium-catalyzed hydrogenation of calcium carbonate was equal to 118 kJ/mol (closed-circuit apparatus). The activation energies for the metal-catalyzed hydrogenations were notably lower than the standard enthalpy of decomposition at 400 °C, namely 174 kJ/mol. Hence, the authors concluded that "[...] $CaCO_3$ directly interacts with H atoms spilt-over from metal surfaces in the first step of the reaction to form CH_4, at least under the conditions studied here (below 698 K)." [26, p. 121]

Yoshida et al. [26] also drew kinetic conclusions from their study. They observed an increasing reaction rate with hydrogen pressure. At sufficiently high hydrogen pressures the reaction rate reached a fixed value. They concluded that this is due to a kinetic transformation from slightly higher than first-order at low pressures to zero-order at high pressures. The initial rate v_0 of the carbon monoxide formation (see reaction equations (3.17) and (3.18)) and the hydrogenation (see reaction equation (3.19)) was calculated with equation (3.20), where P_{H_2} represents the hydrogen pressure and a, c, and n are constants. When n equals 1.5 the initial region of the reaction rates was described satisfactorily.

$$v_0 = \frac{P_{H_2}^n}{a + c\ P_{H_2}^n} \tag{3.20}$$

3.7 Rao et al. 2009: "Investigations of the conversion of inorganic carbonates to methane"

Rao et al. [27] investigated the hydrogenation of calcium carbonate, magnesium carbonate, and mixed calcium transition metal carbonates of the general composition $MCa(CO_3)_2$ and $M^1M^2Ca(CO_3)_3$. The transition metals M investigated were cobalt, nickel, and iron. The experiments were conducted at 550 °C during a reaction time of five hours. The experimental setup consisted of a stainless steel reactor tube (length: 30 cm, diameter 0.6 cm) packed with quartz wool mixed with 50 mg of the solid sample. The quartz wool was placed in the center of the reactor tube. Product analysis was performed with gas chromatography (TCD and FID detectors), mass spectrometry, X-ray diffraction, transmission electron microscopy, and Fourier transform infrared spectroscopy.

The main finding was that the thermal decomposition of the investigated carbonates $MCa(CO_3)_2$ and $M^1M^2Ca(CO_3)_3$ (with M = Co, Ni, or Fe and M^1M^2 = CoNi, NiFe, or FeO) in hydrogen atmosphere leads to the formation of a nano-particulate mixture of calcium oxide, elemental transition metal, and transition metal oxide. These nanoparticles seem to catalyze the methanation of carbon dioxide evolved during the thermal decomposition of carbonates. Therefore, Rao et al. [27] prepared these catalytic nanoparticles of the general composition M/MO/CaO (with M = Co, Ni, or Fe) separately by heating the mixed carbonate $MCa(CO_3)_2$ in hydrogen atmosphere to 550 °C for ten hours.

Table 3.2 (p. 24) shows the conversion level and the yield of carbon dioxide and methane

Table 3.2: Conversion and yield for 50 mg of mixed carbonates heated to 550 °C for 5 hours with 8 ml hydrogen per minute (adapted from Rao et al. 2009 [27], **Traces of C1-C3 hydrocarbons*)

Sample	Conversion [%]	Yield [% CH_4]	Yield [%CO_2]
$CoCa(CO_3)_2$	100	80	20
$NiCa(CO_3)_2$	81	100	0
$FeCa(CO_3)_2$	4	100*	0
$CoNiCa(CO_3)_3$	77	100	0
$NiFeCa(CO_3)_3$	16	100*	0
$FeCoCa(CO_3)_3$	76	100*	0

Table 3.3: Conversion and yield for 50 mg of mixed carbonates with catalysts heated to 550 °C for 5 hours (adapted from Rao et al. 2009 [27], **Traces of C1-C3 hydrocarbons*)

Sample	Hydrogen [mL/min]	Conversion [%]	Yield [% CH_4]	Yield [%CO_2]
$CoCa(CO_3)_2$ + Co/CaO/CoO	8	100	100	0
$CoCa(CO_3)_2$ + Co/CaO/CoO	2.5	100	60	40
$CoCa(CO_3)_2$ + Co/CaO/CoO	3.5	100	100	0
$NiCa(CO_3)_2$ + Ni/CaO	3.5	15	100	0
$FeCa(CO_3)_2$ + Fe/CaO/Fe3O4	8	87	70*	30
$CoNiCa(CO_3)_3$ + NiCo/CaO/CoO	3.5	100	100	0
$NiFeCa(CO_3)_3$ + NiFe/CaO	3.5	64	100*	0
$FeCoCa(CO_3)_3$ + FeCo/CaO/CoO	3.5	50	100*	0

for the hydrogenation of mixed carbonates $MCa(CO_3)_2$ and $M^1M^2Ca(CO_3)_3$ (with M = Co, Ni, or Fe and M^1M^2 = CoNi, NiFe, or FeO). Table 3.3 shows that by adding the above mentioned catalyst, the conversion level rises even for a lower hydrogen flow of 3.5 mL/min. There were also differences in the catalytic activity of the three metals tested. The conversion level of carbonate to methane and/or carbon dioxide increased in the order Co > Ni > Fe and CoNi > NiFe > FeCo. Table 3.4 (p. 25) shows how the catalysts can facilitate the hydrogenation of magnesite and calcite.

3.8 Rao et al. 2013: "Direct conversion of calcium carbonate to C1-C3 hydrocarbons"

In their latest publication concerning the conversion of calcium carbonate to hydrocarbons, Rao et al. [28] reported the formation of not only methane but also the higher hydrocarbons ethine, ethane, and propane. The starting material for the hydrogenation was not pure calcium carbonate $CaCO_3$ but a co-precipitate of calcium and iron carbonate $Ca_{1-y}Fe_yCO_3$ referred to as FeCaCO. Starting materials and products were characterized by gas chromatography, X-ray diffraction, transmission electron microscopy, and Mössbauer spectroscopy. The hydrogenation experiments were conducted in a continuous

Table 3.4: Conversion and yield for 50 mg of magnesite and calcite mixed with various catalyst heated to 550 °C for 5 hours at 3.5 mL hydrogen per minute for $CaCO_3$ and 8 mL hydrogen per minute for $MgCO_3$ (adapted from Rao et al. 2009 [27], **Traces of C1-C3 hydrocarbons*)

Sample	Conversion [%]	Yield [% CH_4]	Yield [% CO_2]
$MgCO_3$ + Co/CaO/CoO	100	100	0
$CaCO_3$ + Co/CaO/CoO	100	100	0
$CaCO_3$ + Ni/CaO	80	100	0
$CaCO_3$ + Fe/CaO/Fe3O4	18	100*	0
$CaCO_3$ + CoNi/CaO/CoO	34	65	35
$CaCO_3$ + NiFe/CaO	40	100*	0
$CaCO_3$ + CoFe/CaO/CoO	89	100*	0

Table 3.5: Product yield in hydrogenation experiments (400 °C, 2 hours), adapted from Rao et al. 2013 [28]

	Yield [%]					
$x_{Fe/Ca}$	CH_4	C_2H_4	C_2H_6	C_3H_8	CO	CO_2
0	0	0	0	0	0	5
0.1	1	2	2	0	1	7
0.5	2	3	5	0	2	12
2	2	3	2	1	8	17
3.5	4	5	3	1	7	34
5	5	7	4	4	6	21

flow, packed bed, stainless steel reactor at atmospheric pressure. Reaction temperatures ranged between 300 and 600 °C. The hydrogen flow was fixed at three ml/min and the reaction time was two hours.

The molar ratio $x_{Fe/Ca}$ of FeCaCO was varied over a range of zero to five. The hydrogenation was carried out at 400 °C and carbon monoxide, carbon dioxide, methane, ethine, ethane, and propane could be detected. Table 3.5 (p. 25) shows the gaseous products of the hydrogenation experiment depending on the molar ratio $x_{Fe/Ca}$ of FeCaCO. The yield of the detected products showed an increasing tendency with the augmentation of the molar ratios. However, the catalytic activity of iron expressed as the turnover number for hydrocarbons[1] had a maximum at a molar ratio of 0.1 and gradually decreased afterwards.

The decomposition products after two hours of heat treatment (referred to as FeCaD with $x_{Fe/Ca} = 0.5$ and $x_{Fe/Ca} = 5$) were further examined. The analysis showed that for $x_{Fe/Ca} = 0.5$ the mixed iron oxide Fe_3O_4 was formed, maybe by reduction of Fe_2O_3. For $x_{Fe/Ca} = 5$ diverse iron compounds could be identified, i.e. α−FeOOH, γ−Fe_2O_3, Fe_3O_4, α−Fe, Θ−Fe_3C, χ−Fe_5C_2, and $CaFe_2O_4$. Many of these iron forms are present in Fischer-Tropsch catalysts. Therefore, Rao et al. [28] concluded that the reaction mechanism of the hydrogenation of FeCaCO could be alike.

Rao et al. [28] state that the formation and adsorption of carbon monoxide is crucial

[1] number of moles of carbon in the carbonate converted to hydrocarbons by one mole of iron present in the respective carbonate

for the formation of hydrocarbons because only then it can react with hydrogen (which is also adsorbed on the surface) to produce hydrocarbons of the form RCH_2 with R = H, CH_2, or CH_3. Furthermore, with carbon monoxide, carbon dioxide, water, and hydrogen present a water-gas-shift reaction equilibrium is possible. This was confirmed by separate experiments when carbon monoxide and water were passed over FeCaD (with $x_{Fe/Ca} = 2$) at 400 °C. In this experiment carbon monoxide was converted into carbon dioxide according to the water-gas-shift reaction (3.1).

The temperature for carbon dioxide formation to start was observed to be at around 130 °C, whereas the carbon monoxide formation started at around 230 °C. Carbon monoxide was only produced when iron was present in the carbonate investigated, which suggests an active role of iron in carbon monoxide formation. Methane and the other hydrocarbons were produced at above 230 °C. In the same temperature range of 250 to 350 °C iron oxides can be reduced to $\alpha-Fe$. This element can therefore be actively involved in the formation of hydrocarbons. Furthermore, Fe_3O_4 present in FeCaD is an active water-gas-shift reaction catalyst. Rao et al. [28] concluded that elemental iron and iron oxide actively catalyze the formation of carbon monoxide, carbon dioxide, and the hydrocarbons methane, ethine, ethane, and propane.

Table 3.5 (p. 25) shows that carbon dioxide was the major product in all experiments. This suggests that the rate of decomposition of the carbonate to carbon dioxide is faster than the reduction of carbon dioxide to monoxide and/or hydrocarbons. The formation of the higher hydrocarbons ethine, ethane, and propane could be explained by the presence of $\chi-Fe_5C_2$, a compound known for its activity in C-C-coupling. Ethine was expected to be formed through $\beta-$elimination or rearrangements of C2-intermediates. The formation of ethine was expected to precede the formation of ethane and propane. The suggestion of Rao et al. [28] for the selective formation of C1-C3 hydrocarbons is that long-chain hydrocarbons would be cracked in a hydrogen-rich atmosphere and that the carbon monoxide to hydrogen ratio formed during the reaction is not suitable for the formation of long chain hydrocarbons.

3.9 Summary

Table 3.6 on page 27 summarizes the reaction apparatuses and analytical techniques used by Reller et al. [21, 24], Padeste et al. [22, 23], Tsuneto et al. [25], Yoshida et al. [26], and Rao et al. [27, 28]. The apparatuses used can be classified into two categories: balances and flow reactors. Gas chromatography was normally used for gas analysis and X-ray-diffraction and electron microscopy for solid state analysis.

Table 3.7 on page 28 shows which carbonates were investigated. The temperature, hydrogen pressure, and the use of a catalyst in the reaction are summarized. The focus of most publications in this field lies on the understanding and improvement of the reaction conditions for the hydrogenation of calcium carbonate [21, 22, 26–28]. The hydrogenation of magnesium carbonate and derivatives is discussed in [21, 23–25, 27].

The working group around Armin Reller, back then working at the University of Zürich, since 2009 professor at the University of Augsburg, published four papers on the thermal decomposition of carbonates [21–24]. Reller et al. 1987 [21] provide some insight into the reaction products and the influence of addition of 10 wt% cobalt, nickel, or copper on

Table 3.6: Summary of the reaction apparatuses and analytic techniques used in the literature reviewed

Apparatus	Analysis	Ref.	Year
Thermo-microbalance	MS, XRD, EM	[21]	1987
Thermo-microbalance	MS, XRD	[22]	1990
Thermo-microbalance	MS, XRD, EM	[23, 24]	1991
Fixed bed flow reactor	GC	[25]	1992
Electrobalance	GC, XRD	[26]	1999
Closed circulation apparatus	GC, XRD	[26]	1999
Tubular reactor	GC, XRD, TEM, FTIR	[27]	2009
Packed bed flow reactor	GC, XRD, TEM, Mössb. spec.	[28]	2013

calcium carbonate hydrogenation. Padeste et al. 1990 [22] investigated the thermal decomposition of calcium carbonate co-precipitated with iron, nickel, cobalt, copper, ruthenium, rhodium, palladium, and silver in hydrogen atmosphere. Padeste et al. 1991 [23] investigated the decompostion of hydromagensite and nickel-doped hydromagnesite in carbon dioxide, nitrogen, and hydrogen. Reller et al. 1991 [24] provide an overview of the work done by the group in the field of the thermochemical reactivity of metal carbonates up to then.

Tsuneto et al. [25] showed the feasibility of the hydrogenation of basic nickel and cobalt carbonate without catalyst and the catalytic hydrogenation of lithium, sodium, potassium, and barium carbonate. Yoshida et al. [26] present a kinetic study of the hydrogenation of calcium carbonate and the influence of the addition of 5 wt% palladium and iridium.

The working group of C. N. R. Rao at the Jawaharlal Nehru Centre for Advanced Scientific Research located in Bangalore, India, published two papers on the topic. The first paper of Rao et al. 2009 [27] is a study of the hydrogenation of calcium carbonate and mixed calcium-transition metal (cobalt, nickel, and iron) carbonates. Rao et. al 2013 [28] focus on the hydrogenation of co-precipitated iron-calcium carbonates.

Interestingly, the publications of Rao et al. [27, 28] refer to the work by Reller et al. [21, 24] and Padeste et al. [22, 23] but do not include references to the papers of Tsuneto et al. [25] and Yoshida et al. [26]. Neither Tsuneto et al. [25] nor Yoshida et al. [26] refer to the work done by Reller et al. [21, 24] and Padeste et al. [22, 23] although the four papers of Rellers' working group [21–24] were published before the work done by Tsuneto et al. [25] and Yoshida et al. [26].

Table 3.7: Summary of the carbonates and reaction conditions in hydrogenation experiments reported in the literature reviewed

Carbonate	T [°C]	P_{H2} [bar]	Catalyst	Ref.
$MgCO_3$	30-680	1	w/o	[21, 24]
	550	n/a	Co/CaO/CoO	[27]
$4\,MgCO_3 \cdot Mg(OH)_2 \cdot 5\,H_2O$	300	1.013	Ni	[25]
$Mg_5(OH)_2(CO_3)_4 \cdot 4\,H_2O$	30-680	1.013	w/o, Ni	[23]
$Co_{0.1}Mg_{0.9}CO_3$	30-680	1	Co	[21]
$Ni_{0.1}Mg_{0.9}CO_3$	30-680	1	Ni	[21]
$Cu_{0.1}Mg_{0.9}CO_3$	30-680	1	Cu	[21]
$CaMg(CO_3)_2$	30-680	1	w/o	[21]
$CaCO_3$	30-680	1	w/o	[21]
	30-720	1.013	Fe, Co, Pd, Ag, Cu	[22]
	30-720	1.013	Ni, Ru, Rh	[22, 24]
	200-400	1.013	Ni, Fe, Co, Pd, Pt, Cu	[25]
	325-725	n/a	Pd, Ir	[26]
	325-725	n/a	Pd, Ir	[26]
	550	n/a	Co/CaO/CoO	[27]
	550	n/a	Ni/CaO	[27]
	550	n/a	$Fe/CaO/Fe_3O_4$	[27]
	550	n/a	CoNi/CaO/CoO	[27]
	550	n/a	NiFe/CaO	[27]
	550	n/a	CoFe/CaO/CoO	[27]
$Co_{0.1}Ca_{0.9}CO_3$	30-680	1	Co	[21]
$CoCa(CO_3)_2$	550	n/a	w/o, Co/CaO/CoO	[27]
$CoNiCa(CO_3)_3$	550	n/a	w/o, NiCo/CaO/CoO	[27]
$Ni_{0.1}Ca_{0.9}CO_3$	30-680	1	Ni	[21]
$NiCa(CO_3)_2$	550	n/a	w/o, Ni/CaO	[27]
$NiFeCa(CO_3)_3$	550	n/a	w/o, NiFe/CaO	[27]
$Cu_{0.1}Ca_{0.9}CO_3$	30-680	1	Cu	[21]
$FeCa(CO_3)_2$	550	n/a	w/o, $Fe/CaO/Fe_3O_4$	[27]
$FeCoCa(CO_3)_3$	550	n/a	w/o, FeCo/CaO/CoO	[27]
$Ca_{1-y}Fe_yCO_3$	300-600	1.013	n/a	[28]
$NiCO_3 \cdot Ni(OH)_2 \cdot 4\,H_2O$	200	1.013	w/o	[25]
$CoCO_3$	200	1.013	w/o	[25]
$BaCO_3$	400	1.013	Ni	[25]
Li_2CO_3	400	1.013	Ni	[25]
Na_2CO_3	400	1.013	Ni	[25]
K_2CO_3	400	1.013	Ni	[25]
$SrCO_3$	30-720	1.013	w/o	[24]

4 Thermodynamic considerations

When talking about chemical equilibrium, the concept of the reaction coordinate ξ is useful. The reaction coordinate quantifies the conversion progress of a chemical reaction. The advantage of using the reaction coordinate is that it has the same value for all participating reaction partners [29]. As the reaction coordinate quantifies change in a system, a consistent way to define it (see equation (4.1)) is by using its change $d\xi$ [30]. A reaction coordinate of zero means that no products are formed, whereas a value near one means that nearly all reactants have been converted into products.

$$d\xi = \frac{dn_i}{\nu_i}, \qquad 0 \leq \xi \leq 1 \tag{4.1}$$

The stoichiometric coefficient ν is negative for reactants and positive for products. Hence, any reaction equation of i components R can be written as given in equation (4.2).

$$\begin{aligned} &\nu_a\ A + \nu_b\ B + ... \rightleftharpoons \nu_x\ X + \nu_y\ Y + ... \\ &\sum_i \nu_i R_i = 0 \end{aligned} \tag{4.2}$$

The most important state function used in chemical thermodynamics is the Gibbs free energy G. The definition of this state function is given in equation (4.3).

$$G = U + PV - TS = H - TS \tag{4.3}$$

At constant temperature and pressure the change of the Gibbs free energy can be calculated with equation (4.4).

$$dG = dU + PdV - TdS = VdP - SdT \tag{4.4}$$

The composition of a thermodynamic system can vary, for example, because of ongoing chemical reactions. The change of the system's composition is accounted for by the change of the chemical potential of the i components. Therefore, equation (4.4) is extended by the term $\mu_i dn_i$ [31].

$$dG = VdP - SdT + \sum_i \mu_i dn_i \tag{4.5}$$

4.1 The free reaction energy $\Delta_R G$

The free reaction energy $\Delta_R G$ for a given temperature and pressure can be defined by equation (4.6). In this representation Δ represents a derivative [30].

$$\Delta_R G = \left(\frac{dG}{d\xi}\right)_{P,T} \tag{4.6}$$

To link the definition of the free reaction energy given in equation (4.6) with the chemical potential, the change of the Gibbs free energy during a reaction is considered. The change of the Gibbs free energy is proportional to the difference in chemical potential between products and reactants times the change of the reaction coordinate.

$$dG = \sum_i \mu_i \cdot dn_i = \left(\sum_{Products} \mu - \sum_{Reactants} \mu\right) \cdot d\xi \tag{4.7}$$

Division of dG by dξ gives the definition of the free reaction energy. Hence, the free reaction energy can be interpreted as the difference between the chemical potentials of products and reactants [30].

$$\Delta_R G = \left(\frac{dG}{d\xi}\right)_{P,T} = \sum_{Products} \mu - \sum_{Reactants} \mu \tag{4.8}$$

4.2 Calculation of the standard free reaction energy

The standard free reaction energy $\Delta_R G^{\ominus}$ can be calculated with equation (4.9). The denomination 'standard' derives from the fact that $\Delta_R G^{\ominus}$ is normally given at 1 atm (1.1013 bar)[1] and a certain temperature. Moreover, the reactants are considered to be in their thermodynamically most stable form. The standard reaction enthalpy $\Delta_R H^{\ominus}$ and the standard reaction entropy $\Delta_R S^{\ominus}$ can be calculated likewise (see equations (4.10) and (4.11)) [29].

$$\Delta_R G^{\ominus} = \sum_{Products} \Delta_f G^{\ominus} - \sum_{Reactants} \Delta_f G^{\ominus} = \sum_i \nu_i \Delta_f G_i^{\ominus} \tag{4.9}$$

$$\Delta_R H^{\ominus} = \sum_i \nu_i \Delta_f H_i^{\ominus} \tag{4.10}$$

$$\Delta_R S^{\ominus} = \sum_i \nu_i \Delta_f S_i^{\ominus} \tag{4.11}$$

The relationship between standard free reaction energy, enthalpy, and entropy for a constant pressure is given in equation (4.12) [29].

$$\Delta_R G^{\ominus} = \Delta_R H^{\ominus} - T\Delta_R S^{\ominus} \tag{4.12}$$

There exist various publications on thermochemical data (like standard enthalpy, entropy, and Gibbs free energy) for a great amount of substances. Some of the data is summarized in handbooks [32, 33] and collections [34, 35].

[1] In some publications $\Delta_R G^{\ominus}$ refers to another pressure, mostly 1 bar

4.3 Chemical equilibrium

The free reaction energy for a general chemical reaction can be calculated with equation (4.13), where Q represents the reaction quotient defined in equation (4.14) [30].

$$\Delta_R G = \Delta_R G^{\ominus} + RT\ ln\ Q \tag{4.13}$$

$$Q := \prod_i a_i^{\nu_i} = \frac{\prod_{Products} a^{\nu}}{\prod_{Reactants} a^{\nu}} \tag{4.14}$$

A reaction system reaches equilibrium when the change of the free reaction energy $\Delta_R G$ reaches zero [36]. To emphasize equilibrium conditions the reaction quotient Q is replaced by the equilibrium constant K. As a result, the standard free reaction energy for a system in equilibrium can be calculated using the temperature T, the ideal gas constant R, and the equilibrium constant K (4.15) [30].

$$\Delta_R G_{equilibrium} = 0 \quad \Rightarrow \quad \Delta_R G^{\ominus} = -RT\ ln\ K \tag{4.15}$$

$$K := Q_{equilibrium} = \left(\prod_i a_i^{\nu_i}\right)_{equilibrium} \tag{4.16}$$

Additionally, if $\Delta_R G^{\ominus}$ is known for a specific temperature T, equation (4.17) can be used to calculate the equilibrium constant K.

$$\Delta_R G^{\ominus} = -RT \ln K \quad \Leftrightarrow \quad K = \exp\left(\frac{-\Delta_R G^{\ominus}}{RT}\right) \tag{4.17}$$

A chemical reaction proceeds towards the minimum of the Gibbs free energy. As long as $\Delta_R G$ is negative the formation of products proceeds voluntarily. Vice versa, for positive values of $\Delta_R G$ the reactant formation proceeds voluntarily. Table 4.1 shows that the value of the standard free reaction energy can be associated with the dominant species of a reaction at equilibrium [31].

Table 4.1: Composition of a reaction mixture at equilibrium, adapted from Smith 2005 [31]

	$\Delta_R G^{\ominus}$	K
negligible reactants	-50	$6 \cdot 10^{8}$
products dominate	-10	57
products equal reactants	0	1
reactants dominate	10	0.02
negligible products	50	$1.7 \cdot 10^{-9}$

4.4 Temperature dependency of the equilibrium constant K

Considering a system at constant pressure, the Gibbs-Helmholtz equation (4.18) can be derived from equation (4.3) using the definition of the entropy as the partial derivative of

the Gibbs free energy with respect to the temperature [31].

$$\left(\frac{\partial\frac{\Delta_R G^\ominus}{T}}{\partial T}\right)_P = -\frac{\Delta_R H^\ominus}{T^2} \tag{4.18}$$

Differentiation of equation (4.17) and replacing $\Delta G^\ominus$ gives the Van't Hoff isochore (4.19) [31].

$$\frac{d\ln K}{dT} = \frac{\Delta_R H^\ominus}{RT^2} \tag{4.19}$$

Integration of the Van't Hoff isochore makes the calculation of the equilibrium constant at two different temperatures possible [29].

$$\int_{K(T_1)}^{K(T_2)} d\ln K = \int_{T_1}^{T_2} \frac{\Delta_R H^\ominus}{RT^2} dT \tag{4.20}$$

If the enthalpy can be considered independent of temperature in the given temperature interval [T_1, T_2], integration gives equation (4.21).

$$\ln K(T_2) = \ln K(T_1) + \frac{\Delta_R H^\ominus}{R}\left(\frac{1}{T_1} - \frac{1}{T_2}\right) \tag{4.21}$$

Otherwise, the temperature dependency of the enthalpy has to be considered (see equation (4.22)). This can be done by using temperature-dependent functions for the specific heat capacity c_p (4.23) [29].

$$\Delta_R H^\ominus(T_2) = \Delta_R H^\ominus(T_1) + \int_{T_1}^{T_2} \Delta c_p \; dT \tag{4.22}$$

$$\Delta c_p = \sum_{Products} n \cdot c_p - \sum_{Reactants} n \cdot c_p \tag{4.23}$$

4.5 Pressure dependency of the equilibrium constant K

Considering a system at constant temperature, the equilibrium constant K_p is independent of the total pressure P.

$$K_p := K(T = const.) = \prod \left(\frac{p_i}{P^\ominus}\right)^{\nu_i} \tag{4.24}$$

$$\frac{\partial \ln K_p}{\partial p}(T = const.) = 0 \tag{4.25}$$

The reaction composition is linked to the equilibrium constant. To emphasize this consideration, the equilibrium constant K_x (4.26) regarding the mole fraction x_i of the i reactants and products is used.

$$K_x = \prod_i x_i^{\nu_i} \tag{4.26}$$

For an ideal gas, the partial pressure p_i is proportional to the mole fraction x_i times the total pressure P.

$$\frac{p_i}{P^{\ominus}} = x_i \cdot \frac{P}{P^{\ominus}} \tag{4.27}$$

Subsequently, the equilibrium constant K_x (4.26) regarding the mole fraction can be rewritten as given in equation (4.28). The change in moles of gaseous components is expressed by Δn, which can be expressed by equation (4.29).

$$K_x = K_p \cdot \left(\frac{P}{P^{\ominus}}\right)^{-\Delta n} \tag{4.28}$$

$$\Delta n = \sum_i \nu_i(gaseous) \tag{4.29}$$

Partial differentiation of equation (4.28), while considering that K_p is independent from temperature, shows the dependence (4.30) of the reaction composition of total pressure.

$$\frac{\partial \ln K_x}{\partial P} = -\frac{\Delta n}{P} \tag{4.30}$$

For an ideal gas this can be rewritten as demonstrated in equation (4.32).

$$p\Delta V = \Delta n RT \tag{4.31}$$

$$\frac{\partial \ln K_x}{\partial P} = -\frac{\Delta V}{RT} \tag{4.32}$$

Equation (4.32) is generally applicable to any reaction equilibrium when the equilibrium constant K_x (as defined in equation (4.26)) is used. The volume change ΔV generally represents the change of volume accompanying one mole of reaction [31].

4.6 Shifting the composition: Le Chatelier's Principle

Le Chatelier's Principle states that:

> "Perturbation of a system at equilibrium will cause the equilibrium position to change in such a way as to tend to remove the perturbation." [31, p. 61]

This principle can be used as a guideline for the effect of the variation of temperature (see equation (4.19), p. 32) or pressure (see equation (4.32), p. 33) on the equilibrium constant. For example, if the standard enthalpy of a reaction $\Delta_R H^{\ominus}$ is positive (endothermic reaction) increasing the temperature will lead to more reaction products. If a positive volume change accompanies the reaction, for instance, in the thermal decomposition of carbonates to oxides and carbon dioxide, application of pressure will shift the equilibrium towards the reactants [31].

4.7 Thermodynamic calculations

4.7.1 HSC Chemistry© 3.0 for Windows

The software HSC chemistry© 3.0 for Windows can be used to perform various thermodynamic calculations. HSC is an abbreviation for enthalpy H, entropy S, and heat capacity C. All calculations performed by the software are based on its database for standard enthalpy, entropy, and heat capacities, or Gibbs free energy values of more than 11,000 compounds [37].

Specific heat values c_p are calculated with the Kelley equation (4.33) [38]. The coefficients A, B, C, and D are taken from the internal database. The calculation of the standard enthalpy H for a specific temperature T is done by using equation (4.34). Standard entropy is calculated with equation (4.35). The values of the enthalpy and entropy of formation at 298.15 K are either taken from the internal database or calculated by integration of the c_p-value between zero and 298.15 K. All integrals are evaluated numerically with internal routines of the software not further described in the documentation [37].

$$c_p = A + B \cdot 10^{-3} \cdot T + C \cdot 10^5 \cdot T^{-2} + D \cdot 10^{-6} \cdot T^2 \tag{4.33}$$

$$H^{\ominus}(T) = H_f(298.15K) + \int_{298.15K}^{T} c_p dT + H_{trans} \tag{4.34}$$

$$S^{\ominus}(T) = S_f(298.15K) + \int_{298.15K}^{T} \frac{c_p}{T} dT + \frac{H_{trans}}{T_{trans}} \tag{4.35}$$

The standard entropy and enthalpy of a reaction are calculated as described in section 4.3. The Δc_p value is calculated as described in equation (4.23) on page 32. The standard free reaction energy $\Delta_R G^{\ominus}$ for a specific temperature T is calculated with equation (4.12) (see page 30). The equilibrium constant K (defined in equation (4.16), p. 31) is calculated with equation (4.17) (see page 31) [37].

4.7.2 The standard free reaction energy from zero to 550 °C

Table 4.1 (p. 31) shows that the value of the standard free reaction energy $\Delta_R G^{\ominus}$ can be linked to the reaction composition at equilibrium for a specific temperature. A highly negative $\Delta_R G^{\ominus}$ tells us, for example, that, when the reaction reaches equilibrium, most of the reactants have been converted into products. Therefore, the value of the standard free reaction energy as a function of temperature $\Delta_R G^{\ominus}(T)$ for the hydrogenation of most of the carbonates described in chapter 2 was simulated with HSC Chemistry© 3.0. The results of these simulations will help to identify possible candidates for experiments in the tubular reaction system.

Carbonates not included in the calculations

Both beryllium carbonate and ammonium aluminum carbonate hydroxide are not included in the simulations. The former because it is unstable and decomposes easily, the latter because it would exceed the objective and time schedule of this thesis. The carbonates of actinoids are either unstable or radioactive. Various carbonates of the rare earth elements exist and are used in research and industry. Nevertheless, this Master's thesis does not

deal with rare earth elements, as this would exceed the objective and time schedule of this thesis.

Simulation parameters and assumptions

The upper limit of the operational temperature range of the tubular reaction system is 550 °C. Subsequently, the standard free reaction energy was calculated between zero and 550 °C. The calculations were performed for a pressure of 1 atm (1.013 bar). Only data of the internal database of HSC Chemistry© 3.0 was used.

The simulations were conducted for the reaction equations given in Table 4.2 (p. 36). The abbreviations given in the first column of Table 4.2 are also used in the Figures 4.1-4.6. Except for iron and cobalt carbonate, only the formation of one oxide form was considered. In the case of iron carbonate the formation of the bivalent FeO, trivalent Fe_2O_3, and the mixed oxide Fe_3O_4 during the hydrogenation was considered. For cobalt carbonate the formation of the bivalent oxide CoO and the mixed oxide Co_3O_4 during hydrogenation was accounted for. In the case of magnesium and copper three different types of carbonates were examined. Furthermore, two types of lead carbonate were considered.

Results

The water produced in the hydrogenation was considered to be gaseous. Indeed, the liquid state would be thermodynamically more stable up to 100 °C at 1 atm. This simplification results in higher values of the standard free reaction energy below 100 °C. Figure 4.1 (p. 38) shows this relationship for the hydrogenation of magnesium carbonate. Magnesium carbonate is taken as an example, the run of the curves stays the same for all other hydrogenation reactions simulated. Both the standard free reaction energies for the hydrogenation producing liquid water and the hydrogenation producing water vapor can be calculated by summation of the value of the standard free reaction energy of the vaporization reaction (4.36) and the standard free reaction energy of either reaction (4.37) or (4.38).

$$2H_2O(l) \rightleftharpoons 2H_2O(g) \tag{4.36}$$

$$MgCO_3(s) + 4H_2(g) \rightleftharpoons MgO(s) + CH_4(g) + 2H_2O(l) \tag{4.37}$$

$$MgCO_3(s) + 4H_2(g) \rightleftharpoons MgO(s) + CH_4(g) + 2H_2O(g) \tag{4.38}$$

Figure 4.2 (p. 38) shows that the carbonates of the first group elements lithium, sodium, potassium, rubidium, and cesium have a positive standard free reaction energy in the selected temperature range. At constant temperature, the free reaction energy increases with the relative atomic number, except from rubidium to cesium.

The standard free reaction energy for the second group elements magnesium, calcium, strontium, and barium is shown in Figure 4.3 (p. 39). Only magnesium carbonate has a negative free reaction energy in the selected temperature range. At constant temperature, the free reaction energy increases with the relative atomic number. In the simulated temperature range, the standard free reaction energy increases with temperature for all carbonates of the first and second group elements.

Figures 4.4 (p. 39) and 4.5 (p. 40) show that lead carbonate and the carbonates of

Table 4.2: Reaction equations for the simulation of the standard free reaction energy at a constant pressure of 1 atm

Abbreviation	Reaction equation
Li2CO3	$Li_2CO_3(s) + 4H_2(g) \rightleftharpoons Li_2O(s) + CH_4(g) + 2H_2O(g)$
Na2CO3	$Na_2CO_3(s) + 4H_2(g) \rightleftharpoons Na_2O(s) + CH_4(g) + 2H_2O(g)$
K2CO3	$K_2CO_3(s) + 4H_2(g) \rightleftharpoons K_2O(s) + CH_4(g) + 2H_2O(g)$
Rb2CO3	$Rb_2CO_3(s) + 4H_2(g) \rightleftharpoons Rb_2O(s) + CH_4(g) + 2H_2O(g)$
Cs2CO3	$Cs_2CO_3(s) + 4H_2(g) \rightleftharpoons Cs_2O(s) + CH_4(g) + 2H_2O(g)$
MgCO3	$MgCO_3(s) + 4H_2(g) \rightleftharpoons MgO(s) + CH_4(g) + 2H_2O(g)$
Mg2(OH)2CO3*3H2O	$Mg_2(OH)_2CO_3 \cdot 3\,H_2O + 4\,H_2(g) \rightleftharpoons$ $2\,MgO + CH_4(g) + 6\,H_2O(g)$
MgCO3*3H2O	$MgCO_3 \cdot 3\,H_2O + 4H_2 \rightleftharpoons MgO(s) + CH_4(g) + 5H_2O(g)$
CaCO3	$CaCO_3(s) + 4H_2(g) \rightleftharpoons CaO(s) + CH_4(g) + 2H_2O(g)$
SrCO3	$SrCO_3(s) + 4H_2(g) \rightleftharpoons SrO(s) + CH_4(g) + 2H_2O(g)$
BaCO3	$BaCO_3(s) + 4H_2(g) \rightleftharpoons BaO(s) + CH_4(g) + 2H_2O(g)$
MnCO3	$MnCO_3(s) + 4H_2(g) \rightleftharpoons MnO(s) + CH_4(g) + 2H_2O(g)$
FeO	$FeCO_3(s) + 4H_2(g) \rightleftharpoons$ $FeO(s) + CH_4(g) + 2H_2O(g)$
Fe2O3	$2FeCO_3(s) + 7H_2(g) \rightleftharpoons$ $Fe_2O_3(s) + 2CH_4(g) + 3H_2O(g)$
Fe3O4	$3FeCO_3(s) + 11H_2(g) \rightleftharpoons$ $Fe_3O_4(s) + 3CH_4(g) + 5H_2O(g)$
CoO	$CoCO_3(s) + 4H_2(g) \rightleftharpoons CoO(s) + CH_4(g) + 2H_2O(g)$
Co3O4	$3CoCO_3(s) + 11H_2(g) \rightleftharpoons$ $Co_3O_4(s) + 3CH_4(g) + 5H_2O(g)$
NiCO3	$NiCO_3(s) + 4H_2(g) \rightleftharpoons NiO(s) + CH_4(g) + 2H_2O(g)$
CuCO	$CuCO_3(s) + 4H_2(g) \rightleftharpoons CuO(s) + CH_4(g) + 2H_2O(g)$
Cu2(OH)2CO3	$Cu_2(OH)_2CO_3 + 4H_2(g) \rightleftharpoons$ $2CuO(s) + CH_4(g) + 3H_2O(g)$
Cu3(OH)2(CO3)2	$\frac{1}{2}Cu_3(OH)_2(CO_3)_2 + 4H_2(g) \rightleftharpoons$ $\frac{3}{2}CuO + CH_4(g) + \frac{5}{2}\,H_2O(g)$
ZnCO3	$ZnCO_3(s) + 4H_2(g) \rightleftharpoons ZnO(s) + CH_4(g) + 2H_2O(g)$
Ag2CO3	$Ag_2CO_3(s) + 4H_2(g) \rightleftharpoons Ag_2O(s) + CH_4(g) + 2H_2O(g)$
CdCO3	$CdCO_3(s) + 4H_2(g) \rightleftharpoons CdO(s) + CH_4(g) + 2H_2O(g)$
PbCO3	$PbCO_3(s) + 4H_2(g) \rightleftharpoons PbO(s) + CH_4(g) + 2H_2O(g)$
PbO*PbCO3	$PbO \cdot PbCO_3(s) + 4H_2(g) \rightleftharpoons 2\,PbO + CH_4(g) + 2\,H_2O(g)$

the transition metals manganese, iron, cobalt, nickel, copper, zinc, silver, and cadmium all have a negative standard free reaction energy in the temperature range considered. The standard free reaction energy shows a tendency to increase between zero and 550 °C. Nevertheless, the gradient of the standard free reaction energy with temperature (slope of the curves depicted in Figures 4.1 - 4.6) varies from carbonate to carbonate. At zero °C the highest value is -53 kJ/mol CH_4 for manganese carbonate, the lowest is -117 kJ/mol CH_4 for copper carbonate. At 550 °C the highest value is -29 kJ/mol CH_4 for the hydrogenation of cobalt carbonate to the mixed oxide Co_3O_4, the lowest is -97 kJ/mol CH_4 for copper carbonate.

Figure 4.4 (p. 39) shows the differences in the standard free reaction energy for varying products. The three types of iron oxides considered (FeO, Fe_2O_3, and Fe_3O_4) show a slightly different behavior. They lie within approx. 20 kJ/mol CH_4 between zero and 550 °C but have different gradients. The gradient of the curve rises in the order FeO < Fe_3O_4 < Fe_2O_3. The two oxides considered for cobalt (CoO and Co_3O_4) lie within 22 kJ/mol CH_4 at zero °C and 33 kJ/mol CH_4 at 550 °C. This is due to the larger gradient of the hydrogenation of cobalt carbonate to the mixed oxide Co_3O_4 compared to the gradient for the hydrogenation producing the bivalent oxide CoO.

Figure 4.6 (p. 40) shows the differences in the standard free reaction energy for carbonates of the same element but with different composition. Basic magnesium carbonate trihydrate and magnesium carbonate trihydrate have a decreasing standard free reaction energy with temperature. In contrast, magnesium carbonate shows a slightly increasing standard free reaction energy between zero and 550 °C. The absolute value of the gradient for the hydrogenation of basic magnesium carbonate trihydrate and magnesium carbonate trihydrate is larger than that for the hydrogenation of magnesium carbonate. The standard free reaction energy for the hydrogenation of lead carbonate and lead carbonate oxide is quite similar in the simulated temperature range. The hydrogenation of azurite $Cu_3(OH)_2(CO_3)_2$ and malachite $Cu_2(OH)_2CO_3$ show a decreasing standard free reaction energy with temperature. On the contrary, the hydrogenation of copper carbonate shows an increasing standard free reaction energy with temperature.

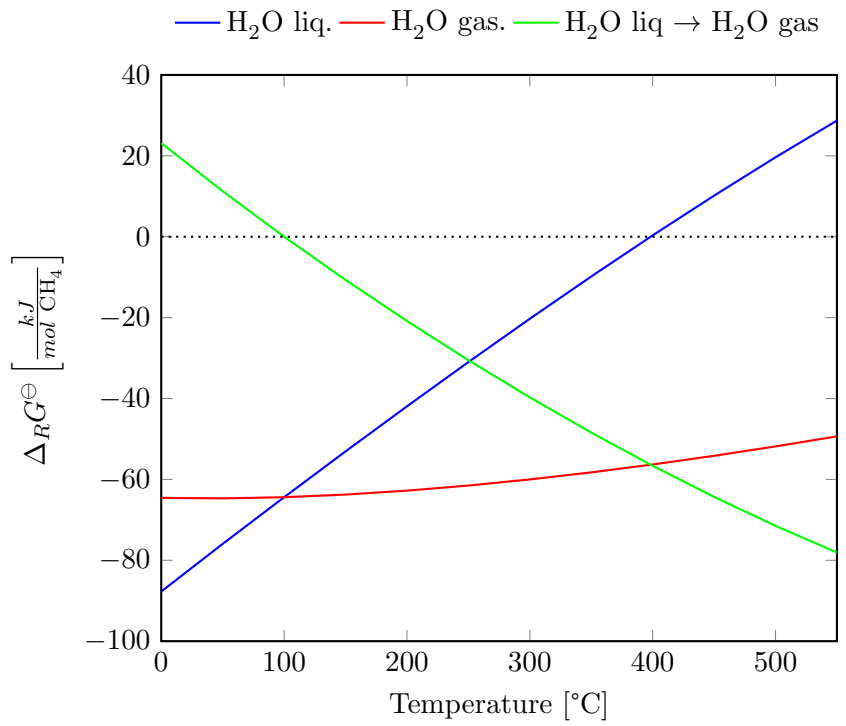

Figure 4.1: Standard free reaction energy at 1 atm for reactions (4.37) (p. 35, *blue*), (4.38) (p. 35, *red*), and (4.36) (p. 35, *green*)

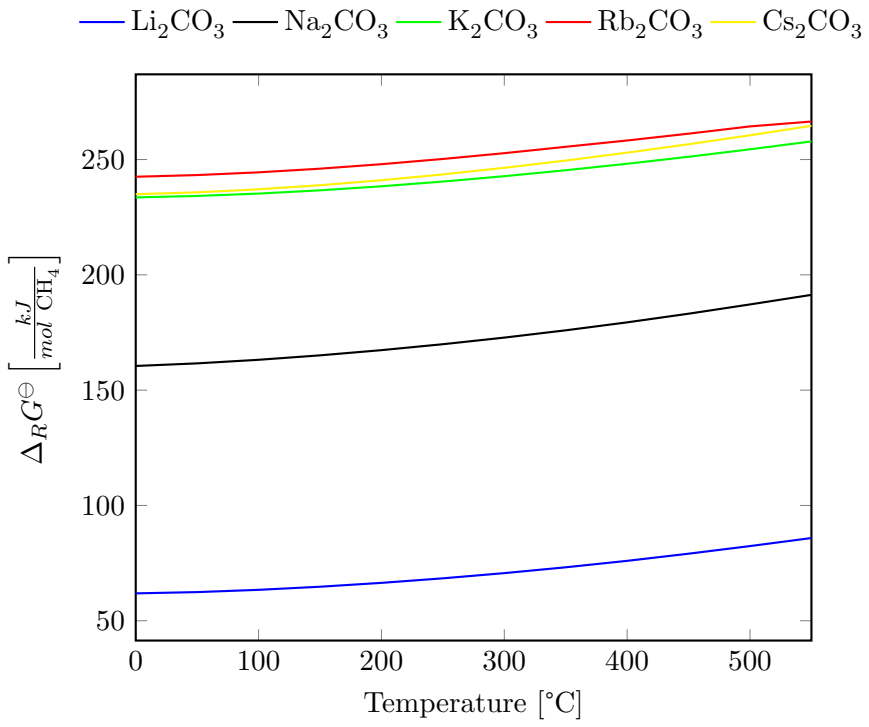

Figure 4.2: Standard free reaction energy for methane production using first group carbonates at 1 atm

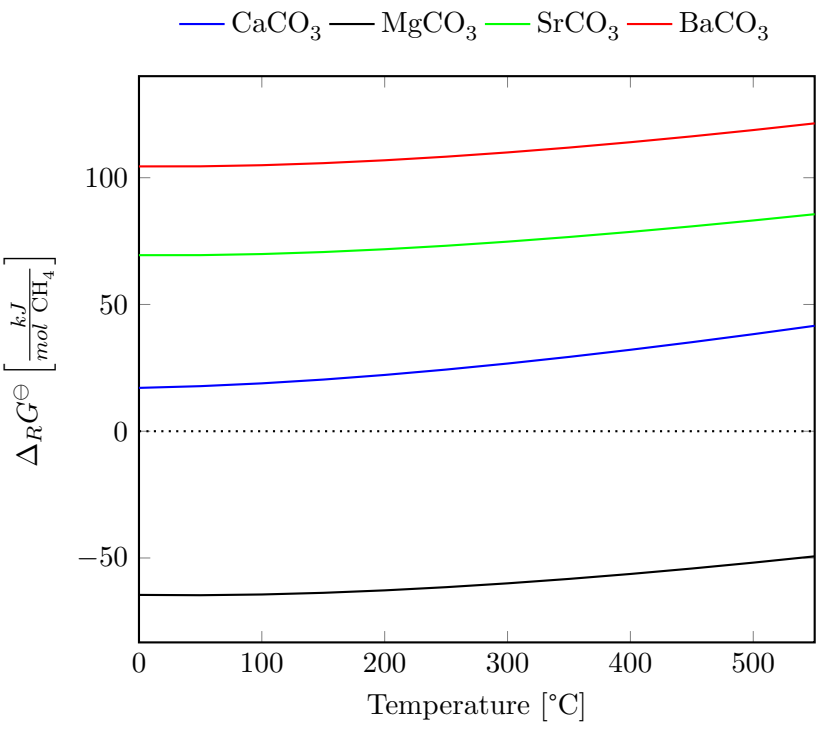

Figure 4.3: Standard free reaction energy for methane production using second group carbonates at 1 atm

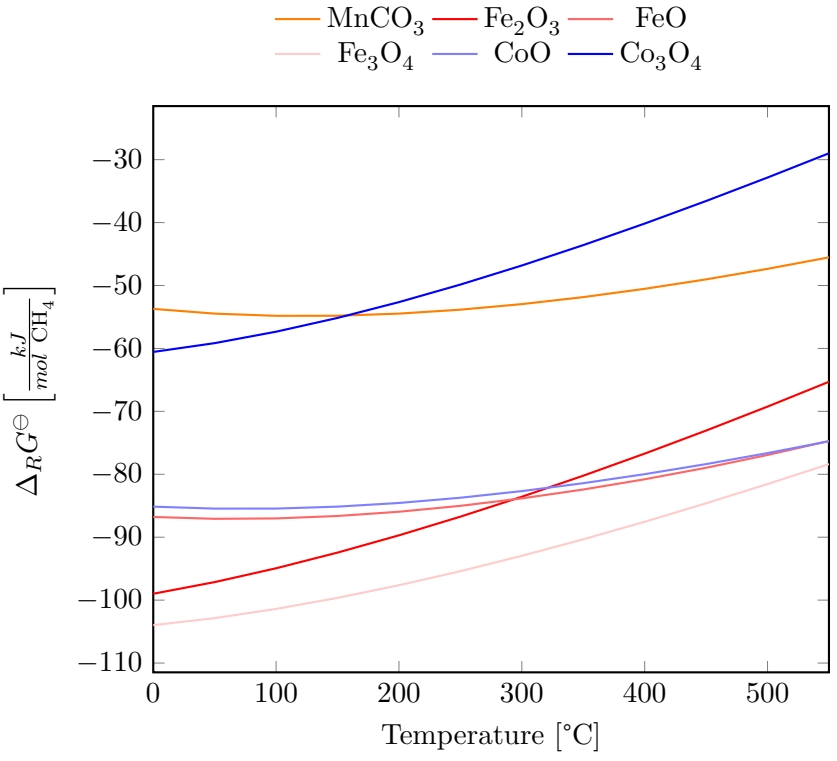

Figure 4.4: Standard free reaction energy for methane production using other main group and transition metal carbonates at 1 atm, Part 1

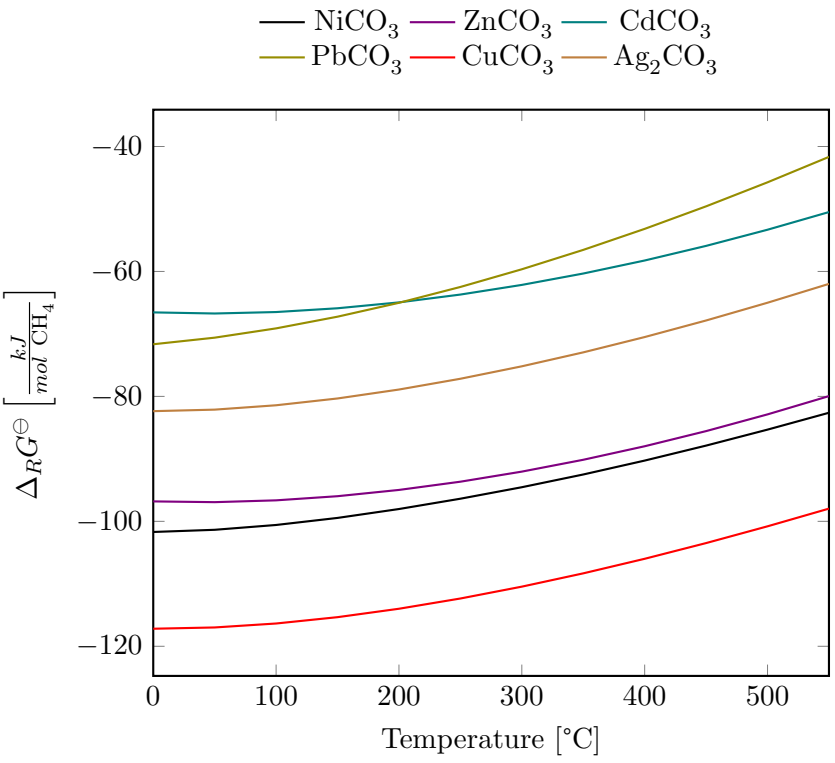

Figure 4.5: Standard free reaction energy for methane production using other main group and transition metal carbonates at 1 atm, Part 2

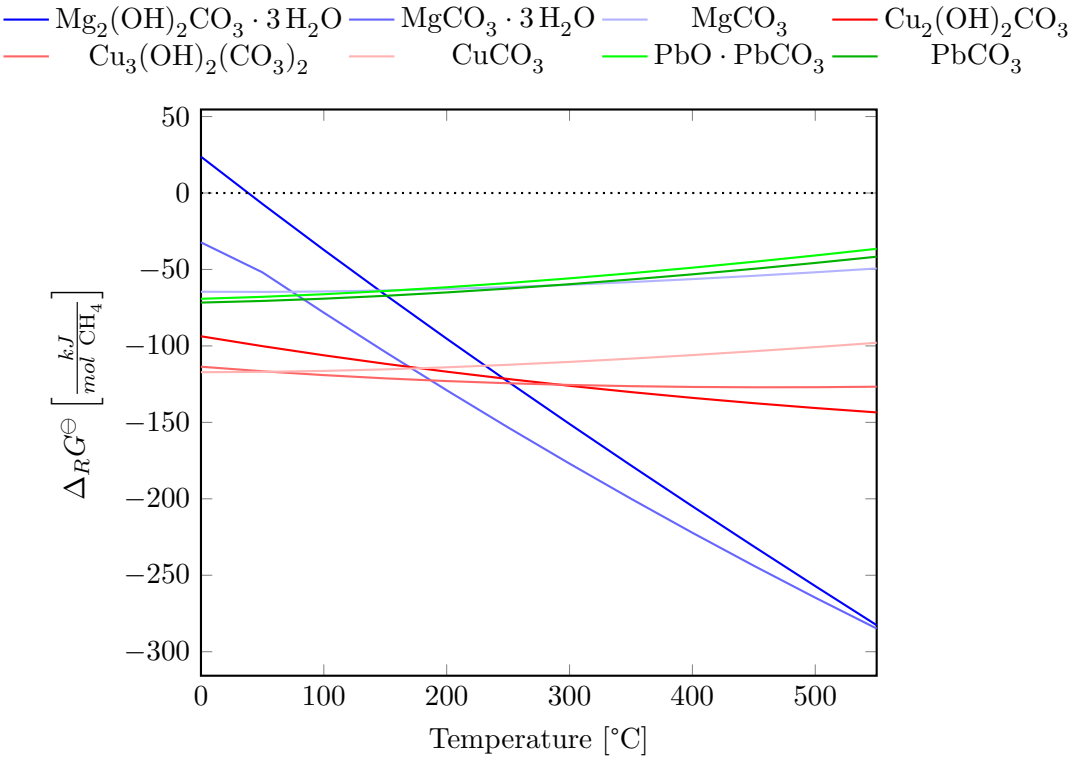

Figure 4.6: Standard free reaction energy for methane production using some basic main group and transition metal carbonates at 1 atm

5 Thermogravimetric experiments - Preliminary studies of the thermal stability of selected carbonates

5.1 Theoretical background of thermogravimetry

The *International Confederation for Thermal Analysis and Calorimetry* (ICTAC) defines thermogravimetry as follows:

> "A technique in which the mass of a substance is measured as a function of temperature while the substance is subjected to a controlled temperature programme." [39]

The typical setup for thermogravimetric experiments consists of the following components [40]:

- Thermo-microbalance consisting of a furnace, sample holder, balance, and multiple sensors
- Equipment for gas pre- and post-treatment
- Equipment and interfaces for data acquisition, storage, and manipulation

For more comprehensive studies of evolved gases during thermogravimetric experiments a combination of a thermo-microbalance with mass spectrometry, Fourier-transform infrared spectroscopy, and other analytical techniques is possible [41].

The measured variable is the mass as a function of temperature and time. There exist various temperature programs, which can also be combined. In isothermal experiments the temperature of the sample is held at a specific constant value. In dynamic thermogravimetry the sample is heated with a specific, mostly constant rate. Quasi-isothermal thermogravimetry is a combination of the isothermal and dynamic mode. In between heating intervals with constant heating rate the sample is kept at a specific temperature until the mass change is very low [41]. In controlled rate thermal analysis the heating rate is adjusted until a constant rate of mass change is approached. The sometimes so-called 'high resolution thermogravimetry' is characterized by a variation of the heating rate according to current mass change. When the mass change rate is high, the heating rate is decreased until the mass loss is completed. Afterwards, the heating rate is increased again until the next mass loss begins [42].

Thermogravimetry (TG) finds a broad field of application. Polymers have been extensively studied with TG and other thermal analysis techniques such as differential scanning

calorimetry (DSC). The determination of characteristic temperatures like the glass transition temperature is one example for information gained by polymer TG/DSC. Compounds with pharmaceutical application have been 'fingerprinted' using standard TG techniques. Additionally, raw materials like coals and oil shales can be characterized with standard TG techniques [41]. In this work, TG will be applied to selected inorganic carbonates in inert nitrogen and reductive hydrogen atmosphere.

5.1.1 Examination of typical thermogravimetric curves

Thermogravimetric results are usually represented in a diagram - the so-called thermogram or simply TG curve. The ratio of the actual mass to the initial mass $\frac{m(T)}{m_0}$ in percent is plotted on the ordinate and the temperature on the abscissa. Alternatively, the mass loss can be plotted on the ordinate (in milligram or another weight measure) and instead of temperature, time can be used as the independent variable [40]. Conventionally, a mass loss is plotted downwards and a mass gain upwards [42].

For comparability reasons, it is preferential to use dimensionless measures. Therefore, in this work the ratio of the actual mass to the initial mass will be used as the ordinate in a TG curve. If the chemical composition of the investigated substance is known, the percentaged mass representation exhibits further advantages. A mass change can be linked to possible reaction mechanisms without evolved gas, liquid, and solid analysis. Nevertheless, only analysis of all reaction partners and products will allow reproducible results.

The initial temperature T_i (also called onset or procedural decomposition temperature) is the temperature where a mass loss is detected first. As the detection depends on the sensitivity of the equipment used, T_i is not a very useful and reproducible information. The final temperature T_f is the temperature at which the sample reaches its final mass. T_f depends on various factors like the sensitivity of the equipment and the run of the curve at higher temperatures. Therefore, the extrapolated onset $T_{e,o}$ and final $T_{e,f}$ temperature can be used to characterize thermogravimetric events more precisely [42].

Additional information to complement thermogravimetry is gained by differential thermogravimetry (DTG). In differential thermogravimetry the first derivative of the mass change over time $\frac{dm}{dt}$ or over temperature $\frac{dm}{dT}$ is calculated. A local maximum $T_{p,max}$ in the DTG curve corresponds to the maximum reaction rate of a mass gain in a TG experiment. A local minimum $T_{p,min}$, on the other hand, corresponds to the maximum reaction rate of a mass loss in a TG experiment [42]. From basic calculus we know that local extrema of the derivative represent points of inflection of the respective function. DTG curves make small mass changes better recognizable and therefore help to identify subtle reactions otherwise not recognized. Furthermore, the peak area of a DTG peak directly corresponds to the mass loss of a selected TG event [42].

Dunn [42] and Hemminger and Cammenga [40] describe two different ways to determine the extrapolated onset $T_{e,o}$ and final $T_{e,f}$ temperature. In both cases, a tangent to a characteristic point $p_{char} = (m_{char}; T_{char})$ of the TG curve is used. The difference between the two methods is the determination of T_{char}. Hemminger and Cammenga [40] use the temperature at a local extremum $T_{p,max}$ or $T_{p,min}$ of the DTG curve. $T_{p,max}$ or $T_{p,min}$ therefore lies in the point of inflection of the TG curve. Dunn [42], on the contrary, uses the temperature $T_{0.5}$ of the half fractional weight loss α. The fractional weight loss is

calculated between the starting and end mass of a selected TG event. In the evaluation of the TG experiments conducted, the method of Hemminger and Cammenga [40] is used. The author of this Master's thesis considers the temperature at a local extremum $T_{p,max}$ or $T_{p,min}$ - with the concurrent maximum rate of reaction - as a more significant value than the temperature $T_{0.5}$ of the half fractional weight loss α.

5.1.2 Influencing values: How to optimize thermogravimetric results

There exist various influencing values that can lead to misinterpretation of a TG curve. Hemminger and Cammenga 1989 [40], Hill et al. 1995 [41], and Dunn 2000 [42] give a comprehensive overview with additional background information and extensive bibliographies. In the following, only the most important aspects are outlined.

Vibrations always lead to weighing errors. Therefore, any thermogravimetric equipment should be placed vibration-free. This is an absolute requirement, as in many experiments small mass changes in the range of 0.01 mg should be registered correctly.

The position of the temperature sensor has to be indicated, as there is a systematic difference between the temperature of the sample and the oven [40]. Furthermore, the measurement of the sample temperature can be done in different ways. Temperature sensors are most commonly thermocouples. The optimal position for the sensor would be in direct contact with the sample [42]. This is often impossible, for example, because of the sample holder. Different manufacturers offer more or less sophisticated constructions. The result of the non-ideal position of the thermocouple is a systematic failure in the measurement of the sample temperature. Therefore, temperature calibration is crucial [40, 42].

No furnace can produce a totally homogeneous temperature field. For optimal results, a hot zone should exist. In this zone, the temperature should be homogeneously distributed. Therefore, the best position of the sample is this hot zone [42].

Heat transfer also occurs within the sample. To reach a homogeneous temperature distribution within the sample, a certain time is necessary [43]. The solid sample should therefore be finely ground and placed as a thin film in the sample pan [42].

The heating rate has great influence on the run of the TG and DTG curve. Generally, a high heating rate leads to a shift of the peaks of the DTG curve to higher temperatures [44]. Additionally, an excessive heating rate can lead to a change in the reaction mechanism and totally different thermograms [42].

The gas used in thermogravimetric experiments has influences on the buoyancy and the heat transfer within the oven. Buoyancy effects lead to an apparent mass gain. Most generally, the apparent mass gain increases with the density of the used gas [40]. The heat transfer within the oven depends on the thermal conductivity of the used gas [42].

5.2 Experimental

5.2.1 General considerations

The thermogravimetric experiments were conducted with the help of Bernhard Marius, BSc. with a Netzsch Jupiter STA 449C thermo-microbalance. Netzsch also provided the equipment for gas pre- and post-treatment, data acquisition, storage, and manipulation.

Aluminum oxide sample pans were used in all measurements. The flow rate was kept at 30 ml/min when the purge gas was nitrogen only. When nitrogen and hydrogen were used together the flow rate of each gas was kept at 50 ml/min. The heating rate was set to 5 K/min, if not mentioned differently. The experiments were conducted in atmospheric conditions. The temperature program was set to heating up the samples from about 30 °C to about 700 °C. The sample temperature was measured with a thermocouple mounted at the sample holder, directly beneath the sample pan. The investigated samples were nickel carbonate (Alfa Aesar, 98 %, anhydrous), manganese carbonate (Alfa Aesar, min. 44 % manganese), magnesium carbonate granulate (a special sample of MagGranMC provided by Magnesia Germany), and siderite (a special sample of July 2, 2013 provided by VA Erzberg). The composition of the siderite sample with an iron carbonate content ($FeCO_{3_{sample}}$) of 71.01 wt% is given in Table 5.1. The iron carbonate content of the sample was calculated according to equation (5.1).

$$FeCO_{3_{sample}} = \frac{Fe_{Sample}}{\frac{AW_{Fe}}{MW_{FeCO3}}} = \frac{34.23}{\frac{55.845}{115.853}} = 71.01\ \%wt \tag{5.1}$$

Table 5.1: Composition of the siderite sample of July 2, 2013 in weight percent as analyzed by VA Erzberg

Component	%wt
Fe	34.23
CaO	7.27
SiO_2	2.59
MgO	3.92
Mn	2.01
Al_2O_3	1
S	0.023
P	0.021
Na_2O	0.033
K_2O	0.347
Hg	$2.76 \cdot 10^{-4}$

5.2.2 Matlab routine for the analysis of the thermogravimetric data

Description of the Matlab routine

The measured thermogravimetric data was analyzed with a Matlab routine called TGAnalysisCarbonates.m (see appendix pp. 87 ff.). The job of this routine is the determination of some characteristic values of a single step in a TG curve. Furthermore, the theoretical carbon, carbon monoxide, carbon dioxide, oxygen, hydroxide, and water content P_{sample} according to the suggested formula of the investigated substance is calculated with equation (5.2). Comparison of the P_{sample} value and the actual mass loss of the examined TG

step can give hints for possible reactions and gaseous products.

$$P_{sample}[\%] = 100 \cdot \frac{MW_P}{MW_{sample}} \tag{5.2}$$

The DTG values are calculated by approximating the derivative with the differential quotient of two proximate data points using equation (5.3). If a mass loss occurs between temperature T_1 and temperature T_2 (with $T_1 < T_2$), the DTG value is negative.

$$\frac{dm}{dT} \approx \frac{\Delta m}{\Delta T} = \frac{m(T_2) - m_(T_1)}{T_2 - T_1} \tag{5.3}$$

The point of inflection of the TG curve is calculated by determining the minimum of the DTG values in an indicated temperature and mass interval using the internal *min()*-function of Matlab. With this information at hand, the tangent of inflection is calculated according to equation (5.4) (T_{PoI}...Temperature at point of inflection, equal to $T_{p,min}$ of DTG curve; k_w...slope of the linear equation at a point of inflection; b_w...intercept for the linear equation at the point of inflection). For the calculation of the extrapolated onset $T_{e,o}$ and final $T_{e,f}$ temperature the method described by Hemminger and Cammenge [40] (see also section 5.1.1, p. 42) is used. The tangent of inflection is subtended with the starting mass line and end mass line to determine $T_{e,o}$ and $T_{e,f}$ according to equations (5.5) and (5.6) .

$$m(T_{PoI}) = k_w \cdot T_{PoI} + b_w \tag{5.4}$$

$$T_{e,o} = \frac{m_{start} - b_w}{k_w} \tag{5.5}$$

$$T_{e,f} = \frac{m_{end} - b_w}{k_w} \tag{5.6}$$

The TG curve, the tangent of inflection, and the user defined starting and end mass line are presented in a plot. Additionally, the calculated data is stored in a text file. Figure 5.1 shows the plot generated by TGAnalysisCarbonates.m for the thermogravimetric data of manganese carbonate under nitrogen.

Practical use of the Matlab routine

At first, the raw data of a TG experiment is stored in a text file. This file can only contain numeric data with the data columns separated by space characters. The required user input of TGAnalysisCarbonates.m has to be completed. The starting and end temperature (`TstartUser` and `TendUser`) and the starting and end mass (`mstart` and `mend`) are initialized with a first guess. Then the routine is executed. Visual analysis of the plot and more detailed analysis with the data cursor allow a second, more precise guess for `TstartUser`, `TendUser`, `mstart`, and `mend`. This procedure is repeated until the values for the extrapolates onset $T_{e,o}$ and final $T_{e,f}$ temperature are satisfactory.

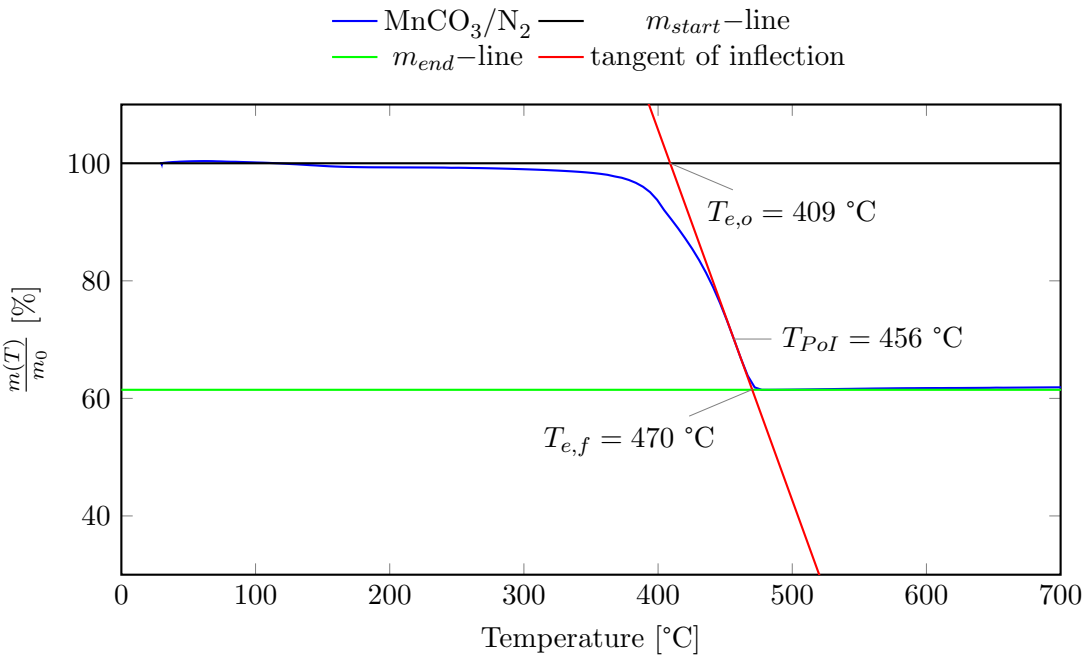

Figure 5.1: TG curve of manganese carbonate with tangent of inflection and extrapolated onset and final temperature as calculated with TGAnalysisCarbonates.m

5.3 Results

5.3.1 Assumptions

All four samples were investigated in inert nitrogen and reductive hydrogen atmosphere. The aim of these experiments was to identify possible differences in the run of the TG curves depending on the gas used. The mass loss of a step in a TG curve can be linked to possible gaseous products. In inert nitrogen atmosphere, it seems plausible that the metal carbonate decomposes to an oxide releasing carbon monoxide or dioxide as depicted in reaction equations (5.7) and (5.8). The presence of hydrogen can lead to reduction of carbon dioxide in a reverse water-gas-shift reaction (5.9). Some metal oxides can catalyze such a reaction [45]. However, the reversibility of the water-gas-shift reaction has to be kept in mind. Moreover, metal oxides can be reduced to elemental metals in the presence of hydrogen (see reaction equation (5.10)). The gases evolved during the thermogravimetric experiments could not be analyzed. Therefore, only the possible thermal decomposition is discussed in the next section.

$$\mathrm{MCO_3} \rightleftharpoons \mathrm{MO_2} + \mathrm{CO} \tag{5.7}$$

$$\mathrm{MCO_3} \rightleftharpoons \mathrm{MO} + \mathrm{CO_2} \tag{5.8}$$

$$\mathrm{CO_2} + \mathrm{H_2} \rightleftharpoons \mathrm{CO} + \mathrm{H_2O} \tag{5.9}$$

$$\mathrm{MO} + \mathrm{H_2} \rightleftharpoons \mathrm{M} + \mathrm{H_2O} \tag{5.10}$$

5.3.2 Limitations

The experimental setup did not allow the analysis of the evolved gas during the heat up of the samples. The solid residue after the thermogravimetric experiments was not analyzed. Furthermore, the experiments were realized only once. As a consequence, there is no statistical certainty about the thermogravimetric data presented in this work. The purpose of the thermogravimetric experiments and the interpretation of the experimental data is to obtain a first impression of the thermal behavior of the selected samples.

5.3.3 Interpretation of the thermogravimetric curves

Magnesium carbonate

Figure 5.2 (p. 49) shows a comparison of the TG curve of magnesium carbonate with different heating rates (5 and 10 K/min) and purge gases. A heating rate of 10 K/min leads to a different run of the curve when nitrogen is used as the purge gas. When this heating rate is applied, only one step in the TG curve, associated to a mass loss of 48.3 %, can be seen.

At a lower heating rate of 5 K/min, on the other hand, three steps can be seen. The first step is broad and starts at about 50 °C and ends at about 350 °C. The extrapolated onset temperature $T_{e,o}$ could be allocated to 204 °C and the extrapolated final temperature $T_{e,f}$ to 296 °C, corresponding to a mass loss of 16.0 %. The temperature corresponding to the maximum rate of reaction evaluated at the point of inflection T_{PoI} equals 262 °C. The second step is sharper and ends at about 460 °C, with a $T_{e,o}$ of 400 °C, a $T_{e,f}$ of 453 °C, and a T_{PoI} of 435 °C, corresponding to a mass loss of 24.7 %. The second and third step are clearly separated by a plateau, whereas the third step terminates at about 500 °C. The third step is hallmarked by a $T_{e,o}$ of 473 °C, a $T_{e,f}$ of 499 °C, and a T_{PoI} of 483 °C, corresponding to a mass loss of 16.1 %. The total mass loss sums up to 56.8 %. *As a heating rate of 10 K/min leads to apparent loss of information, all other thermogravimetric experiments were conducted at a heating rate of 5 K/min.*

Hydrogen present in the purge gas at the same heating rate of 5 K/min leads to the loss of the third TG step observed for pure nitrogen. The first, broad TG step is hallmarked by a $T_{e,o}$ of 185 °C, a $T_{e,f}$ of 268 °C, and a T_{PoI} of 236 °C, corresponding to a mass loss of 16.0 %. Between 350 and 500 °C the extrapolated onset temperature $T_{e,o}$ could be allocated to 402 °C and an extrapolated final temperature $T_{e,f}$ to 456 °C corresponding to a mass loss of 40.8 %. The temperature corresponding to the maximum rate of reaction evaluated at the point of inflection T_{PoI} equals 436 °C. The total mass loss stays the same, irrespective which purge gas is used. The temperature interval $[T_{e,o}, T_{e,f}]$ of the TG steps, on the contrary, is decreased by 15 to 50 °C.

Figure 5.3 (p. 49) shows that the total mass loss, independent of the purge gas and heating rate, could correspond to the formation of carbon dioxide by thermal decomposition of magnesium carbonate. The intermediate steps can not be assigned to a specific process as neither the gaseous product nor the solid residue were analyzed. Nevertheless, the thermogravimetric data can be compared to the findings of Padeste et al. 1991 [23] (see section 3.3, p. 18). The TG curves in this publication [23] show a similar behavior. Therefore, the sample examined in this work may not consist of pure magnesium carbon-

ate but basic mangesia or hydromagnesite. Furthermore, the total mass loss of 56.8 % is higher than the calculated carbon dioxide content of magnesium carbonate (52.2 %), which could also be due to weighing errors or further reactions to take place. These assumption have indeed to be supported by further experimental analysis.

Nickel carbonate

Figure 5.4 (p. 50) shows that between about 30 and 215 °C the run of the TG curve does not depend on the purge gas. The mass loss at 215 °C is 15 %. When hydrogen is present in the purge gas, a rapid mass loss of about 37 % with a $T_{e,o}$ of 227 °C, a $T_{e,f}$ of 263 °C, and a T_{PoI} of 245 °C occurs. Nitrogen atmosphere, in contrast, leads to a broader TG step after 215 °C. This step corresponds to a mass loss of 21.8 %, leading to an end mass of 63.2 % with a $T_{e,o}$ of 262, a $T_{e,f}$ of 331 °C, and a T_{PoI} of 293 °C. The end mass for hydrogen atmosphere, on the contrary, is 51.9 %.

Figure 5.5 (p. 50) shows that the first TG event can not be assigned to a specific component of nickel carbonate. Moreover, the first TG event corresponds to a relatively slow, but constant mass loss with temperature. The end mass of the sample when nitrogen is used as a purge gas shows that carbon dioxide could be released and the solid residue could consist of nickel oxide. Hydrogen, on the other hand, leads to a higher mass loss in one step. This could correspond to the parallel thermal decomposition and reduction of the oxide to elemental nickel.

Manganese carbonate

Figure 5.6 (p. 51) shows that in the case of manganese carbonate the TG curve does not change profoundly when hydrogen is added to the purge gas. In both cases only one TG step can be seen, corresponding to a mass loss of 38-40 %. Between 30 °C and the onset temperature the curves constantly differ by two percent. This could be due to buoyancy effects or minor weighing errors. Additionally, the extrapolated onset and final temperature are shifted to lower values when hydrogen is used. $T_{e,o}$ decreases from 409 to 403 °C, $T_{e,f}$ decreases from 470 to 444 °C. The temperature of maximum reaction rate determined at the point of inflection decreases from 456 to 435 °C. Figure 5.7 (p. 51) shows that most possibly carbon dioxide was released during the thermogravimetric experiment.

Siderite

The iron carbonate content of the siderite sample is 71.01 %wt (see section 5.2.1, p. 43 for further explanation and calculation). Therefore, the thermogram was re-calculated to pure iron carbonate according to equation (5.11). This assumption only holds if the residue of the siderite sample (see Table 5.1, p. 44) does not change during the heat up.

$$m(T)_{norm.} = m(T) \cdot FeCO_{3,sample} + (100 - FeCO_{3,sample})\ [\%wt] \qquad (5.11)$$
$$m(T)_{norm.} = m(T) \cdot 71.01 + 28.99\ \%wt$$

Figure 5.8 (p. 53) shows that a hydrogen-containing atmosphere can notably shift the onset temperature of a TG step. Furthermore, not only the characteristic temperatures

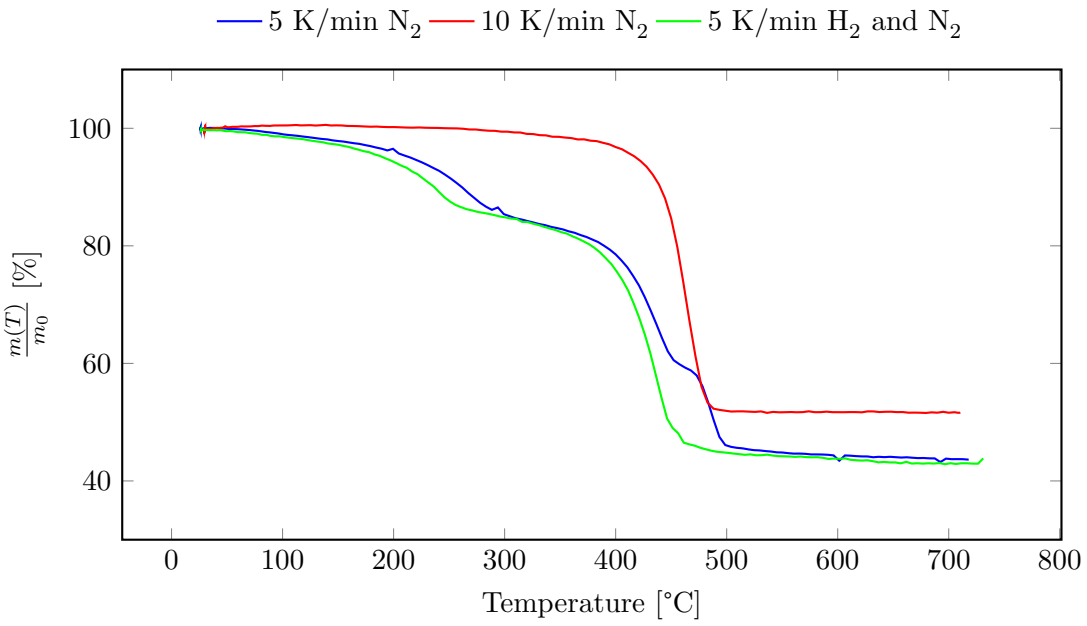

Figure 5.2: Thermogravimetric curves of magnesium carbonate

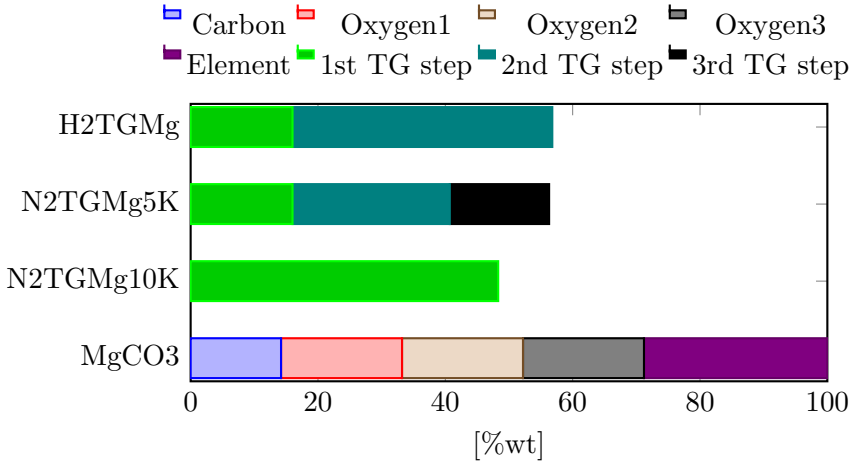

Figure 5.3: Composition of magnesium carbonate compared to the mass loss encountered in the thermogravimetric experiments. *H2TGMg: nitrogen and hydrogen flow 50 ml/min each, heating rate at 5 K/min; N2TGMg5K nitrogen flow of 30 ml/min and 5 K/min heating rate; N2TGMg10K nitrogen flow of 30 ml/min and 10 K/min heating rate*

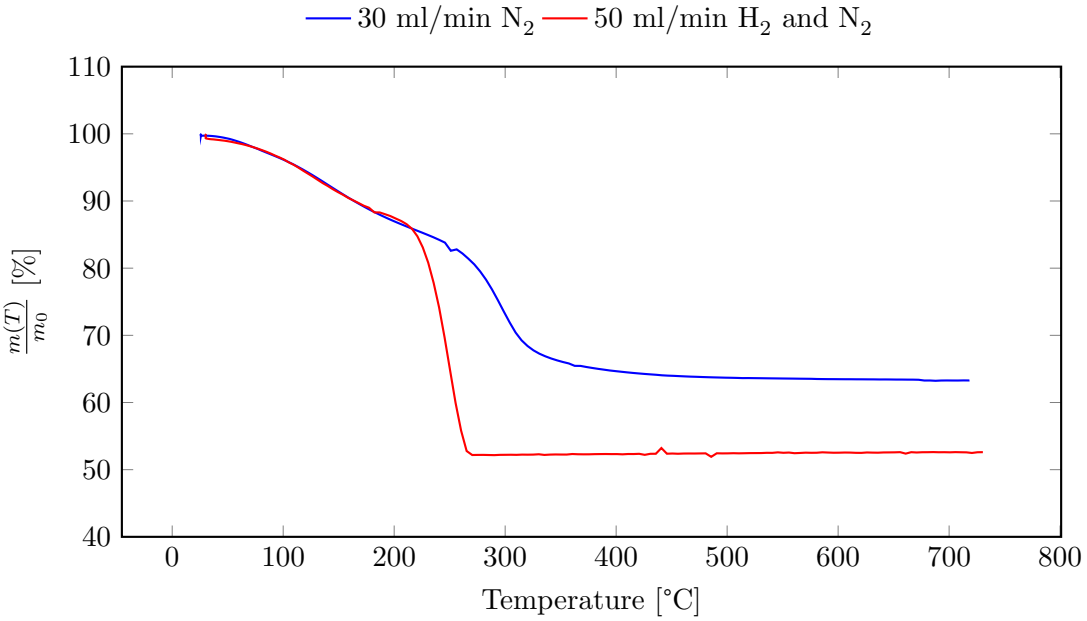

Figure 5.4: Thermogravimetric curves of nickel carbonate

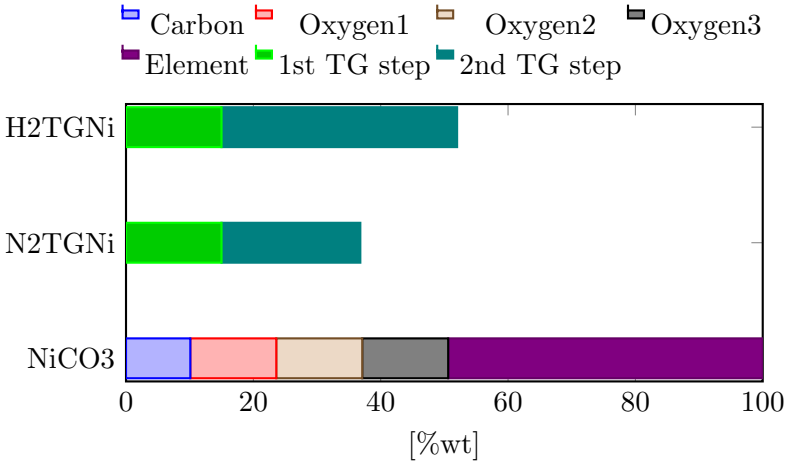

Figure 5.5: Composition of nickel carbonate compared to the mass loss encountered in the thermogravimetric experiments. *N2TGNi: nitrogen flow of 30 ml/min, H2TGNi: nitrogen and hydrogen flow 50 ml/min each*

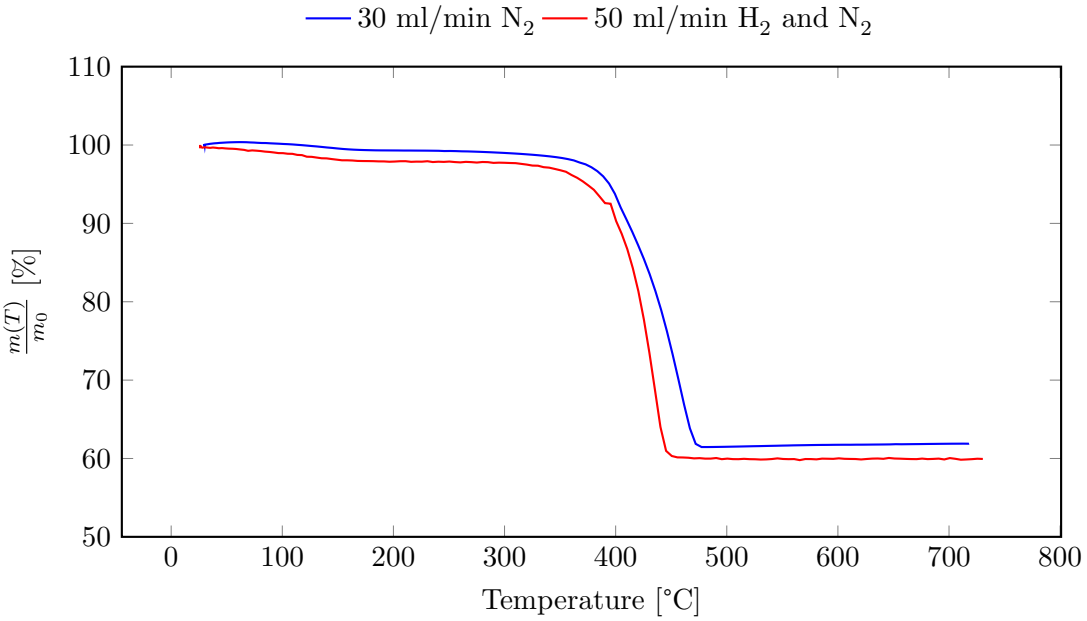

Figure 5.6: Thermogravimetric curves of manganese carbonate

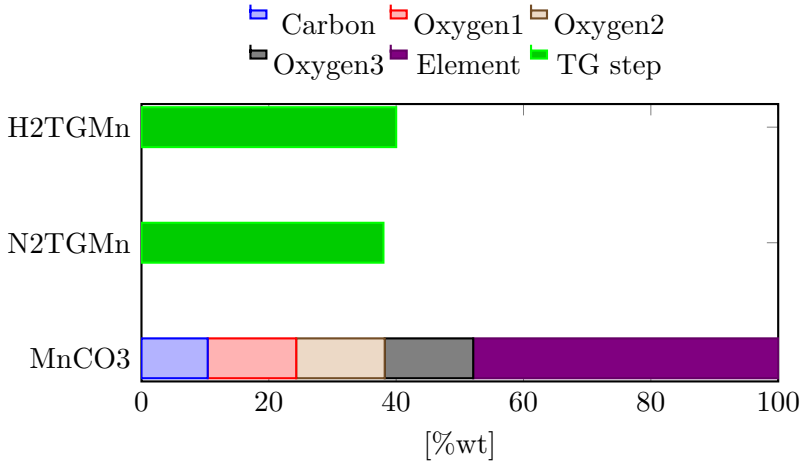

Figure 5.7: Composition of manganese carbonate compared to the mass loss encountered in the thermogravimetric experiments. *N2TGMn: nitrogen flow of 30 ml/min, H2TGMn: nitrogen and hydrogen flow 50 ml/min each*

are shifted, also the end mass corresponding to this TG step is decreased. This could be a sign for a different reaction or reaction mechanism to occur.

Nitrogen atmosphere leads to a mass loss of 26 % with a $T_{e,o}$ of 462 °C, a $T_{e,f}$ of 502 °C, and at T_{PoI} of 478 °C. These temperatures are decreased when hydrogen is present, namely to a $T_{e,o}$ of 402 °C, a $T_{e,f}$ of 445 °C, and at T_{PoI} of 426 °C. The mass loss, on the other hand, increases from 26 to 33 %.

Hydrogen atmosphere leads to a broad step in the thermogram after the first characteristic TG step described above. This broad step also seems to occur when nitrogen is present, but at a considerably higher temperature. The end mass of about 54 % is reached at about 650 °C when hydrogen is present. Nitrogen atmosphere, indeed, leads to an end mass of 68 % at 718 °C.

Figure 5.9 (p. 53) shows that the assignment of mass losses to reactions occuring during a thermogravimetric experiment is not easy without further gas and solid analysis. Additionally, it is not known if the residue of the sample consists of further carbonic acid salts which could be decomposed. Nevertheless, the mass loss in nitrogen atmosphere could be due to the thermal decomposition of iron carbonate to iron oxide and carbon dioxide. The use of hydrogen could have led to the formation of elemental iron. The total mass loss of 32.6 % is significantly higher than the carbon dioxide content of iron carbonate (27.0 %) but still lower than the theoretical carbonate content (36.8 %).

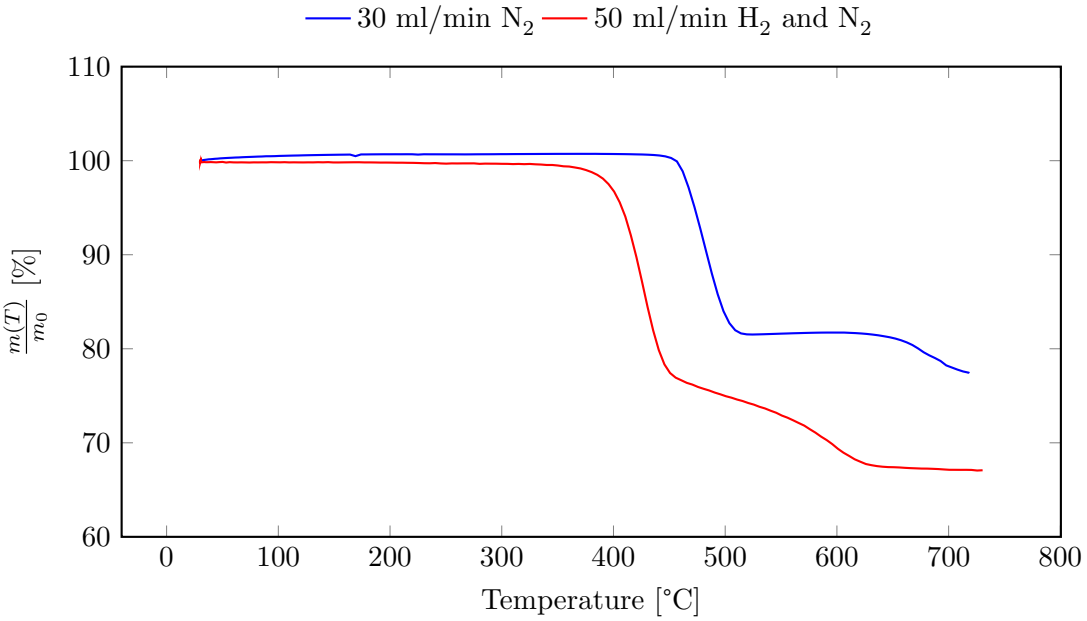

Figure 5.8: TG curves of siderite under nitrogen and hydrogen

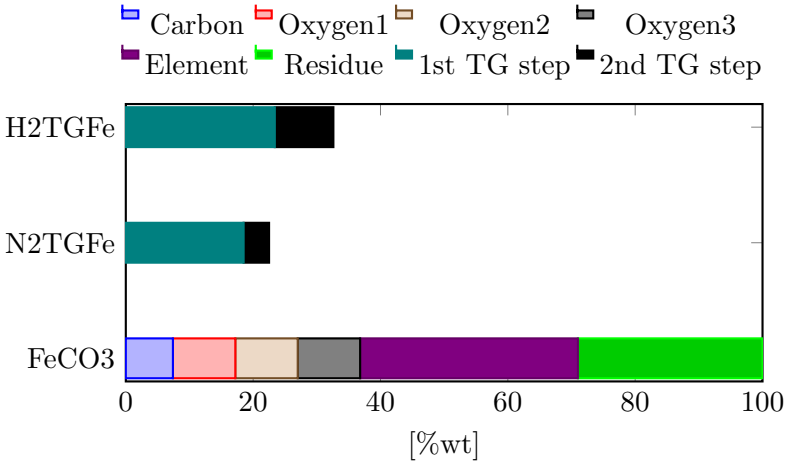

Figure 5.9: Composition of the siderite sample compared to the mass loss encountered in the thermogravimetric experiments. *N2TGFe: nitrogen flow of 30 ml/min; H2TGFe: nitrogen and hydrogen flow 50 ml/min each*

6 Commissioning of the tubular reactor system

6.1 Description of the reactor system

The reactor system was manufactured by Parr Instruments[1]. All pipes connecting parts of the reactor system are made of stainless steel with an outer diameter of 6.35 mm (0.25 inch). The reactor tube has an inner diameter of 2.54 cm (1 inch) and can be used for pressures as high as 345 bar at a maximum of 550 °C internal temperature. A casing with a pre-heating coil is placed inside the reactor tube to locate the thermocouples for internal temperature measurements. The heater consists of three separately controllable heating zones with an internal thermocouple for each zone. Figure 6.1 (p. 55) shows a picture and the process diagram of the reactor system issued by Parr Instruments. The system installed at the CEET does not include a mass flow controller at the third gas input and includes only one liquid input with a HPLC pump. Nevertheless, these options can be added later.

6.1.1 Product handling

There are three gas inputs, whereas two of them can be controlled with a Bronkhorst massflow controller (MFC). Liquids can be introduced into the reactor with a Knauer 'Smartline 100' HPLC pump at a maximum flow rate of 50 ml/min. The placement of powdery reactants is not as simple as the introduction of gases and liquids. Two possibilities have been tested during the commissioning: the impregnation of glass wool with a powder and the placement of the powder in a cartridge. Therefore, the stainless steel cartridge depicted in Figures 6.2 and 6.3 (p. 56) was designed by the author and manufactured at the CEET. The use of the cartridge disclosed various advantages compared to the use of the glass wool:

- Easier placement into the reactor
- Easier and more precise weighing before and after the reaction
- Easier handling of hazardous substances

Gaseous and liquid reaction products are transported by the constant gas stream. A condenser is placed after the reactor tube outlet. The cooling medium of the condenser has to be gaseous or liquid. The cooling medium of the reactor setup commissioned is water cooled with a thermostat to 13 °C. Condensed liquids are collected in a 1200 ml

[1] Manufacture-code: 5403C-SS-230-ST3(24)-4500-PCC-GF(2)-PLLF(1)-ISP-ITW-CHX-GLS(1200ml)-AP-CE/PED

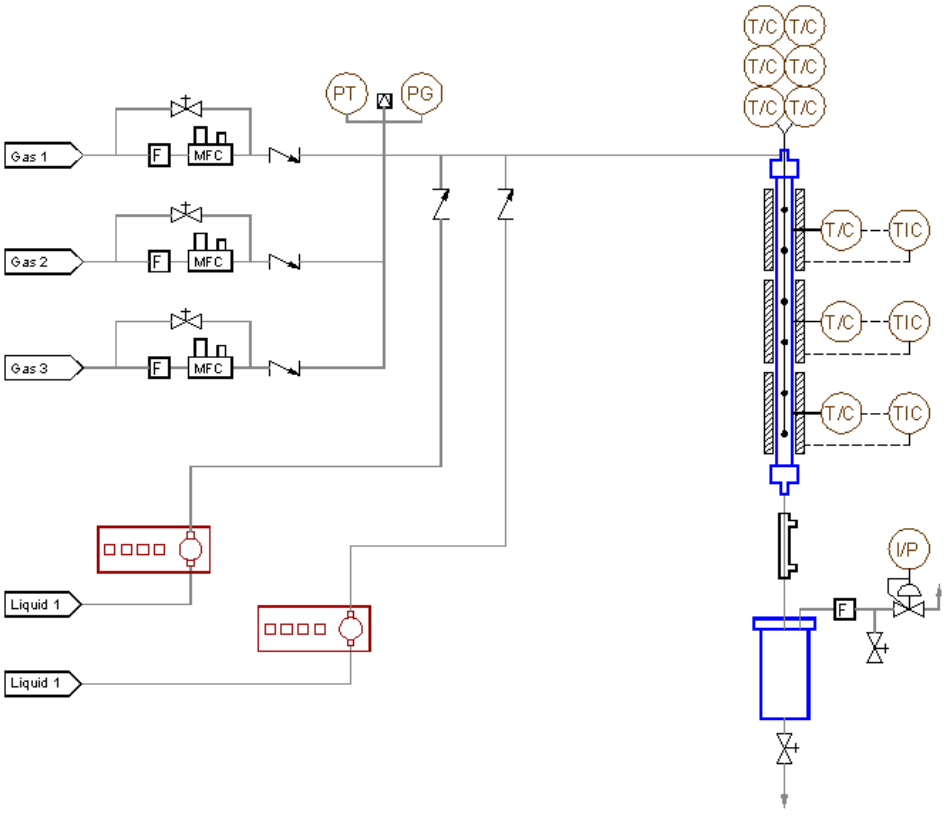

Figure 6.1: Picture and process diagram (provided by Parr Instruments) and of the reactor system. The system installed at the CEET does not include a mass flow controller at the third gas input and includes only one liquid input with a HPLC pump.

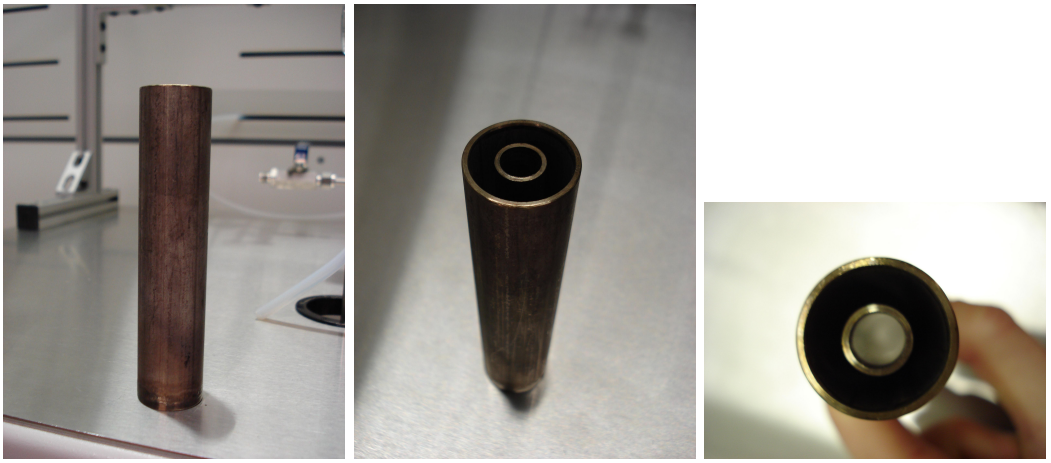

Figure 6.2: Cartridge for powder handling

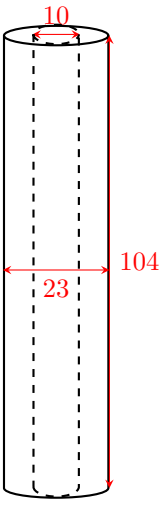

Figure 6.3: Sketch of the cartridge 1:1.67, wall thickness = 1.5 mm, measures are given in mm including the wall

high-pressure condensing vessel. The gaseous outlet of the reactor is controlled by an ABB back pressure regulator. As this regulator does not allow a continuous flow at pressures below 20 bar, the author installed a bypass with a manually adjustable valve.

6.1.2 Reactor control system

A Parr 4871 Process controller together with the SpecView HMI (human machine interface) is used to control the reactor system via a point-to-point Ethernet connection. The process variables that can be adjusted are the gas and liquid input flow, the output of the back pressure regulator, and the power of the three heaters. The current value of the reactor pressure and the temperature inside the reactor at six different positions are visualized in different windows. Figure 6.4 (p. 58) shows the main window of the SpecView HMI. The user interface was programmed by technicians during the setup of the reactor system by Parr Instruments. A detailed description of the control system is given in the document `914147 - Tubular Reactor Control System.doc` created on the July 22, 2013 during the setup of the reactor system by technicians of Parr Instruments. Additionally, the user can alter the views and settings using the configuration mode of the SpecView HMI.

The general way to adjust a process variable is to create a 'loop' and a controller for the wanted process variable. Such a controller shows the process variable (PV), the set point (SP), the controller output, and the status of the controller (auto or manual). Four buttons are integrated in a controller. The SP button is used to change the set point, the OP button is used to adjust the controller output in a range from -5 to 105 %. To be able to manually alter the controller output, the controller has to be set to manual mode. This can be done with the A/M button. Clicking the PAR button opens a separate window to display the controller parameters like the alarm set points. Most of the controller parameters can be changed in that window.

The value of all process variables and parameters is automatically logged. The user can create log reports for selected variables in a predefined time span. With this feature at hand, experimental data can be stored and analyzed with other programs and routines.

6.2 Gas analysis equipment

6.2.1 Description of the equipment

The gaseous output of the reactor has to be analyzed continuously. Therefore, an ABB Advance Optima 2020 continuous gas analyzer system for carbon monoxide, carbon dioxide, methane, and hydrogen detection was purchased. The analyzer system consists of two 486.6 by 177.8 mm (19 by 7 inch) housings. The first housing contains the control unit, the second housing contains the two analyzers. A Uras26 infrared photometer is used for the carbon monoxide, carbon dioxide, and methane detection in a range of 0 to 100 vol%. A Caldos27 thermal conductivity analyzer is used for the hydrogen detection in a range of 0 to 100 vol%. The gas analyzers need a continuous gas flow of 10-90 l/h at a relatively constant temperature in the range of 5-50 °C. The power supply of the central unit is integrated in the housing and can be directly connected to a socket. The analyzers need additional power supply of 95 W (Uras26) and 12 W (Caldos27), respectively, at 24 V DC. Therefore, a RS AS-120P 120 W desktop power supply was purchased. To supply

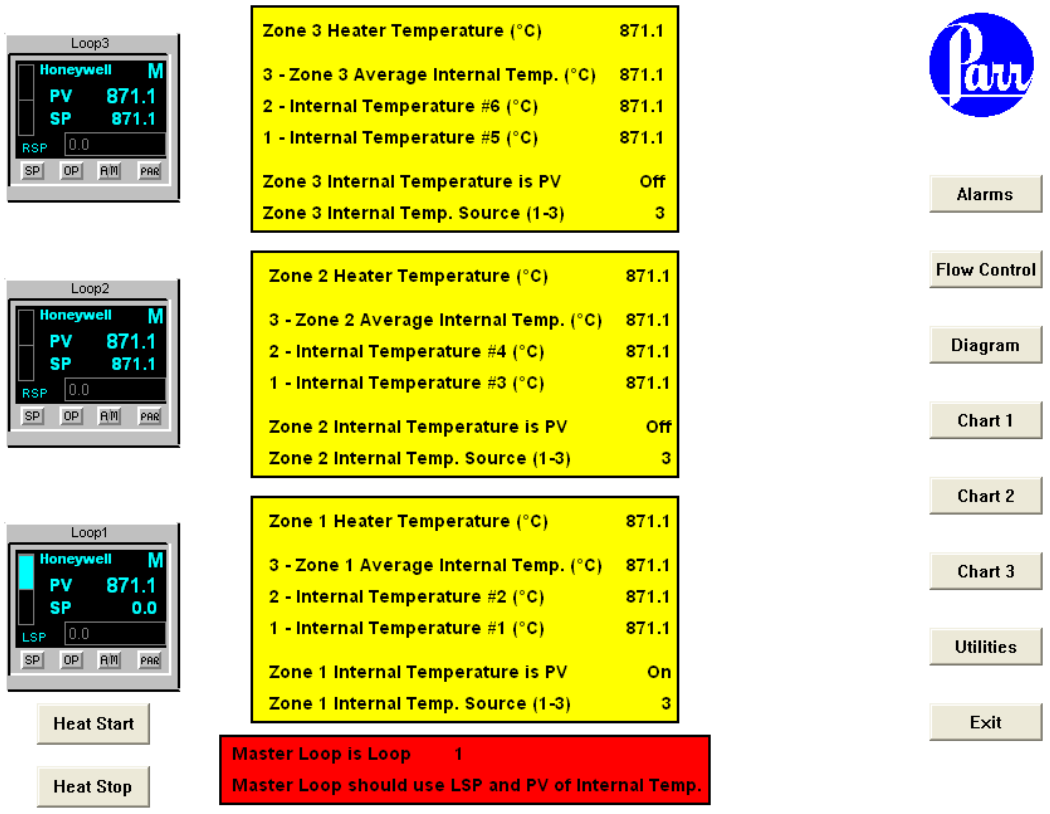

Figure 6.4: Main window of the SpecView HMI in its version of July 2013

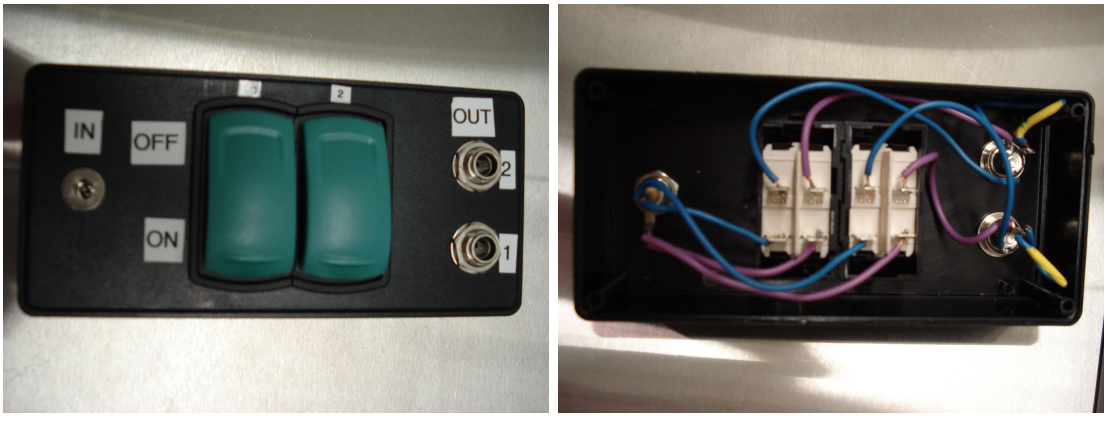

Figure 6.5: Switch box for the power supply of the analyzers, blue: +, violett: -

both analyzer modules, the switch box depicted in Figure 6.5 on page 58 was designed and assembled in the lab. Standard plugs and sockets (central pin = plus) were used for this box.

The analyzed gas stream should not contain condensable gases, as this would adulterate the measurements and lead to problems with the analyzers. As a consequence, gas conditioning and the installation of a pump was necessary. The pump installed is a two-way Behr diaphragm pump. The pumping rate of the first pumping way can be controlled with a potentiometer. This pumping way is used in the setup installed during this Master's thesis. The second pumping way runs constantly at maximum rate. As there is no flow indicator, the flow rate was determined experimentally (see Section 6.3.1, p. 61). A Hartmann und Braun CGEK-5 sample gas cooler is used to achieve a constant sample gas temperature and remove condensable gases. The sample gas cooler has two gas in- and outputs. Condensed gases of the first input are removed by a peristaltic pump. This input is used in the experimental setup installed during this Master's thesis. Condensed gases of the second input are collected in a container. The display of the sample gas cooler shows the temperature at the surface of the chiller.

6.2.2 Analyzer rack

The sample gas cooler, the diaphragm pump, the control unit housing, and the analyzer housing had to be installed into a common rack. Therefore, the building kit system *Item24* (distributed by Haberkorn in Austria) was used. This kit system is based on aluminum profiles with T-slot nuts. A lot of additional equipment to connect profiles and mount equipment is available. The profile used for the analyzer rack is called 'Profile 8 40 x 40, natural' with an edge length of 40 mm. This profile was selected because of its robustness and the fact that most additional equipment like rebate profiles is only available for this kind of profile. To allow future adaptions of the rack, the profiles were connected with angle brackets as most other connectors would need manipulation (threading, drilling, etc.) of the profile. Figure 6.6 (p. 60) shows the flowchart of the analyzer rack, including the pin numbers for connecting the sample and purge gas lines.

Figure 6.7 (p. 60) shows pictures of the rack from different perspectives. The total height of the rack without wheels is 1420 mm, the width is 456 mm, and the depth without equipment is 413 mm. At the bottom of the rack a stainless steel collection pan (437 x 395 mm) is placed on four rebate profiles without further fixation. The sample gas cooler is mounted above this pan by direct fixation with four M8 screws at two points of two profiles at the back of the rack. Above the sample gas cooler a stainless steel plate (446 x 146 mm, referred to as 'platform') is mounted on rebate profiles with four M5 screws and screw nuts. The pump, the power supply, and the switch box for the analyzer unit are placed on the platform. On the right hand side of the platform (seen from the front) a switchable 5-way outlet strip is mounted on a profile using two M5 screws. The analyzer and control unit housings are mounted above the platform. They rest on two rebate profiles, each. Moreover, the housings are attached to the front of the rack with four M6 screws (two on each side). The top of the rack is covered with a 446 x 403 mm stainless steel plate. This top plate is mounted with four M8 screws and screw nuts to four 'V8 40' angle brackets.

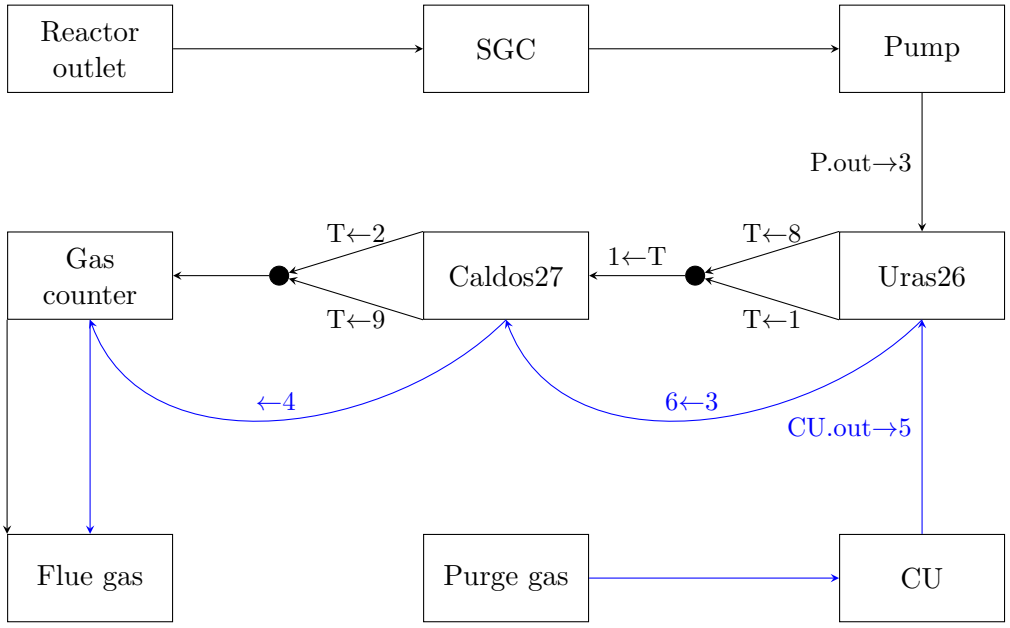

Figure 6.6: Flowchart of the analyzer rack, pin numbers are reprinted near arrows; black: sample gas line, blue: purge gas line, SGC: sample gas cooler, CU: central unit, T:tee

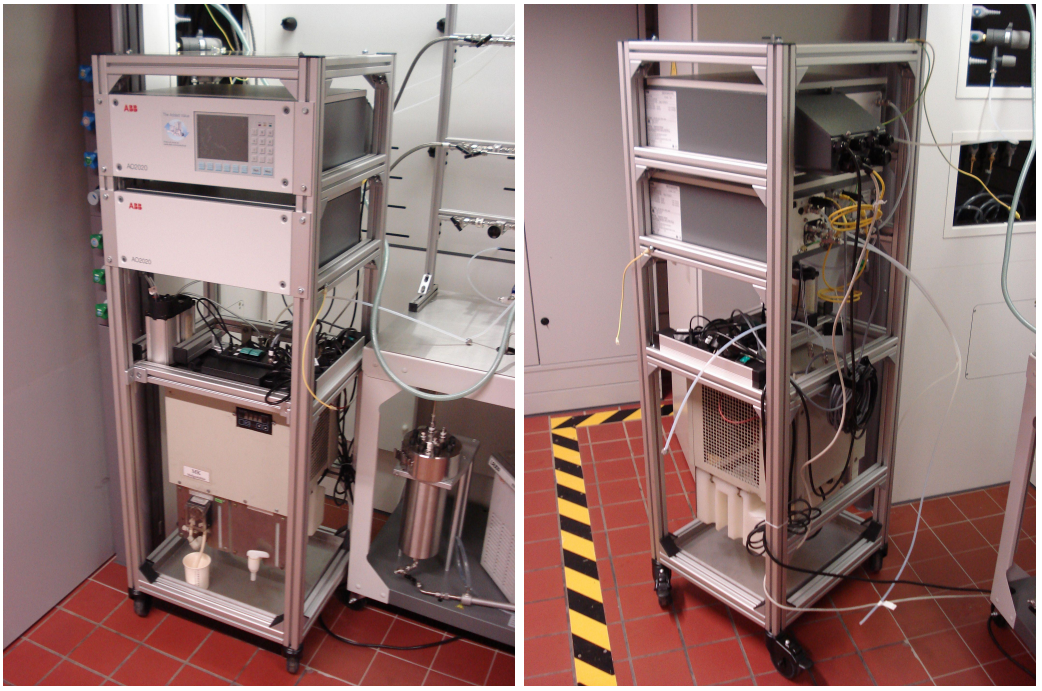

Figure 6.7: Analyzer rack from different perspectives: front view (left), back view (right)

Table 6.1: Results of the experiments conducted to determine the flow rate of the pump

Pumping way	Poti. position	Nr. of exp.	Flow rate [l/h]
I (adjustable)	10 o'clock	5	49 ± 2
I	12 o'clock	10	51 ± 5
I	3 o'clock	5	106 ± 4
I	maximum	10	130 ± 6
II (not adjust.)	n/a	10	120 ± 11

6.3 Commissioning experiments

6.3.1 Determination of the pump flow rate

The two-way Behr diaphragm pump is used to supply the gas analyzers with a continuous gas stream sidelined from the reactor gas outlet. The first pumping way can be controlled using a potentiometer. Unfortunately, there are no marks surrounding this potentiometer to indicate the pump duty. The second pumping way works at a constant rate. To determine the flow rate of both pumping ways, the following experimental procedure was used:

A graduated 500 ml cylinder is filled with water and a container with a capacity of at least 10 l is half filled with water. A support stand with a support clamp suitable for the graduated cylinder is placed behind the container. Then, the open end of the graduated cylinder is closed with one hand and submerged into the half filled container, so that only a 3-5 cm broad part of the cylinder is filled with air, the rest of the graduated cylinder should remain full of water. The graduated cylinder is fixed to the support stand with the clamp. A hose is connected to a pumping way of the Behr diaphragm pump. This hose is then introduced into the graduated cylinder. The pump, most possibly placed at a higher level than the cylinder and container, is turned on and the time required to displace the water in the graduated cylinder and the displaced volume are measured simultaneously.

Table 6.1 shows the results of the experiments. The flow rate for pumping air at 25 °C could be determined to be 51 ± 5 l/h when the adjustable pumping way I is used with the potentiometer in 12 o'clock position. The necessary flow rate for the analyzers is 10-90 l/h. Therefore, the adjustment with the hoses connected to the adjustable pumping way I with the potentiometer in 12 o'clock position is used in the analyzer rack commissioned.

6.3.2 Heating experiments

The purpose of the heating experiments was to investigate the temperature distribution within the reactor tube and the response of the analyzers to possible gaseous products. No heating program was used. Instead, the heater power was adjusted manually in order to reach a specific temperature inside the reactor. Furthermore, the pressure constancy and its dependence on the gas flow rate was investigated. The aim was to keep the pressure constant while the pump for the analyzers sidelined a continuous flow. This was done by manually changing the gas flow rate using the SpecView HMI and adjusting the valve of the bypass around the back pressure regulator.

The temperature measured inside the reactor tube (T1 - T6), the heater temperatures,

the reactor pressure, and the gas flow rates were recorded using the SpecView HMI. The concentration of carbon monoxide, carbon dioxide, methane, and hydrogen was measured continuously with the ABB Uras26 and Caldos27 analyzers. As there was no software available to record the concentration data, the data was noted every few minutes and when a concentration change took place. The powder cartridge (depicted in Figure 6.2, p. 56) was used in all four heating experiments.

Figures 6.8 (p. 64) to 6.11 (p. 73) show physically non-existent 'negative pressures' inside the reactor. This is due to the representation of atmospheric conditions by the pressure indicator of the reactor. This indicator shows a value between -0.2 and zero bar when the reactor is operated at atmospheric conditions.

Heating of magnesium carbonate in nitrogen atmosphere

5.160 g (61.20 mmol) of magnesium carbonate granulate (a special sample of MagGranMC provided by Magnesia Germany) were placed into the cartridge and loaded into the reactor tube from the bottom. Two spacers with a total length of 178 mm were placed below it. Therefore, the nearest thermocouple to the sample is T2. After the experiment the reactor was cooled to room temperature over night. The sample did not show any visible changes. The weight loss of the sample was 2.684 g (31.83 mmol) equal to 52.02 wt%. Figure 6.8 (p. 64) shows two diagrams with the relevant experimental information. No liquids were found in the condensing vessel and only carbon dioxide could be detected in the flue gas. The course of the experiment can be divided into the following phases:

1. Heat with full power to reach 490-510 °C at T4
2. Hold temperature inside the reactor by heating with varying power
3. Turn off heaters
4. Cool-down and shutdown

In the first phase (until minute 88) the heaters were set to full power until the temperature of thermocouple T4 indicated a relatively constant temperature of 500 °C. Figure 6.8 (p. 64) shows that it took 70 minutes to increase the temperature of the mid heater from room temperature to 550 °C. The three heaters show a comparable heat-up behavior in the starting phase. Nevertheless, the heating rate decreases from bottom to top. After 88 minutes a temperature of 497 °C was reached at T4.

In the second phase (minute 88 to 261) the heating power of all three heaters was adjusted manually to reach a relatively constant temperature of 500 °C at T4. The heater temperatures show a saw-tooth form in this phase. The temperatures inside the reactor, on the other hand, show a sinusoidal form. Even though the heaters operate in a comparable temperature range, the temperature difference inside the reactor remains at a relatively constant high level. Table 6.2 (p. 63) shows the mean temperature inside the reactor between minute 100 and 225. The mean temperature can be sorted in the following form: T4 (506 ± 8 °C) > T3 (499 ± 8 °C) > T5 (488 ± 7 °C) > T2 (459 ± 8 °C) > T6 (417 ± 7 °C) > T1 (356 ± 6 °C). In the mid of the reactor tube (T4 and T3) and one positions above (T5) and below (T2) the temperature is relatively equally distributed (459 ± 8 to 506 ± 8 °C).

Table 6.2: Thermocouple position from top to bottom and mean temperature between minute 100 and 225 (magnesium carbonate in nitrogen atmosphere)

Position	T_{av} [°C]
T6	417 ± 7
T5	488 ± 7
T4	506 ± 8
T3	499 ± 8
T2	459 ± 8
T1	356 ± 6

At the outermost positions T6 (top) and T1 (bottom), however, the temperature drops notably.

Figure 6.8 (p. 64) shows that after 51 minutes at a temperature of 170 °C (measured at T2) carbon dioxide was detected for the first time. The carbon dioxide concentration then gradually rose to 3.2 vol% (minute 105, 461 °C at T2) and dropped back to zero (minute 235). This behavior could be due to the complete thermal decomposition of magnesium carbonate to magnesium oxide and carbon dioxide. Furthermore, the mass loss of the sample accounts for 52.02 wt%. The carbon dioxide content of magnesium carbonate accounts for 52.20 mol% (= wt%). The difference between these values is relatively small, namely 0.18 wt%.

The nitrogen flow rate was manually adjusted to reach a constant reactor pressure in the range of 0.7-1.0 bar. Therefore, the nitrogen flow was set to 500 sccm at the beginning of the experiment, then raised to 800 sccm (minute 17) to increase the reactor pressure and decreased to 500 sccm (minute 25) at first and then to 450 sccm (minute 33) to hold the pressure. As the reactor pressure was still between 1.2 and 1.3 bar, the nitrogen flow was decreased to 400 sccm (minute 81) until the pressure reached 0.7 bar (minute 107). The flow was increased to 450 sccm again (minute 119). This resulted in an average pressure of 0.70 ± 0.03 bar between minute 107 and 251.

The experiment was stopped when the carbon dioxide concentration reached zero vol% (minute 235) and the cool-down phase was introduced. The mid and bottom heaters were turned off at minute 200 and the top heater at minute 238. The heater temperature and the temperature inside the reactor in the respective heating zone gradually decreased after the shutdown of the heater. The faster cooling after minute 251 was due to opening of the heating jacket.

Heating of magnesium carbonate in 20 vol% hydrogen atmosphere

5.069 g (60.16 mmol) of magnesium carbonate granulate (a special sample of MagGranMC provided by Magnesia Germany) were placed into the cartridge and loaded into the reactor tube from the bottom. Two spacers with a total length of 178 mm were placed below it. Therefore, the nearest thermocouple to the sample is T2. After the experiment the reactor was cooled to room temperature over night. The sample did not show any visible changes. The weight loss of the sample was 2.5787 g (30.58 mmol) equal to 50.87 wt% (mol%). Figure 6.9 (p. 67) shows two diagrams with the relevant experimental information. No

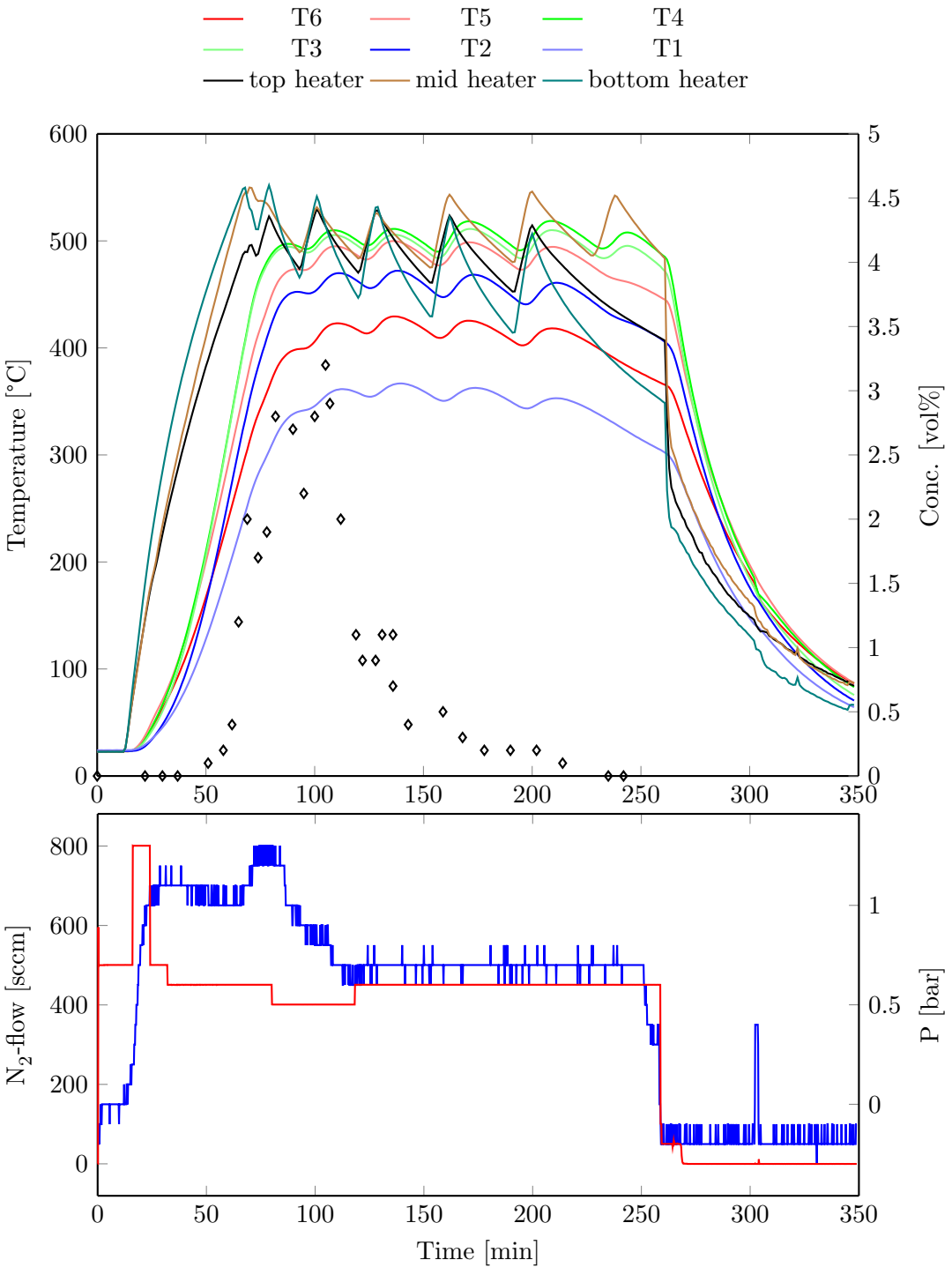

Figure 6.8: Heating of magnesium carbonate in nitrogen atmosphere. *Above:* Temperature inside the reactor (T6: top to T1: bottom), heater temperatures, and carbon dioxide concentration in the flue gas (diamonds). *Below:* Pressure (blue) and nitrogen flow (red)

liquids were found in the condensing vessel. The only gases detected were carbon dioxide and hydrogen.

Before the heaters were turned on, the reactor was filled with nitrogen at a flow rate of 200 sccm. Then, the hydrogen flow was turned on and the ratio of nitrogen to hydrogen flow was always kept at 4:1. Therefore, the theoretical hydrogen concentration in the flue gas is 20 vol%. This preparation phase is not shown in Figure 6.9 (p. 67). Figure 6.9 (p. 67) shows the course of the experiment starting shortly before the heaters were turned on for the first time. In the first 37 minutes shown in the upper diagram of Figure 6.9 (p. 67) the hydrogen concentration in the flue gas increased from 14 to 19.1 vol% as the hydrogen flow was turned on shortly before. Between minute 37 and 273 the average concentration of hydrogen in the flue gas reached 19.5 ± 0.1 vol%. The course of the experiment can be divided into the following phases:

1. Heat with full power to reach 235-245 °C at T2
2. Hold temperature
3. Heat with full power to reach 315-325 °C at T2
4. Hold temperature
5. Heat with varying power to slowly reach 430-470 °C at T3
6. Turn off heaters
7. Cool-down and shutdown

In the first phase all three heaters were set to full power until the bottom heater reached 404 °C (minute 40). Then the heaters were turned off until the temperature inside the reactor stayed constant over several minutes. No change in the flue gas composition took place and the heaters were turned back on (minute 80) in full power until the bottom heater reached 438 °C (minute 90). The temperature inside the reactor started to increase simultaneously to the heater temperature. Carbon dioxide was detected for the first time at minute 93 and 282 °C at T2 in a concentration of 0.2 vol%. T2 reached 316 °C at minute 102. The heaters were turned back on again at minute 104, first at full power for several minutes. Then the heaters were operated in varying power settings.

At the beginning of the fifth phase, temperature T2 shows a broad peak with a local maximum at minute 138 and a temperature of 433 °C. T2 decreases to 418 °C until minute 157 and increases henceforward to 469 °C at minute 235. The temperature is not equally distributed inside the reactor. Table 6.3 (p. 66) shows that the mean temperature at the mid positions T4 and T3 and the second top position T5 lie within 50 °C. The mean temperature can be sorted in the following way: T4 (484 ± 23 °C) > T3 (478 ± 22 °C) > T5 (473 ± 16 °C) > T2 (442 ± 16 °C) > T6 (408 ± 12 °C) > T1 (342 ± 11 °C).

The carbon dioxide concentration increased successively in the third, forth, and in the beginning of the fifth phase of the experiment until it reached 1.7 vol% at minute 123 (T2 at 383 °C, heaters turned off). It dropped to 1.3 vol% at minute 126 and rose again when the mid and bottom heaters were turned back on. Furthermore, the carbon dioxide concentration continuously decreased between minute 134 (432 °C at T2) and 181 (426 °C

Table 6.3: Thermocouple position from top to bottom and mean temperature between minute 138 and 268 (magnesium carbonate in 20 vol% hydrogen atmosphere)

Position	T_{av} [°C]
T6	408 ± 12
T5	473 ± 16
T4	484 ± 23
T3	478 ± 22
T2	442 ± 16
T1	342 ± 11

at T2) from 2 to 0.6 vol%. Between minute 181 and 273 the carbon dioxide concentration increased from 0.6 vol% to 1.8 vol% (minute 200, 452 °C at T2) and decreased back to zero vol%. As no more carbon dioxide could be detected after minute 273, the bottom and top heater were turned off. The heating jacket was opened at minute 308. The total mass loss (50.87 wt%) nearly corresponds to the carbon dioxide content of pure magnesium carbonate (52.20 wt%), the difference of 1.33 wt% could be due to a too short reaction time or weighing errors. The decay of the carbon dioxide concentration between minute 138 and 157 proceeded concurrently to the heaters being turned off and a temperature loss at T2. This could be a sign for the endothermic character of the thermal decomposition of magnesium carbonate. The reaction enthalpy[2] $\Delta_R H$ for the thermal decomposition of magnesium carbonate lies in the range of 98.019 kJ/mol at 400 °C to 96.291 kJ/mol at 500 °C. Furthermore, the carbon dioxide concentration started to rise again when the heaters were turned back on.

The lower diagram in Figure 6.9 (p. 67) shows that the nitrogen to hydrogen ratio was kept at 4:1 until the cool down phase of the experiment. Until minute 280 the pressure inside the reactor varied between 0.5 and 0.9 bar, with an mean value of 0.8 ± 0.2 bar. The mean total flow until minute 280 was relatively constant at 468 ± 24 sccm. At the beginning of the cool-down phase the nitrogen flow was increased for six minutes to 640 sccm and the hydrogen flow to 160 sccm for four minutes before it was turned off. The nitrogen flow was set to 200 sccm for 10 minutes, then increased to 500 sccm for 17 minutes to replace remaining hydrogen before the system was turned off.

Heating of siderite in nitrogen atmosphere

4.005 g of ground siderite (a special sample of July 2, 2013 provided by VA Erzberg, for composition see Table 5.1, p. 44) with an iron carbonate content of 2.844 g (24.56 mmol) were placed into the cartridge and loaded into the reactor tube from the bottom. Two spacers with a total length of 178 mm were placed below the cartridge. Therefore, the nearest thermocouple to the sample is T2. After the experiment the reactor was cooled to room temperature over night. The sample color changed from brown to black. The weight loss of the sample was 0.283 g. No liquids were found in the condensing vessel. The only gas detected was carbon dioxide.

Before the heaters were turned on, the reactor was filled with nitrogen at a flow rate of

[2]Enthalpy values calculated with HSC Chemistry© 3.0 for Windows

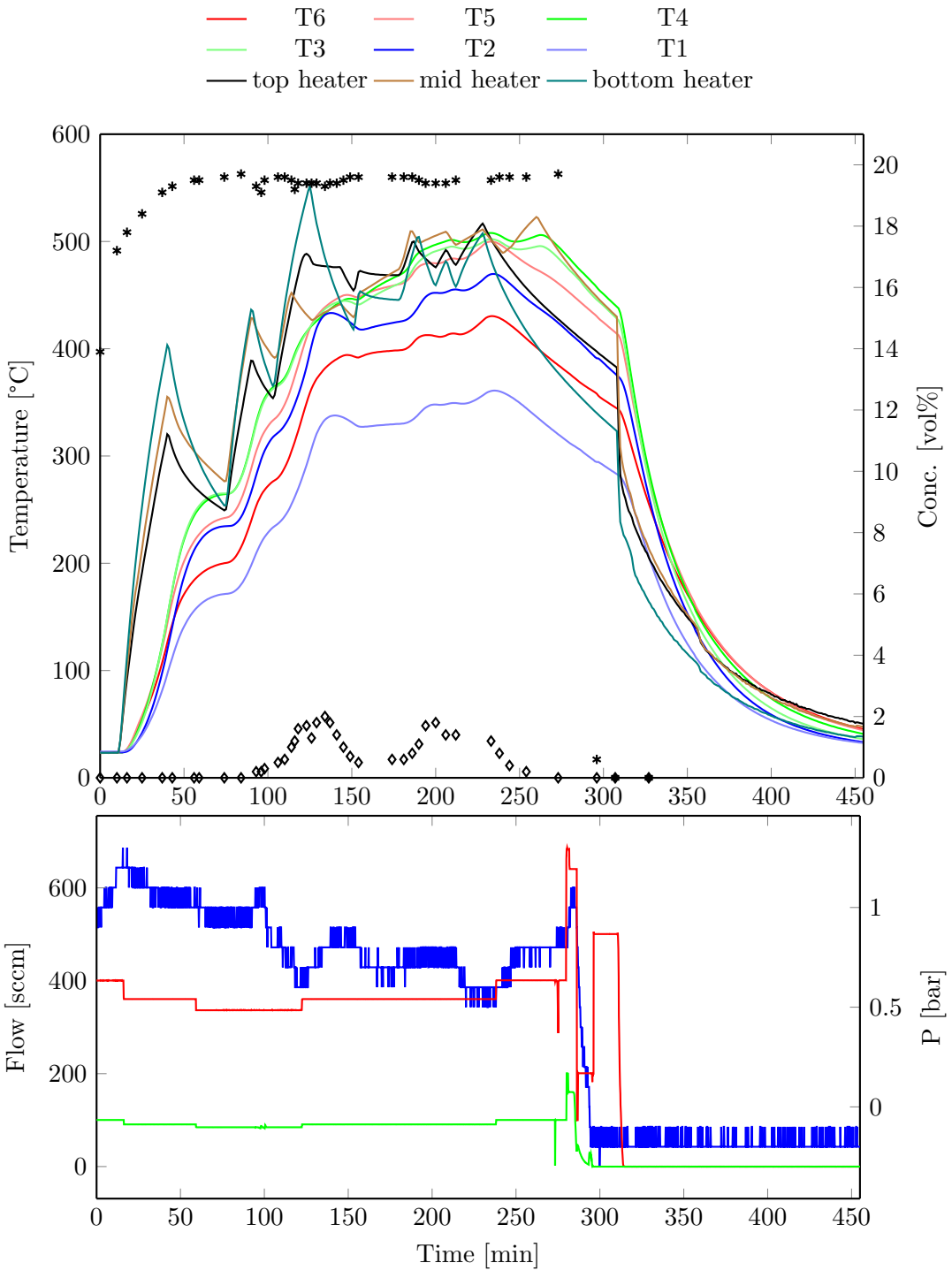

Figure 6.9: Heating of magnesium carbonate in hydrogen atmosphere. *Above:* Temperature inside the reactor (T6: top to T1: bottom), heater temperatures, carbon dioxide (diamonds), and hydrogen (asterisk) concentration in the flue gas. *Below:* Pressure (blue), nitrogen flow (red), and hydrogen flow (green)

Table 6.4: Thermocouple position from top to bottom and average temperature between minute 125 and 275 (siderite in nitrogen atmosphere)

Position	T_{av} [°C]
T6	412 ± 10
T5	478 ± 9
T4	486 ± 7
T3	491 ± 7
T2	479 ± 12
T1	378 ± 13

680 sccm to reach a reactor pressure of 1.0 bar. This preparation phase is not shown in Figure 6.10 (p. 70). Figure 6.10 (p. 70) shows two diagrams with the relevant experimental information of the course of the experiment starting shortly before the heaters were turned on for the first time. The experiment can be divided into the following phases:

1. Heat with full power to reach 305-315 °C at T2
2. Stop heating and wait for several minutes
3. Heat with varying power to slowly reach 450-490 °C at T2 and hold temperature
4. Turn off heaters
5. Cool-down and shutdown

All three heaters were set to full power at the beginning of the experiment. The bottom heater was turned off at 408 °C after 33 minutes, the mid heater at 412 °C after 41 minutes, and the top heater at 383 °C after 40 minutes. T2 reached 306 °C after 67 minutes and slowly increased to 315 °C seven minutes later at minute 74, denoting the end of phase two.

In the third phase of the experiment, the heaters were operated in varying power settings to slowly reach 450 °C at T2. At minute 125 T2 reached 450 °C and stayed above this temperature until minute 275. The mean temperature at T2 between minute 125 and 275 accounts for 479 ± 12 °C.

The bottom heater was turned off first, at minute 234 with a temperature of 550 °C. The mid and top heater were turned off simultaneously at minute 248 with a temperature of 507 (mid) and 503 (top) °C. By turning off the last heater, the cool-down phase began. The heating jacket was opened at minute 334.

As in the heating experiments with magnesium carbonate, the heat was not equally distributed within the reactor tube. Table 6.4 (p. 68) shows that the temperatures of the central part (T5, T4, T3, T2) of the reactor tube lie within 29 °C between minute 125 and 275. The outermost positions T1 and T6 show a higher deviation from the temperature in the central part.

Figure 6.10 (p. 70) shows that until minute 301 (in the mid of the cool down phase) the nitrogen flow rate was varied between 250 and 400 sccm, with a mean value of 294 ± 26 sccm. In the same time interval, the pressure varied between 0.7 and 1.6 bar, with a mean value of 0.9 ± 0.2 bar. In the cool-down phase the analyzers were disconnected from the

reactor as no more carbon dioxide was detected after minute 279. At minute 301 the bypass around the back pressure regulator (BPR) was opened to decrease the pressure to 0.3 bar and immediately closed again. The BPR was set to automatic mode and a set point of 0.8 bar. This was done to test the time needed to increase the pressure 0.5 bar at a constant nitrogen flow of 50 sccm. After 24 minutes the reactor pressure reached 0.8 bar, the pressure increase rate at 50 sccm can therefore be calculated to be 0.02 bar/min. Until minute 336 the pressure was kept at 0.8 ± 0.1 for 10 minutes by the BPR in automatic mode. The bypass around the BPR was fully opened and atmospheric pressure conditions were established immediately.

At minute 156 and 479 °C at T2 carbon dioxide was detected for the first time at a concentration of 0.1 vol%. The carbon dioxide concentration in the flue gas gradually increased to reach 0.3 vol%. It stayed constant at 0.3 vol% from minute 182 (495 °C at T2) to 205 (493 °C at T2) and decreased back to zero at minute 279. As the temperature in the central part of the reactor stayed relatively constant between minute 125 and 275 (see Table 6.4, p. 68) this increase and decline could be due to complete thermal decomposition or a high activation energy of the reaction, so that the thermal energy supplied is not high enough for a complete thermal decomposition. If the whole mass loss of 0.2832 g corresponds to the iron carbonate content of the sample, the mass loss of iron carbonate would account for 9.96 wt% (mol%). However, the carbon dioxide content of iron carbonate accounts for 37.99 wt% (mol%). Therefore, the thermal decomposition could have proceeded but not be completed in the experiment.

Heating of siderite in 20 vol% hydrogen atmosphere

4.046 g of ground siderite (a special sample of July 2, 2013 provided by VA Erzberg, for composition see Table 5.1, p. 44) with an iron carbonate content of 2.873 g (24.80 mmol) were placed into the cartridge and loaded into the reactor tube from the bottom. Four spacers with a total length of 278 mm were placed below the cartridge. Therefore, the nearest thermocouple to the sample is T3. The reactor was cooled to room temperature over night. The sample color changed from brown to black. The weight loss of the sample was 1.1436 g. No liquids were found in the condensing vessel. The Uras26 module of the ABB analyzer detected carbon dioxide and carbon monoxide in the flue gas. The Caldos27 analyzer showed a measurement drift during the experiment and needed to be calibrated afterwards. Therefore, no hydrogen concentration in the flue gas is shown in Figure 6.11 (p. 73).

Before the heaters were turned on, the reactor was filled with nitrogen to reach a reactor pressure of 1.0 bar. Then, the hydrogen flow was turned on and the ratio of nitrogen to hydrogen flow was mostly kept at 4:1. This preparation phase is not shown in Figure 6.11 (p. 73). Figure 6.11 (p. 73) shows two diagrams with the relevant experimental information of the course of the experiment starting shortly before the heaters were turned on for the first time. The experiment can be divided into the following phases:

1. Heat with full power to reach a heater temperature of 400-480 °C
2. Heat with varying power to slowly reach 430 °C at T3
3. Hold temperature at T3 between 430 and 505 °C

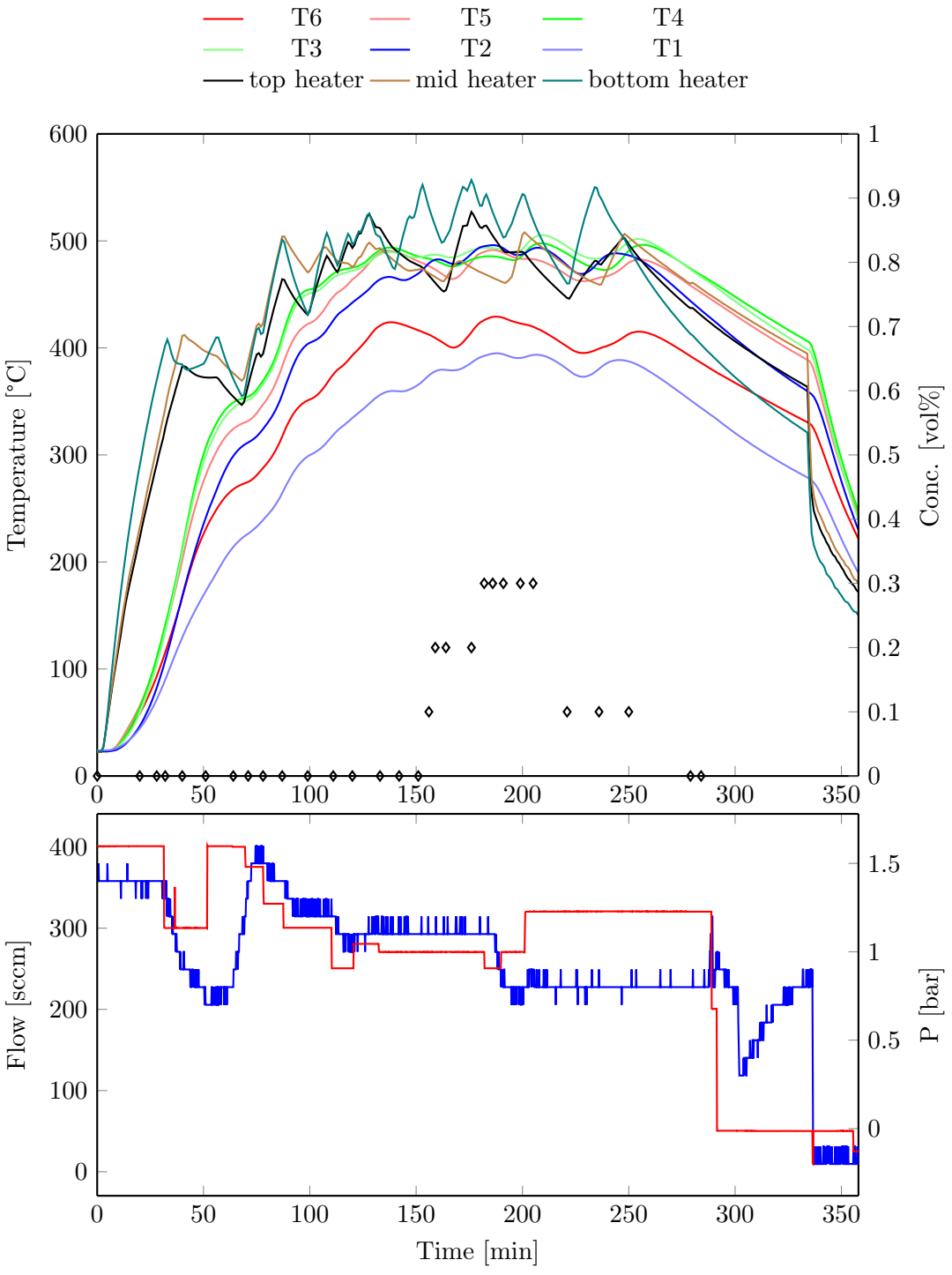

Figure 6.10: Heating of siderite in nitrogen atmosphere. *Above:* Temperature inside the reactor (T6: top to T1: bottom), heater temperatures, carbon dioxide concentration in the flue gas (diamonds). *Below:* Pressure (blue) and nitrogen flow (red)

Table 6.5: Thermocouple position from top to bottom and average temperature between minute 86 and 287 (siderite in 20 vol% hydrogen atmosphere)

Position	T_{av} [°C]
T6	391 ± 23
T5	459 ± 25
T4	472 ± 24
T3	473 ± 25
T2	456 ± 29
T1	365 ± 27

4. Turn off heaters

5. Cool-down and shutdown

All three heaters were set to full power at the beginning of the experiment. At minute 47 they were turned off simultaneously. The bottom heater showed a temperature of 479 °C, the mid heater 439 °C, and the top heater 409 °C, denoting the end of phase one. In the second and third phase of the experiment the heaters were operated with varying power settings.

The top heater was turned off first, at minute 211 and a temperature of 516 °C. The bottom and top heater were turned off simultaneously at minute 215 with a temperature of 509 (mid) and 511 (bottom) °C. By turning off the last heater, the cool-down phase began. The heating jacket was opened at minute 287. The second phase ended when T3 reached 431 °C at minute 86. The third phase lasted until the heating jacket was opened at minute 287, as the temperature at T3 fell below 430 °C.

Like in the three preceding heating experiments, the heat was not equally distributed within the reactor tube. Table 6.5 (p. 71) shows the temperature inside the reactor for the third phase. The central part (T5, T4, T3, T2) of the reactor tube lies within 64 °C between minute 86 and 287. The outermost positions T1 and T6 show a higher deviation from the temperature in the central part.

Carbon dioxide was first detected at minute 117 (444 °C at T3) in a concentration of 0.1 vol%. The carbon dioxide concentration gradually increased to 0.6 vol% (minute 163, 485 °C at T3), dropped back to 0.5 vol% (minute 173, 485 °C) for 20 minutes, increased again to 0.7 vol% (minute 194, 504°C) and quickly decreased to zero at minute 221. The carbon monoxide concentration shows a comparable run to the carbon dioxide concentration. The difference between the two concentrations is that the carbon monoxide concentration accounts for roughly half of the carbon dioxide concentration between minute 140 and 221. The reason for the carbon dioxide production could be the thermal decomposition of iron carbonate to iron oxide. If the total mass loss of 1.1436 g corresponds to the iron carbonate content of the sample, the mass loss of iron carbonate would account for 39.81 wt% (mol%). This value is 1.82 wt% (mol%) higher than the carbon dioxide content of iron carbonate (37.99 %). This could be due to weighing errors, decomposition of other components of the siderite sample, or a starting reduction of iron carbonate to elemental iron, as suggested in the interpretation of the thermogravimetric experiment (see section 5.3.3, p. 48).

Thermally produced carbon dioxide could react with hydrogen to yield carbon monoxide in a reverse water-gas-shift reaction (see reaction equation 5.9, p. 46). The free reaction energy[3] $\Delta_R G$ for the reverse water gas shift reaction accounts for 14.076 kJ/mol at 400 °C and decreases to 10.618 kJ/mol at 500 °C. Furthermore, the iron oxide produced by the thermal decomposition could catalyze the reverse water-gas-shift (cf. literature review Rao et al. 2013 [28], pp. 24 ff. and Grenoble et al. 1981 [45]).

The lower diagram in Figure 6.5 (p. 71) shows that the nitrogen to hydrogen ratio was not always at 4:1. The hydrogen concentration indicated by the Caldos27 analyzer module showed a major drift during the experiment. Therefore, the hydrogen flow was varied between minute 30 and 78 to see the response of the analyzer. As the indicated value seemed irreproducible, the hydrogen concentration in the flue gas is not depicted in the upper diagram in Figure 6.5. Consequently, the hydrogen flow was regulated to 20 vol% by keeping the nitrogen to hydrogen flow ratio at 4:1 at the reactor input. The hydrogen supply was cut off at minute 246. The nitrogen flow was increased from 280 to 400 sccm when the hydrogen supply was cut off to replace remaining hydrogen before the system was turned off. Between minute 78 and 246 the nitrogen to hydrogen ratio was always at 4:1, with a mean nitrogen flow of 279 ± 15 and a mean hydrogen flow of 70 ± 4.

The varying pressure until minute 80 can be explained by the variation of the hydrogen flow. The increase of the reactor pressure between minute 105 and 115 could be due to the initiating thermal decomposition. The fast decrease of the pressure from 1.6 to 0.7 bar occurred because the bypass around the BPR was manually opened to decrease the reactor pressure. The pressure drop at minute 286 was due to opening the bypass around the BPR to reduce the reactor pressure to atmospheric level during the shutdown phase. The mean pressure between minute 135 and 246 was 0.76 ± 0.05 bar, between minute 246 and 286 0.62 ± 0.06 bar.

[3] Values calculated with HSC Chemistry© 3.0 for Windows

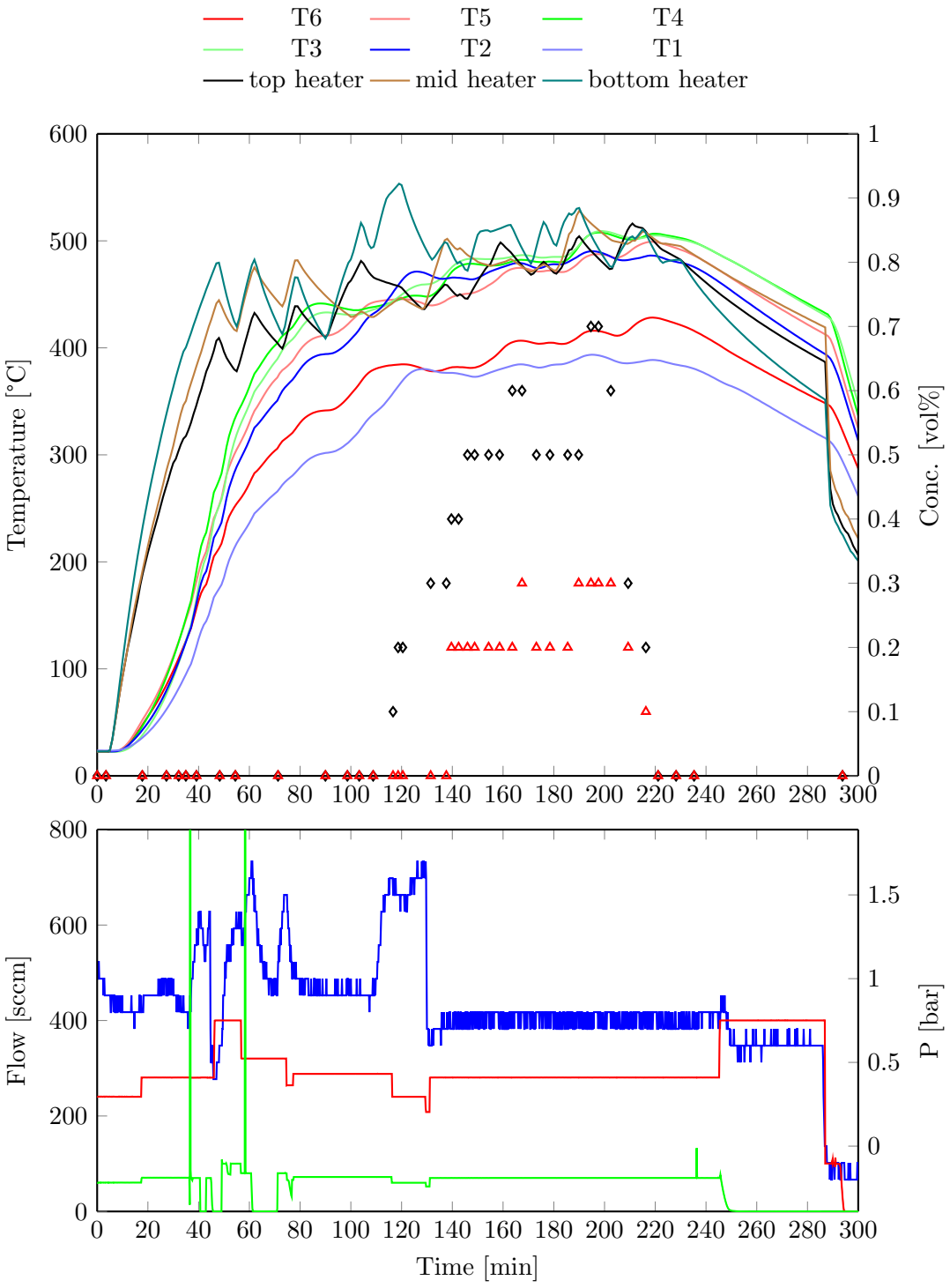

Figure 6.11: Heating of siderite in hydrogen atmosphere. *Above:* Temperature inside the reactor (T6: top to T1: bottom), heater temperatures, carbon dioxide (diamonds), and carbon monoxide (triangles) concentration in the flue gas. *Below:* Pressure (blue), nitrogen flow (red), and hydrogen flow (green)

7 Conclusions and possible future work

The thermodynamic calculations for the hydrogenation of magnesium, lead, manganese, iron, cobalt, nickel, copper, zinc, silver, and cadmium carbonate to methane revealed a negative standard free reaction energy between zero and 550 °C at 1 atm. As a consequence, these hydrogenation reactions are thermodynamically favorable, but could still be kinetically hindered. The literature review showed that the hydrogenation of inorganic carbonates has already been investigated by four different working groups. This field of research started in 1987 with the publication of Reller et al. [21] and is still worked on, as the latest publication dates from 2013 (Rao et al. [28]). The focus lies on the hydrogenation of calcium and magnesium carbonate and derivatives. In summary, the research done by Reller et al. [21–24], Rao et al. [27, 28], Tsuneto et al. [25], and Yoshida et al. [26] showed that the thermal decomposition of inorganic carbonates in hydrogen atmosphere mainly yields carbon monoxide and methane, besides carbon dioxide - the major product of the thermal decomposition in inert atmosphere. Rao et al. 2013 [28] were also able to produce C2 and C3 hydrocarbons with iron/calcium carbonate co-precipitates. Tsuneto et al. [25] and Yoshida et al. [26] suggest that the methane production proceeds directly at the solid/gas interface without intermediate carbon dioxide production. Reller et al. [21–24] and Rao et al. [27, 28], on the contrary, suggest that the thermal decomposition with the concurrent carbon dioxide production has to precede further reductions. Future work could include thermodynamic calculations for the carbon monoxide production in a reverse water-gas-shift reaction, and the hydrogenation of carbon dioxide to formic acid, formaldehyde, methanol, and higher hydrocarbons.

In this work, four carbonates were investigated in thermogravimetric experiments in nitrogen and 50 vol% hydrogen atmosphere: siderite with a 71.01 wt% iron carbonate content and synthetic magnesium, manganese, and nickel carbonate. Nitrogen atmosphere led to a mass loss most possibly corresponding to the thermal decomposition of the carbonates to carbon dioxide and metal oxides. The temperature corresponding to the maximum rate of reaction evaluated at the point of inflection T_{PoI} decreased for all four samples when hydrogen was present. Additionally, mass losses significantly higher than the calculated carbon dioxide content could be observed in the case of siderite and nickel carbonate, possibly corresponding to the reduction of the carbonate to the respective metal. Future thermogravimetric experiments should include evolved gas and solid state analysis to clearly identify reaction products. Furthermore, catalysts for specific hydrogenation products, higher pressures, and isothermal experiments would be desirable.

The commissioning included the design and assembly of: an analyzer rack, a switch box, and a powder cartridge. The analyzer rack could be successfully coupled to the reactor system. The powder cartridge enables easier powder handling compared to the impregnation of glass wool with powder. Heating experiments with magnesium carbonate and siderite with nitrogen and 20 vol% hydrogen flow were conducted. The Uras26 analyzer

Table 7.1: Summary of characteristic temperatures identified in the thermogravimetric experiments

Sample	Atmosphere	$T_{e,o}$ [°C]	T_{PoI} [°C]	$T_{e,f}$ [°C]
$MgCO_3$	N_2	n/a[1]; 204; 400; 474	n/a[1]; 262; 437; 483	n/a[1]; 296; 453; 499
	N_2:H_2 (1:1)	185; 402	236; 436	268; 456
Siderite	N_2	462	478	502
	N_2:H_2 (1:1)	402	426	445
$MnCO_3$	N_2	409	470	456
	N_2:H_2 (1:1)	403	444	435
$NiCO_3$	N_2	n/a[1]; 262	n/a[1]; 293	n/a[1];331
	N_2:H_2 (1:1)	n/a[1]; 227	n/a[1]; 245	n/a[1];263

[1] Broad TG step where no reproducible value could be calculated

showed reproducible concentration values, whereas the Caldos27 analyzer showed a major drift one of the experiments and had to be re-calibrated. The heating experiments showed that the central part of the reactor tube can reach a narrow heat distribution (measured at thermocouples T2-T5) within approximately 80 minutes when all heaters are set to full power (see Figure 6.8, p. 64). The outermost positions of the reactor tube (thermocouples T1 and T6), on the contrary, show a major temperature decline compared to the nearest thermocouple (T2 and T5), although two thermocouples measure the temperature of the same heating zone. Carbon dioxide was detected in all four heating experiments, carbon monoxide only when siderite was heated in 20 vol% hydrogen atmosphere. Carbon dioxide could most possibly be produced by the thermal decomposition of the samples. In the case of magnesium carbonate, the mass loss in nitrogen and 20 vol% hydrogen atmosphere corresponded approximately to the calculated carbon dioxide content of 52.20 wt%. When siderite was heated in nitrogen for more than five hours the mass loss was 9.96 wt%. Indeed, the calculated carbon dioxide content of iron carbonate accounts for 37.99 wt%. Therefore, the thermal decomposition could have proceeded only partially, possibly because of a too low temperature, a high activation energy, or matrix effects. Heating of siderite in 20 vol% hydrogen led to a mass loss of 39.81 wt%. This value 1.82 wt% higher than the calculated carbon dioxide content could be due to weighing errors, the decomposition of matrix elements, or a starting reduction of iron carbonate to iron. The carbon monoxide production during the heating of siderite in 20 vol% hydrogen atmosphere could be explained by a reverse water-gas-shift reaction of carbon dioxide and hydrogen.

Tables 7.1 and 7.2 (p. 76) show a summary of characteristic data identified in the thermogravimetric and heating experiments. Carbon dioxide was first detected at 170 °C when magnesium carbonate was heated in the reactor in nitrogen atmosphere. This temperature is 34 °C lower than the $T_{e,o}$ determined in the thermogravimetric experiments. The TG curve, indeed, shows a slow mass decrease starting at 50 °C. The temperature of maximum carbon dioxide concentration (3.2 vol%) of the heating experiment in nitrogen atmosphere accounts for 461 °C. This temperature lies within the range of the T_{PoI} of the second and third step of the thermogravimetric experiment (437 and 483 °C). When 20 vol% hydrogen were used during the heating of magnesium carbonate in the reactor, the temperature for

Table 7.2: Summary of some characteristic temperatures, experimental times, and carbon dioxide concentrations identified in the heating experiments

Sample	Atmosphere	T [°C]	Thermoc. pos.	t [min]	CO_2 [vol%]
$MgCO_3$	N_2	170	T2	51	0.1
		461	T2	105	3.2
	N_2:H_2 (4:1)	282	T2	93	0.2
		383	T2	123	1.7
		432	T2	134	2.0
		426	T2	181	0.6
		452	T2	200	1.8
Siderite	N_2	479	T2	156	0.1
		495	T2	182	0.3
		493	T2	205	0.3
	N_2:H_2 (4:1)	444	T3	117	0.1
		485	T3	163	0.6
		485	T3	173	0.5
		504	T3	194	0.7

the first detection of carbon dioxide in 0.2 vol% increased to 282 °C. In the thermogravimetric experiments with 50 vol% hydrogen, on the contrary, the $T_{e,o}$ decreased by 19 °C to 185 °C. As the concentration data of the heating experiments was taken by handwritten notes, this difference could be due to missing data points for 0.1 vol% carbon dioxide. In order to avoid this problem, software for data acquisition and storage should be used in the future. The temperatures at maximum carbon dioxide concentration in the heating experiments (432 °C at 2.0 vol% CO_2 and 452 °C at 1.8 vol% CO_2), however, were within the range of the T_{PoI} of the second step identified in the thermogravimetric experiments (436 °C). In the case of siderite, the temperatures of the first detection of carbon dioxide and maximum carbon dioxide concentration that were identified in the heating experiments were in the range of the $T_{e,o}$ and T_{PoI} identified in the thermogravimetric experiments. Taken together, the findings of the heating experiments complement the findings of the thermogravimetric experiments and support the assumption that a thermal decomposition of the respective carbonate with the accompanying release of carbon dioxide was observed. Indeed, future investigations should make use of GC-MS and/or FTIR for gas analysis and XRD and/or electron microscopy for solid analysis to fortify the results.

As the Parr tubular reactor system was only commissioned during this Master's thesis, further interesting research is now possible. Adaptions of the reactor system could include the retrofitting to a recycle reactor and the integration of mass flow indicators to allow mass balances of the reactor. Furthermore, the non-isothermal heat distribution within the reactor should be investigated.

Bibliography

(1) Zevenhoven, R.; Eloneva, S.; Teir, S. Chemical fixation of CO2 in carbonates: Routes to valuable products and long-term storage. *Catalysis Today* **2006**, *115*, 73–79.

(2) Holleman, A. F.; Wiberg, E.; Wiberg, N., *Lehrbuch der Anorganischen Chemie*, 102nd ed.; Walter de Gruyter: Berlin, 2007.

(3) Housecroft, C.; Sharpe, A., *Anorganische Chemie*, 2nd ed.; Pearson Education: München, 2006.

(4) Ludwig, R.; Kornath, A. In spite of the chemist's belief: Carbonic acid is surprisingly stable. *Angewandte Chemie International Edition* **2000**, *39*, 1421–1423.

(5) *Ullmann's encyclopedia of industrial chemistry: Online version*, 5th ed.; Wiley-VCH: http://onlinelibrary.wiley.com/book/10.1002/14356007, June 2013.

(6) Lenk, W.; Prinz, H.; Steinmetz, A. In *Ullmann's encyclopedia of industrial chemistry*; Wiley-VCH Verlag: Weinheim, Germany, 2010.

(7) Simons, E. L.; Cairns, E. J.; Sangermano, L. D. Purification and preparation of some caesium compounds. *Talanta* **1966**, *13*, 199–204.

(8) Bick, M.; Prinz, H.; Steinmetz, A. In *Ullmann's encyclopedia of industrial chemistry*; Wiley-VCH Verlag: Weinheim, Germany, 2010.

(9) Flessner, T.; Doye, S. Cesium carbonate: A powerful inorganic base in organic synthesis. *Journal für praktische Chemie* **1999**, *341*, 186–190.

(10) Ali, A.; Hasan, M.; Zaki, M. Dawsonite-type precursors for catalytic Al, Cr, and Fe oxides: Synthesis and characterization. *Chemistry of Materials* **2005**, *17*, 6797–6804.

(11) Li, G.-C.; Liu, Y.-Q.; Guan, L.-L.; Hu, X.-F.; Liu, C.-G. Meso/macroporous γ-Al2O3 fabricated by thermal decomposition of nanorods ammonium aluminium carbonate hydroxide. *Materials Research Bulletin* **2012**, *47*, 1073–1079.

(12) Donaldson, J. D.; Beyersmann, D. In *Ullmann's encyclopedia of industrial chemistry*; Wiley-VCH: Weinheim, Germany, 2005.

(13) Antonsen, D. H.; Meshri, D. T. In *Kirk-Othmer encyclopedia of chemical technology*; John Wiley & Sons, Inc.: Hoboken, NJ, USA, 2005.

(14) Wayne Richardson, H. In *Kirk-Othmer encyclopedia of chemical technology*; John Wiley & Sons, Inc.: Hoboken, NJ, USA, 2003.

(15) Brumby, A. et al. In *Ullmann's encyclopedia of industrial chemistry*; Wiley-VCH Verlag: Weinheim, Germany, 2008.

(16) Kanari, N.; Mishra, D.; Gaballah, I.; Duprac, B. Thermal decomposition of zinc carbonate hydroxide. *Thermochimica Acta* **2004**, *410*, 93–100.

(17) Rohe, D. M. M.; Wolf, H. U. In *Ullmann's encyclopedia of industrial chemistry*; Wiley-VCH: Weinheim, Germany, 2000.

(18) Schulte-Schrepping, K.-H.; Piscator, M. In *Ullmann's encyclopedia of industrial chemistry*; Wiley-VCH Verlag: Weinheim, Germany, 2000.

(19) Connelly, N. G., *Nomenclature of inorganic chemistry*; Royal Society of Chemistry, I., Ed.; RSC Publishing: Cambridge, 2005.

(20) McGill, I. In *Ullmann's encyclopedia of industrial chemistry*; Wiley-VCH: Weinheim, Germany, 2000.

(21) Reller, A.; Padeste, C.; Hug, P. Formation of organic carbon compounds from metal carbonates. *Nature* **1987**, *329*, 527–529.

(22) Padeste, C.; Reller, A.; Oswald, H. R. The influence of transition metals on the thermal decomposition of calcium carbonate in hydrogen. *Materials Research Bulletin* **1990**, *25*, 1299–1305.

(23) Padeste, C.; Oswald, H.; Reller, A. The thermal behaviour of pure and nickel doped hydromagnesite in different atmospheres. *Materials Research Bulletin* **1991**, *26*, 1263–1268.

(24) Reller, A.; Emmenegger, R.; Padeste, C.; Oswald, H.-R. Thermochemical reactivity of metal carbonates. *CHIMIA International Journal for Chemistry* **1991**, *45*, 262–266.

(25) Tsuneto, A.; Kudo, A.; Saito, N.; Sakata, T. Hydrogenation of solid state carbonates. *Chemistry Letters* **1992**, 831–834.

(26) Yoshida, N.; Hattori, T.; Komai, E.; Wada, T. Methane formation by metal-catalyzed hydrogenation of solid calcium carbonate. *Catalysis Letters* **1999**, *58*, 119–122.

(27) Jagadeesan, D.; Eswaramoorthy, M.; Rao, C. N. R. Investigations of the conversion of inorganic carbonates to methane. *ChemSusChem* **2009**, *2*, 878–882.

(28) Jagadeesan, D.; Sundarayya, Y.; Madras, G.; Rao, C. N. R. Direct conversion of calcium carbonate to C1-C3 hydrocarbons. *RSC Advances* **2013**, *3*, 7224.

(29) Daubert, T. E., *Chemical engineering thermodynamics*; McGraw-Hill: New York, 1985.

(30) Atkins, P. W.; Paula, J. d., *Physikalische Chemie*, 4th ed.; Wiley-VCH Verlag: Weinheim, 2006.

(31) Smith, E. B., *Basic chemical thermodynamics*, 5th ed.; Clarendon Press: Oxford, 2005.

(32) *Perry's chemical engineer's handbook*, 8th ed.; McGraw-Hill New York: 2008.

(33) Lide, D. R., *CRC handbook of chemistry and physics on CD-ROM*; CRC Press: Boca Raton, Fla., 2007.

(34) *NIST-JANAF termochemical tables*, 4th ed.; Chase, M. W., National Institute of Standards and Technology US Department of Commerce, Eds.; American Chemical Society: Washington, DC, 1998.

(35) Barin, I., *Thermochemical data of pure substances*, 2nd ed.; Wiley-VCH: Weinheim, 1993.

(36) Muller, P. Glossary of terms used in physical organic chemistry: IUPAC Recommendations 1994. *Pure and Applied Chemistry* **1994**, *66*, 1077–1184.

(37) Roine, A. Outokumpu HSC chemistry for Windows user's guide for version 3.0.; Outokumpu Research Oy, Finnland, 1997.

(38) Maier, C. G.; Kelley, K. K. An equation for the representation of high-temperature heat content data. *Journal of the American Chemical Society* **1932**, *54*, 3243–3246.

(39) Mackenzie, R. Nomenclature in thermal analysis, part IV. *Thermochimica Acta* **1979**, *28*, 1–6.

(40) W. F. Hemminger, H. K. C., *Methoden der Thermischen Analyse*; Springer: Berlin, Heidelberg, New York, 1989.

(41) Hill, J. O. In *Encyclopedia of analytical science*, Townshend, A., Ed., 10 vols.; Academic Press Ltd.: London, 1995; Vol. 9.

(42) Dunn, J. G. In *Encyclopedia of analytical chemistry*, Meyers, R. A., Ed., 15 vols.; Wiley-VCH: New York, Weinheim, 2000; Vol. 15.

(43) J. Szekely J. W. Evans, H. Y. S., *Gas-solid reactions*; Academic Press: 1976.

(44) Buckman, N.; Hawkins, N. Improving resolution in thermogravimetric analysis. *Chemistry in Australia* **1994**, *61*, 566–566.

(45) Grenoble, D.; Estadt, M.; Ollis, D. The chemistry and catalysis of the water gas shift reaction: 1. The kinetics over supported metal catalysts. *Journal of Catalysis* **1981**, *67*, 90–102.

List of Figures

List of Tables

List of abbreviations and symbols

a, a_i	Activity, activity of component i
AACH	Ammonium aluminum carbonate hydroxide
AW	Atomic weight
b_w	Intercept for a linear equation at a point of inflection
BPR	Back pressure regulator
Cat.	Catalyst, catalysis
CEET	Institute for Chemical Engineering and Environmental Technology
CtM	Conversion of the respective carbonate to methane
CU	Central unit
c_p	Specific heat capacity
$\Delta_R G$	Free reaction energy
$\Delta_f G$	Free formation energy
$\Delta_R H$	Reaction enthalpy
$\Delta_f H$	Enthalpy of formation
$\Delta_R S$	Reaction entropy
$\Delta_f S$	Entropy of formation
DSC	Differential scanning calorimetry
DTA	Differential thermal analysis
DTG	Differential thermogravimetry
eq.	Equilibrium
FID	Flame ionization detector
FTIR	Fourier transform infrared spectroscopy
G	Gibbs free energy
gas.	Gaseous
GC	Gas chromatography
HMI	Human machine interface
HPLC	High performance liquid chromatography
K	Equilibrium constant
k_w	Slope of a linear equation at a point of inflection
K_p	Equilibrium constant at constant temperature
K_x	Equilibrium constant regarding the mole fraction x_i of component i
$K_{sn,X}$	Nth dissociation constant of acid X
liq.	Liquid
M	Metal or transition metal
m_0	Initial mass of a sample in an experiment
m_{end}	End mass of a TG event
min, min.	Minute, minimum

MFC	Mass flow controller
mol%	Mol percent
Möss. spec.	Mössbauer spectroscopy
MS	Mass spectrometry
m_{start}	Start mass of a TG event
Mt	Megatons
m_T	Mass of a sample at a temperature T
MW	Molecular weight
μ	Chemical potential
n/a	Not applicable
NMR	Nuclear magnetic resonance (spectroscopy)
ν	Stoichiometric coefficient
$\ominus$	Denominates a quantity at 1 atm
P	Pressure
PCC	Precipitated calcium carbonate
Poti.	Potentiometer
P_{sample}	Percentage content of P in sample
p_i	Partial pressure of component i
PV	Process variable
Q	Reaction quotient
R	Reactants or ideal gas constant
RE	Rare earth element
Ref.	Reference
S	Entropy
sccm	Standard cubic centimeters per minute
SGC	Sample gas cooler
SP	Set point
STP	Standard temperature and pressure
T	Temperature
T_0	Temperature at which the standard free reaction energy equals zero
T1-T6	Thermocouple position inside the reactor from top (T6) to bottom (T1)
T_{av}	Mean temperature
TCD	Thermal conductivity detector
TEM	Transmission electron microscopy
$T_{e,o}$	Extrapolated onset temperature
$T_{e,f}$	Extrapolated final temperature
T_i	Initial temperature
T_f	Final temperature
TG	Thermogravimetry, thermogravimetric
$T_{p,max}$	Temperature at a local maximum of a DTG curve
$T_{p,min}$	Temperature at a local minimum of a DTG curve
T_{PoI}	Temperature at the point of inflection
TPH	Temperature-programmed hydrogenation
U	Internal energy
UV	Ultra violet

V	Volume
vol%	Volume percent
w/o	Without
wt%	Weight percent
ξ	Reaction coordinate
$x_{i/j}$	Molar ratio of i to j
XRD	X-ray diffraction

Matlab routine TGAnalyisCarbonates.m

```
1  %TGAnalysisCarbonates
2  clc,
3  clear,
4  close all,
5
6  %User Input
7  inputdirectory = '';
8  inputfilename = '';  %This file must only include numeric data, column 1 =
       Temperature, column 2 = time, column 3 = mass in percent
9  outputdirectory = '';
10 outputfilename = '';
11 molName = '';
12 molFormula = '';
13 Mol = 0;    %Molecular weight of the analyzed molecule
14 TstartUser = 0;        %Start Temperature for min(dm/dT) calculation
15 TendUser = 0;          %End Temperature for min(dm/dT) calculation
16 mstart = 0;            %Starting mass of TG event in percent
17 mend = 0;               %End mass of TG event, if left at 0 then the minimum
       mass of the whole experiment will be used
18 saveresults = 1;         %If set to 0 no results are saved, if set to 1
       results are saved
19
20 %Initalisation
21 %Assignment of columns in input data
22 Tcolumn = 1;     %Temperature in °C
23 tcolumn = 2;     %time in min
24 mcolumn = 3;     %mass in percent
25 dmcolumn = 4;    %dm/dT in %/°C
26 lastRow = 0;     %Last Row counter
27 Tw = 0; %Temperature at point of inflection in °C
28 kw = 0; %Slope at point of inflection in %/°C
29 bw = 0; %T-axis Intercept
30 mw = 0; %Mass at point of inflection
31
32 Ts = 0; %Starting temperature of TG event
33 Te = 0; %End temperature of TG event
34
35 rowTstart = 1;
36 rowTend = 1;
37
38 C = 12.011;       %Carbon atomic number in g/mol
39 O = 15.999;       %Oxygen atomic number in g/mol
40 H = 1.0079;       %Hydrogen atomic number
41 H2O = 18.02;      %Molecular weight of water in g/mol
42
43 C_Mol = 100* (C/Mol);            %Carbon in molecule in %
44 O_Mol = 100 * (O/Mol);           %Oxygen in molecule in %
```

```
45 H2O_Mol = 100 * (H2O/Mol);        %Water in molecule  in %
46 CO_Mol = 100 * ((C+O)/Mol);       %Carbon monoxide in molecule in %
47 CO2_Mol = 100 * ((C + 2*O)/Mol);%Carbon dioxide in molecule in %
48 OH_Mol = 100 * ((O+H)/Mol);       %Hydroxide in molecule in %
49
50 %Preparation of data Matrix for further manipulation
51 file = [inputdirectory, inputfilename];
52 data = load(file);
53 data = data(:,1:3); %Only columns T t mass are important
54
55 %clearance of cool down curve with Tmax of Tcolumn
56 for n = 1:length(data)
57     if data(n,Tcolumn) == max(data(:,Tcolumn))
58         lastRow = n;
59     end
60 end
61 data = data(1:lastRow,:);
62
63 %Add column 4 = dm/dT
64 data(1:end-1,dmcolumn) = (data(2:end,mcolumn)-data(1:end-1,mcolumn))./(data
       (2:end,Tcolumn)-data(1:end-1,Tcolumn));
65
66 %Smoothing the raw data:
67 %Replace values out of upper and lower limit of dm/dT with zeros
68 lowerLimit = -1;
69 upperLimit = 0.01;
70 for n = 1:length(data)
71     if  data(n,dmcolumn) < lowerLimit || data(n,dmcolumn) > upperLimit
72         data(n,dmcolumn) = 0;
73     end
74 end
75
76 %Search of row-numbers for T-range where the minimum has to be determined
77 while data(rowTstart,Tcolumn) < TstartUser
78    rowTstart = rowTstart + 1;
79 end
80 while data(rowTend,Tcolumn) < TendUser
81     rowTend = rowTend + 1;
82 end
83
84 %Determination of kw, Tw, mw, bw, Ts, Te
85 kw = min(data(rowTstart:rowTend,dmcolumn));
86
87 for TwRow = 1:length(data)
88     if data(TwRow,dmcolumn) == kw
89         Tw = data(TwRow,Tcolumn);
90         mw = data(TwRow,mcolumn);
91     end;
92 end
93
94 if mend == 0
95     mend = min(data(:,mcolumn));
96 end
97
98 bw = mw - kw*Tw;
```

```
99  Ts = (mstart - bw)/kw;
100 Te = (mend - bw)/kw;
101
102 %Plot
103 plot(data(:,Tcolumn), data(:,mcolumn),'b-', [0 max(data(:,Tcolumn))], [mstart
        mstart], 'g-', [0 max(data(:,Tcolumn))], [mend mend], 'r-', [0 -bw/kw],
    [bw 0], 'y-');
104 grid on;
105 legend boxoff;
106 ylim([0 120]);
107 xlim([min(data(:,Tcolumn)) max(data(:,Tcolumn))]);
108 xlabel('Temperature [°C]');
109 ylabel('Mass [%]');
110
111 %Save Results
112 if saveresults == 1
113 file = [outputdirectory, molName, ' Results.txt']; %Assemble the filename for
        the results
114 fid = fopen(file, 'w');
115 fprintf(fid, '***RESULTS FOR %s ***\n', molName);
116 fprintf(fid, 'The maximum gradient (kw) between %3.0f and %3.0f °C is %5.4f
    %%\\°C \n', TstartUser, TendUser, kw);
117 fprintf(fid, 'The temperature at maximum gradient and point of inflection is
    %5.2f °C \n', Tw);
118 fprintf(fid, 'The extrapolated onset temperature is %5.2f °C \n', Ts);
119 fprintf(fid, 'The extrapolated final temperature is %5.2f °C \n', Te);
120 fprintf(fid, 'The starting mass is %4.1f %% \n', mstart);
121 fprintf(fid, 'The end mass is %4.1f %% \n', mend);
122 fprintf(fid, 'The mass difference is %4.1f %% \n', mstart-mend);
123 fprintf(fid, 'The suggested molecular formula for %s is %s \n', molName,
    molFormula);
124 fprintf(fid, 'Theoretical Carbon in %s: %4.1f %% \n', molName, C_Mol);
125 fprintf(fid, 'Theoretical Oxygen in %s: %4.1f %% \n', molName, O_Mol);
126 fprintf(fid, 'Theoretical Carbon monoxide in %s: %4.1f %% \n', molName,
    CO_Mol);
127 fprintf(fid, 'Theoretical Carbon dioxide in %s: %4.1f %% \n', molName,
    CO2_Mol);
128 fprintf(fid, 'Theoretical Water in %s: %4.1f %% \n', molName, H2O_Mol);
129 fprintf(fid, 'Theoretical Hydroxide in %s: %4.1f %% \n', molName, OH_Mol);
130 fclose(fid);
131 mstartline = [ 0 mstart; max(data(:,Tcolumn)) mstart ];
132 mendline = [0 mend; max(data(:,Tcolumn)) mend];
133 tangentofinflection = [0 bw; -bw/kw 0];
134 save([outputdirectory, molName, ' PlotdataTGA.txt' ], 'data', '-ascii'); %
    Column1: Temperature [°C], column2: Time [min], column3: Mass [%],
    column4: dm/dT [%/°C]
135 save([outputdirectory, molName, ' mstartline.txt' ], 'mstartline', '-ascii');
136 save([outputdirectory, molName, ' mendline.txt' ], 'mendline', '-ascii');
137 save([outputdirectory, molName, ' ToI.txt' ], 'tangentofinflection', '-ascii'
    );
138 end
```